Accepted Manuscript

Title: Electrospun polyimide nanofibers and their applications

Author: Yichun Ding Haoqing Hou Yong Zhao Zhengtao Zhu Hao Fong

PII: S0079-6700(16)30038-7
DOI: http://dx.doi.org/doi:10.1016/j.progpolymsci.2016.06.006
Reference: JPPS 991

To appear in: *Progress in Polymer Science*

Received date: 28-7-2015
Revised date: 8-6-2016
Accepted date: 27-6-2016

Please cite this article as: Ding Y, Hou H, Zhao Y, Zhu Z, Fong H, Electrospun polyimide nanofibers and their applications, *Progress in Polymer Science* (2016), http://dx.doi.org/10.1016/j.progpolymsci.2016.06.006

This is a PDF file of an unedited manuscript that has been accepted for publication. As a service to our customers we are providing this early version of the manuscript. The manuscript will undergo copyediting, typesetting, and review of the resulting proof before it is published in its final form. Please note that during the production process errors may be discovered which could affect the content, and all legal disclaimers that apply to the journal pertain.

ACCEPTED MANUSCRIPT

Electrospun polyimide nanofibers and their applications

Yichun Ding[a,b], Haoqing Hou[a1]haoqing@jxnu.edu.cn, Yong Zhao[b], Zhengtao Zhu[b], Hao Fong[b*]hao.fong@sdsmt.edu

[a]College of Chemistry and Chemical Engineering, Jiangxi Normal University, Nanchang, Jiangxi 330027, China

[b]Program of Biomedical Engineering, South Dakota School of Mines and Technology, Rapid City, South Dakota 57701, USA

Tel.: 1 605 394 1229

Abstract

Aromatic polyimides (PIs) are high-performance polymers with rigid heterocyclic imide rings and aromatic benzene rings in their macromolecular backbones. Owing to excellent mechanical properties and thermal stability, as well as readily adjustable molecular structures, PIs have been widely adopted for many applications related to electronics, aerospace, automobile, and other industries. In recent years, PI fibers prepared by electrospinning of polyamic acid (PAA) precursor nanofibers followed by imidization (commonly known as electrospun PI nanofibers) have attracted growing interests. Herein, the preparation, evaluation, and application of electrospun PI nanofibers are reviewed. PI polymers and the electrospinning technique are introduced first followed by the preparation of electrospun nanofibers of homo-PI, co-PI, blend-PI, and PI

ACCEPTED MANUSCRIPT

composite. Subsequently, the mechanical and thermal properties of electrospun PI nanofibers are presented; in particular, the mechanical properties of individual electrospun PI nanofibers are highlighted. Thereafter, various applications of electrospun PI nanofibers are outlined, including reinforcement of composites, Li-ion battery separators, fuel cell proton exchange membranes, sensors, microelectronics, high-temperature filtration media, super-hydrophobic PI nanofibers, and PI-based carbon nanofibers. In the final section of conclusions and perspectives, future research endeavors and high-value applications of electrospun PI nanofibers are discussed.

Keywords

Polyimide, Electrospinning, Nanofibers, Properties, Applications

Abbreviations

AAI	$[CH_3COCH{=}C(O\text{-})CH_3]_3Fe$
AAPTMI	5(6)-amino-1-(4'-aminophenyl)-1,3-trimethylindane
ACAT	N,N'-bis(4'-aminophenyl)-1,4-quinonenediimine
AIE	aggregation-induced emission
BDAF	2,2-bis[4-(4-aminophenoxy)phenyl]hexafluoropropane
blend-PI	blend-polyimide
BPA	4,4'-diaminobiphenyl
BPDA	3,3',4,4'-biphenyl-tetracarboxylic dianhydride
BSAA	4,4'-(4,4'-isopropylidenediphenoxy)-bis(phthalic anhydride)
BTDA	benzophenone-3,3',4,4'-tetracarboxylic dianhydride
ECNFs	electrospun carbon nanofibers
CN-TPA	cyano triphenylamine
co-PI	co-polyimide
DATPP	diaminotetraphenylporphyrin
DDS	4,4'-diaminodiphenylsulphone
DEDAC	dodecylethyldimethylammonium chloride
DHB	3,3'-dihydroxybenzidine
DMAB	dimethylamine borane

Accepted Manuscript

ACCEPTED MANUSCRIPT

DMOBPA	4,4'-diamino-3,3'-dimethoxydiphenyl
DNT	2,4-dinitrotoluene
ECPF	electroactive co-polyimide fiber
EDLCs	electrical double layer capacitors
EPF	electroactive polyimide fiber
HMDA	hexamethylenediamine
HPMDA	1,2,4,5-cyclohexanetetracarboxylic dianhydride
HQDPA	1,4-bis (3',4'-dicarboxyphenoxy) benzene dianhydride
LIBs	lithium ion batteries
MeO-PA	methoxy-containing polyamide
MeO-PAA	methoxy-containing polyamic acid
MeO-PI	methoxy-containing polyimide
MWNTs	multi-wall carbon nanotubes
M-5	poly(hydroquinone-diimidazopyridine)
NB	nitrobenzene
NEPF	non-electroactive polyimide fiber
NMP	N-methylpyrrolidinone
ODA	4,4'-oxydianiline
ODPA	4,4'-oxydiphthalic anhydride
OH-PAA	hydroxy-containing polyamic acid
OH-PI	hydroxy-containing polyimide
PA	2,4,6-trinitrophenol
PAA	polyamic acid
PAI	poly(amide-imide)
PAN	polyacrylonitrile
PANi	polyaniline
PA6	polyamide 6
PBI	polybenzimidazole
PBO	polybenzoxazole
PECNFs	highly porous electrospun carbon nanofibers
PDA (PPD)	p-phenylenediamine
PDT	poly(dodecylthiophene)
PEO	polyethylene oxide
PFOS	perfluorooctanesulfonic acid
PHA	polyhydroxyamide
PI	polyimide
PI-co-PBO	poly(imide-co-benzoxazole)
PI-g-PMMA	polyimide nanofibers grafted with poly(methyl methacrylate)
PLLA	poly(lactic acid)
PMDA	pyromellitic dianhydride

Accepted Manuscript

ACCEPTED MANUSCRIPT

PMIL	polymer melt infiltration lamination
PMMA	poly(methyl methacrylate)
PRM	2,5-bis(4-aminophenyl)pyrimidine
PSF	polysulfone
PVdF-HFP	poly(vinylidene fluoride-co-hexafluoropropylene)
PVP	polyvinylpyrrolidone
TBAB	tetrabutyl ammonium bromide
TEGDA-BA	triethylene glycol diacetate-2-propenoic acid butyl ester
TEOS	tetraethoxysilane
TFAH	1,1,1-trifluoro-2,4-pentanedione
TNT	2,4,6-trinitrotoluene trinitrotoluene
UHMWPE	ultra-high molecular weight polyethylene
6FAP	2,2'-bis (4-aminophenyl)hexafluoropropane
6F-BAPP	2,2'-bis[4-(4-aminophenoxy)phenyl]hexafluoropropane
6FDA	2,2'-bis(3,4-dicarboxyphenyl)hexafluoropropane dianhydride

1. Introduction

1.1. Polyimides

Polyimides (PIs) are a class of polymers with macromolecular repeating units containing the functional imide group [1, 2]. PIs may be classified into aliphatic, semi-aromatic, and aromatic groups, while the aromatic PIs are the most important particularly owing to their superior thermal stability, high mechanical properties (*e.g.*, low creep and high strength), and good chemical resistance [3, 4]. For example, the properties of aromatic PIs may be well-retained up to ~450 °C and down to the boiling point of liquid nitrogen (*i.e.*, -196 °C); thus the application temperature ranges of aromatic PIs are considerably broader than those of many other polymers [4]. In addition, aromatic PIs are substantially resistant to combustion and usually do not need to be mixed with flame retardants. In the contents hereinafter, PIs will generally refer to aromatic PIs unless specified otherwise.

Accepted Manuscript

ACCEPTED MANUSCRIPT

PIs can be synthesized through a one-step approach; for example, the solution of a dianhydride and a diamine (with stoichiometric balance) in a phenolic solvent (with a high boiling point) can result in direct formation of PI at temperature higher than 200 °C [1, 2]. Nevertheless, PIs are more commonly made through a two-step approach; for example, a dianhydride and a diamine first react to form a precursor polyamic acid (PAA), which is then converted into the final polymer of PI upon the thermal/chemical imidization [1, 2]. Because of the heterocyclic imide rings and aromatic benzene rings in their macromolecular backbones, PIs possess very high glass transition temperatures and are typically insoluble. Hence, PIs are difficult to be re-processed after the materials/products are produced since the re-processing temperatures would be so high that the decomposition of PIs could often occur. Note that the precursor PAA polymers are not suitable for being processing by extrusion and injection molding techniques because at processing temperatures, PAA is likely undergoing degradation and/or imidization reactions. As a result, the widely adopted method to make PI materials/products consists of the following two steps: (1) preparation of precursor PAA materials *via* polymerization of monomers in polar organic solvents (*e.g.*, DMF, DMAc, and NMP), and (2) formation of the PI products *via* imidization of their PAA precursors. The chemical scheme of a typical two-step method for the preparation of PIs is shown in Fig. 1.

Due to the diversity of both dianhydrides and diamines, the molecular structure and rigidity/flexibility of PIs can be judiciously designed; in consequence, their thermal, mechanical, and other properties may be readily tailored [5, 6]. Since PIs were first made

Accepted Manuscript

ACCEPTED MANUSCRIPT

by Bogert and Renshaw in 1908 [7], they have been produced for various applications [3, 6, 8]. As early as the 1960s, DuPont owned a series of patents for the preparation of PIs [9-12]; and the company also had three major PI products commercially available including Kapton®, Vespel®, and Pyre-ML® [8]; thereafter, DuPont further developed many other PI products for electronics, aerospace, automobile, and other industries [3, 4, 6, 8].

Several conventional methods are used to spin PI fibers (*e.g.*, wet-spinning and dry-jet wet-spinning) [13-19]; and the two-step approach is commonly adopted. In general, precursor fibers of PAA are first obtained by spinning of its solution; subsequently, the PAA fibers are converted into the PI fibers upon imidization. For example, Park *et al*. reported the preparation of PI fibers by dry-jet wet-spinning of a PAA solution followed by thermal imidization [18]. Their studies indicated that the ultimate stress and initial modulus of PAA fibers were 268 MPa and 4.1 GPa, respectively; after imidization at 350 °C for 30 min in nitrogen, the resulting PI fibers exhibited the respective values of 399 MPa and 5.2 GPa.

Conventional PI fibers have diameters in the range from several to hundreds of micrometers; although they have been used for making protective clothes, high-temperature exhaust gas filters, air purification media, and aircraft interior components [20-22], PI fibers with much smaller diameters are in demand especially for the applications involving energy storage/conversion and environment protection [23, 24]. The electrospinning technique provides a straightforward while versatile approach for the convenient preparation of continuous fibers, with typically sub-micrometer diameters (commonly known as electrospun nanofibers) [25-27]; the specific surface areas of electrospun nanofibers are several orders of magnitude larger than those of conventional fibers. In recent years, electrospun PI nanofibers and their applications have attracted growing interests, as evidenced by the increasing numbers of publications related to "polyimide fiber" and "polyimide nanofiber" (Fig. 2). Herein, a comprehensive review and perspective for the development and application of electrospun PI nanofibers is presented.

1.1. Electrospinning

The fiber-processing technique of electrospinning has attracted growing attention since Reneker's group at the University of Akron conducted pioneer studies in the 1990s [28-37]. In the recent two decades, the electrospinning technique has been widely adopted to prepare polymer, ceramic, carbon/graphite, composite, and hierarchically structured fibers with diameters typically ranging from tens of nanometers to several micrometers. Presently, the electrospinning technique and the resulting nanofibers are not only of

ACCEPTED MANUSCRIPT

interest to academia, numerous companies throughout the world have started industrial-scale productions of electrospun nanofibers (and nanofibrous materials) for various applications [38-41]. For example, a company in China is now making electrospun PI nanofibrous mats/nonwovens for the applications of lithium ion battery separators and high temperature filters; and the capacity of one production line has reached ~2,000 m^2 per day (Fig. 3) [42].

1.1.1. Electrospinning process and the resulting nanofibers

As shown in Fig. 4, a simple electrospinning setup/apparatus generally consists of four components: (1) a DC high voltage power supply (with adjustable voltage usually up to 40 kV); (2) a spin dope container (*e.g.*, a syringe on a syringe pump); (3) a spinneret (*e.g.*, a metallic needle on syringe); and (4) a collector (*e.g.*, an electrically grounded rotating device covered with aluminum foil). During electrospinning, a spin dope (*e.g.*, a polymer solution) is placed in a container with spinneret; and a DC high voltage (typically in the range of 5–40 kV) is applied to the spin dope through the spinneret. An electrically grounded collector is placed at a certain distance (usually tens of centimeters) away from the spinneret. When the electrostatic field reaches a critical value, the electric force overcomes the surface tension and the viscoelastic force, and then a jet is ejected and travels straight for a certain distance [43]. Thereafter, the jet starts to bend and form helical loops; and this phenomenon is termed as "bending instability" [36, 37]. The bending instability results in the elongation of an electrospinning jet/filament by thousands of times in a time period of 50 millisecond or shorter, and the solvent evaporation during bending instability is extremely fast [36]; hence, macromolecules in a polymer solution can be oriented during electrospinning, and the orientation can be retained in electrospun nanofibers. Note that electrospun nanofibers are usually collected as overlaid nanofibrous mat/nonwoven on collector.

Although electrospun nanofibers typically have diameters in the range from tens of nanometers to several micrometers, the thinnest electrospun nanofibers with diameters of ~1.6 nm were reported by Huang *et al*. in 2006 [44]. As shown in Fig. 5, electrospun nanofibers can be prepared with different morphological structures such as cylindrical solid nanofibers [45], porous nanofibers [46, 47], hollow nanofibers [48, 49], core-shell nanofibers [50, 51], multi-channel hollow nanofibers [52, 53], ribbon-shaped nanofibers [33, 54], beaded and/or bead-on-string nanofibers [31, 55, 56], and nanofibers with hierarchical structures [57-62]. The large aspect ratio, high specific surface area, and controllable structure of electrospun nanofibers, as well as low density and high porosity of electrospun nanofibrous mats, lead to numerous applications including filtration/separation, energy conversion/storage, environment remediation, and biomedical applications such as tissue engineering [25, 63-68].

ACCEPTED MANUSCRIPT

1.1.2. Alignment of electrospun nanofibers

As a result of bending instability, the traveling path of an electrospinning jet/filament is extremely chaotic; thus electrospun nanofibers are usually collected as almost randomly overlaid mat/nonwoven. Electrospun mats/nonwovens can be directly utilized for some applications (*e.g.*, filtration/separation and wound dressing); however, the unidirectional alignment of electrospun nanofibers is required/crucial for other applications including reinforcement of composites [69-72] and fabrication of microelectronic devices [73-76]. To date, many approaches [77-84] have been explored to acquire well oriented/aligned nanofibers (Fig. 6a) [80]. In 2002, Dersch *et al.* [77] reported that a metal frame could be adopted to collect electrospun PA6 and PLA nanofibers oriented in parallel. As shown in Fig. 6b, Li *et al.* [78] also reported a similar collector (*i.e.*, two parallel stripes made of metals or doped/conductive silicon), and unidirectionally aligned polymeric/ceramic nanofibers could be collected between the two stripes. Additionally, a collector of two parallel rings (Fig. 6c) was reported for obtaining aligned nanofiber yarn [79]. In 2006, an interesting setup for collecting aligned nanofibers was reported by Pan *et al.* [80]; in specific, two metallic needles were respectively applied with positive and negative voltages (Fig. 6d), and those two needles would generate electrospun nanofibers with opposite charges. Upon these two types of electrospun nanofibers met together followed by being collected on a rotating mandrel, a yarn consisting of aligned nanofibers would be obtained. Moreover, well-aligned electrospun nanofibers could also be obtained by electrospinning a polymer solution containing magnetic particles in magnetic field (Fig. 6e) [81]. However, the above methods are restricted by the productivity and/or stability of electrospinning; for example, the method of two parallel electrodes could merely obtain tens to hundreds of unidirectionally aligned nanofibers, while the methods of using oppositely charged spinnerets and magnetic field collector would make the electrospinning process unstable and difficult to control.

For collecting large amount of aligned electrospun nanofibers, a high-speed rotating disc can be used as the collector (Fig. 6f) [82]; and a belt with well-aligned nanofibers can be obtained on the sharp edge of disc collector. In 2004, Katta *et al*. [83] reported a rotating collector consisting of metal wires (Fig. 6g) to make large piece of electrospun nanofibrous mat with high thickness value. To prepare a continuous bundle with aligned electrospun nanofibers, it appears that the collector system containing an electrically grounded water bath and a rotating device might be promising [84, 85] As shown in Fig. 6h, an electrospinning setup with one spinneret can produce ~180 m of aligned nanofiber yarn in an hour [84].

1 Preparation of electrospun polyimide nanofibers

In 1996, Reneker and Chun reported that more than 20 kinds of polymer nanofibers had been successfully prepared *via* the electrospinning technique in their laboratory, and PI was among those polymers [29]; however, they simply indicated that PI nanofibers could be electrospun from its solution with the solvent being phenol, whereas no further

ACCEPTED MANUSCRIPT

information was provided regarding to detailed processing conditions for making electrospun PI nanofibers. In the following 7 years (*i.e.*, from 1997 to 2003), no research activity about electrospun PI nanofibers was reported in literature. This is confusing, since the electrospinning technique was well developed and hundreds of polymers had been electrospun into nanofibers for various applications during those 7 years. Presumably, the reason might be that many PIs are insoluble in common solvents and they are also infusible, leading to the difficulty for being electrospun directly. Starting from 2003, sporadic research endeavors have been gradually reported regarding to the preparations and applications of electrospun PI nanofibers [86-88]. In particular, Hou's group has been very active; and their research activities have included the synthesis of new types of dianhydride and diamine monomers, the preparation of PI nanofibers with high mechanical strength, and various applications of electrospun PI nanofibers [69, 88-102].

As described before, PIs are generally insoluble. Although some polyetherimides (*e.g.*, Ultem® made by GE Plastics) are soluble, the acquired electrospun nanofibers usually have relatively large diameters in micrometers. As a result, electrospun PI nanofibers are typically prepared *via* the two-step method [103]: (1) to electrospin PAA (PI precursor) nanofibers from its solution, and (2) to convert PAA nanofibers into PI nanofibers upon the imidization process. A PAA solution can be made through polymerization of equal molar amount of dianhydride and diamine in protonic organic solvent (*e.g.*, DMF and DMAc) with vigorous mechanical stirring at low temperature (*e.g.*, –15~5 °C) for a time period of 12–72 h [3, 88]. To obtain high molecular weight of PAA and/or to get high viscosity of PAA solution, both dianhydride and diamine have to be purified (*e.g.*, through sublimation), thus the stoichiometric balance can be achieved. Note that diamines are easy to be oxidized by oxygen and dianhydrides are very sensitive to water; therefore, the polymerization has to be carried out in oxygen-free condition (*e.g.*, in N_2) and the solvent has to be desiccated [89, 91]. After electrospinning, the PAA nanofibers are converted into PI nanofibers upon thermal imidization at a temperature in the range of 250–450 °C depending on the molecular structures [88, 89, 93, 104]. The thermal imidization is often carried out in a furnace under constant flow of N_2 or Ar to remove the imidization byproduct of water.

1.2. Electrospun homo-polyimide nanofibers

A homo-PI can be synthesized by polymerization of one dianhydride with equimolar amount of one diamine. Fig. 7 depicts two-step syntheses of two homo-PIs of PMDA-ODA (Fig. 7a) and BPDA-PDA (Fig. 7b). In 2003, Nah *et al.* [86] first reported the two-step method for making electrospun homo-PI nanofibers. In specific, they made a PAA solution (10 wt.%) from pyromellitic dianhydride (PMDA) and 4,4'-oxydianiline (ODA) in N_2 with the solvent of NMP. Subsequently, this PAA solution was used for electrospinning, and the obtained PAA nanofibers were first rinsed with water, then dried at 40 °C for 24 h, and finally imidized with the following procedure: 80 °C for 2 h, 160 °C for 1 h, and 250 °C, 300 °C, 350 °C each for 30 min; and the obtained homo-PI nanofibers had diameters of ~500 nm. In 2006, Zhang *et al.* [105] also prepared

ACCEPTED MANUSCRIPT

electrospun PMDA-ODA PI nanofibers *via* a similar method; however, the diameters of their nanofibers were smaller than 300 nm, and the tensile strength and elongation at break were 19.8 MPa and 4.24%, respectively.

Even though PIs are generally insoluble in common solvents, Kawakami's group synthesized a soluble fluorinated PI of 6FDA-6FAP [106-108], which was made from the monomers of 2,2'-bis(3,4-dicarboxyphenyl) hexafluoropropane dianhydride (6FDA) and 2,2'-bis(4-aminophenyl) hexafluoropropane (6FAP) followed by chemical imidization. The 6FDA-6FAP PI could be dissolved in DMAc, and the resulting solution could be used for electrospinning directly; according to their reported studies, the diameter and morphology of such PI nanofibers could be tailored by using different solvents, adding conductive additives (salts), and adjusting processing parameters [107, 108]. Kawakami *et al.* first prepared the 6FDA-6FAP PI nanofibers with diameters of 416 ± 21 nm [106]; after adding a salt of tetrabutyl ammonium bromide (TBAB) in the solution and controlling the humidity, they prepared bead-free 6FDA-6FAP PI nanofibers with diameters of 33 ± 5 nm [107]. In 2012, they further reported even thinner nanofibers with diameters of 27 ± 5 nm by using hexamethylenediamine (HMDA) as the cross-linking agent [108].

It is well known that the morphology and structure of nanofibers have important impacts on their mechanical properties, and uniform nanofibers usually possess high mechanical strength. Chisca *et al.* [109] and Serbezeanu *et al.* [110] studied the effect of specific viscosity (*i.e.*, polymer concentration in spinning solution) on the morphology of PI nanofibers during electrospinning. Goponenko *et al.* [111] investigated the influence of adding salts on the conglutination of electrospun BPDA-ODA PI nanofibers during thermal imidization. It was revealed that the aging in vacuum before thermal imidization and addition of dodecylethyldimethylammonium chloride (DEDAC) would facilitate the removal of solvent (*e.g.*, DMAc) and reduce the conglutination degree of nanofibers. SEM images acquired from the corresponding electrospun PI nanofibers after different treatments are shown in Fig. 8.

1.3. Electrospun co-polyimide and polyimide copolymer nanofibers

The PIs' molecular structures can be readily adjusted by using different monomers of dianhydride and/or diamine, and there are numerous dianhydride/diamine monomers available for synthesizing PIs [3, 5]. For making homo-PIs, one dianhydride is polymerized with one equimolar diamine. When the types of dianhydride and/or diamine are equal or more than two, the resulting copolymers are termed as co-PIs [112, 113]. Fig. 9 shows a scheme for making BPDA-BPA-ODA co-PI from one dianhydride monomer of 3,3',4,4'-biphenyltetracarboxylic dianhydride (BPDA) and two diamine monomers of *p*-phenylenediamine (BPA) and 4,4'-oxydianiline (ODA) [91]. Similar to homo-PIs, electrospun nanofibers of BPDA-BPA-ODA co-PI can also be prepared *via*

ACCEPTED MANUSCRIPT

the two-step method; *i.e.*, the BPDA-BPA-ODA co-PI nanofibers can be electrospun from co-poly(amide acid) (co-PAA) solution followed by thermal imidization. The BPDA-BPA-ODA co-PI nanofibers possess very high mechanical strength (*i.e.*, tensile strength of 1.1 ± 0.1 GPa and elastic modulus of 6.2 ± 0.7 GPa), since the two different (*i.e.*, rigid-rod-like and flexible) components may result in synergistic enhancement effect [91]. Peciulyte *et al.* [114] reported the preparation of BPDA-PDA-ODA co-PI nanofibers by the two-step method, and the influence of stepwise increase of temperature on the morphology and properties of co-PI nanofibers was investigated. Yao *et al*. also prepared the aligned BPDA-PDA-ODA co-PI nanofibers, which had high mechanical strength and could be used for reinforcement of composites [70, 115].

Polybenzoxazole (PBO) is a rigid-rod type of aromatic polymer with excellent chemical and thermal stabilities. Electrospun PBO nanofibers have been prepared from polyhydroxyamide (PHA) and methoxy-containing polyamide (MeO-PA) [116, 117]. Recently, Hou *et al.* have reported that methoxy-containing polyimide (MeO-PI) and hydroxy-containing polyimide (OH-PI) nanofibers could be partially or completely converted into poly(imide-co-benzoxazole) (PI-co-PBO) [102] and polybenzoxazole (PBO) [118] nanofibers at elevated temperatures, respectively. As shown in Fig. 10a, the preparation of heat-resistant electrospun PBO nanofibers from OH-PI includes three steps: hydroxy-containing polyamic acid (OH-PAA) was first synthesized from 3,3’,4,4’-biphenyltetracarboxylic dianhydride (BPDA) and 3,3’-dihydroxybenzidine (DHB); subsequently, OH-PI nanofibers were obtained by electrospinning of OH-PAA solution followed by thermal imidization at 310–370 °C; thereafter, the OH-PI nanofibers were further treated at 450 °C to be converted into PBO nanofibers through intra-molecular rearrangement. The obtained PBO nanofibers exhibited excellent thermal stability and thermo-mechanical properties; in particular, the 5% decomposition temperature of electrospun PBO nanofibers was as high as 643 °C, and the PBO nanofiber belt had the tensile strength of 537 MPa and the modulus of 8.3 GPa at room temperature; while at a high temperature of 350 °C, the tensile strength and modulus were 490 MPa and 7.1 GPa, indicating that the retention ratios were over 90% and 80%, respectively.

Unlike OH-PI, MeO-PI is only able to be converted into PBO partially; *i.e.*, the copolymer of poly(imide-co-benzoxazole) (PI-co-PBO) can be formed [102]. As shown in Fig. 10b, methoxy-containing polyamic acid (MeO-PAA) is first made from the monomers of BPDA and 4,4’-diamino-3,3’-dimethoxydiphenyl (DMOBPA). Thereafter, the resulting MeO-PAA is converted into methoxy-containing polyimide (MeO-PI) upon thermal imidization at 300–370 °C. Finally, the PI-co-PBO is prepared by further treatment at 400–450 °C. It is necessary to note that MeO-PI is only able to be partially converted into PI-co-PBO, because the complete conversion of MeO-PI into PBO may require much higher energy as compared with OH-PI [102]. Nonetheless, the prepared electrospun PI-co-PBO nanofiber belt still exhibited superior tensile strength (559 MPa),

ACCEPTED MANUSCRIPT

good storage modulus (11.2 GPa), high 5% decomposition temperature (590 °C), and excellent retention (*i.e.*, ≥ 90%) of tensile strength and modulus at 200 °C.

Poly(amide-imide) (PAI) is a copolymer that contains both amide and imide groups in its macromolecular backbone; intriguingly, these two groups have a synergistic enhancement effect on mechanical properties [119, 120]. Lee *et al.* [121] studied two different types of thermoplastic resins to synthesize a co-PAI (Fig. 11a); subsequently, the obtained co-PAI was electrospun into nanofibers followed by glycerol coating and then thermal imidization under tension at an elevated temperature to improve the mechanical properties (Fig. 11b and 11c). Their results indicated that, to apply tension during the thermal imidization at high temperature would substantially improve the mechanical strength of the resulting nanofibers; in specific, the specimen upon the treatment with glycerol and then being thermally imidized at 330 °C under tension exhibited initial modulus and tensile strength of 50.6 and 5.65 GPa, respectively.

1.4. Electrospun blend-polyimide nanofibers

Compared with the synthesis of new PIs from new monomers, the strategy of making PI copolymers seems to be a simple approach to obtain PIs with new structures and properties. However, the sequence of repeating units and the structure of macromolecules acquired through copolymerization are typically random without precise control, thus the properties of the resulting co-PIs are different from time to time. From the practical perspective, it is therefore more convenient and cost-effective to make the blend of PIs (blend-PIs) with tunable properties by mixing existing/available PIs [122-124]. For example, He *et al.* prepared blend-PI (BPDA-BPA/BPDA-ODA) nanofibers from two PAAs [96]. Fig. 12 shows the difference of preparing co-PI nanofibers and blend-PI nanofibers. For the preparation of blend-PI nanofibers, the solutions of BPDA-BPA PAA and BPDA-ODA PAA were synthesized separately followed by blending and/or mechanical stirring; the blend-PAA solution was then electrospun into nanofibers, while the final blend-PI nanofibers were obtained upon thermal imidization. The prepared blend-PI nanofibers consisted of rigid component (BPDA-BPA) and flexible component (BPDA-ODA), and exhibited higher strength and toughness than each individual homo-PI nanofibers. Furthermore, the mechanical properties could be readily tailored by changing the molar ratio of rigid component *versus* flexible component. The discussion about the reinforcement mechanism of blend-PI nanofibers can be found in ***Section 3.1.2***.

1.5. Electrospun polyimide composite nanofibers

The superior thermal stability, high mechanical strength, and good chemical resistance of PIs make them suitable for the preparation of functional electrospun PI composite nanofibers for a wide range of applications (*e.g.*, catalysis, sensor, microelectronics, energy, and others) [125-133]. In general, there are two methods for making electrospun PI composite nanofibers: (1) direct mixing other components (*e.g.*, inorganic particles

ACCEPTED MANUSCRIPT

and their precursors) into PAA solution before electrospinning; and (2) post treatment and/or surface modification of PI nanofibers after electrospinning.

1.5.1. Direct mixing before electrospinning

It is straightforward to make electrospun composite nanofibers by direct dispersing nanoscale fillers in spin dope. To date, many PI composite nanofibers have been prepared by direct addition of nano-fillers into PAA solutions for electrospinning followed by thermal imidization; the nano-fillers include carbon nanotubes (CNTs) [92, 133-139], graphene [139], graphene oxide (GO) [140, 141], meso-phase pitch (MP) [142], as well as the nanoparticles of SiO_2 [143-146], Al_2O_3 [146], $BaTiO_3$ [94, 104, 135], γ-Fe_2O_3 [147], and core-shell Fe-FeO [148]. The obtained electrospun PI composite nanofibers exhibited considerably improved mechanical strength, electric/thermal conductivity, thermal stability, and other properties.

In addition to nanoparticles, some precursors of inorganic materials can also be added into PAA solutions for making electrospun PI composite nanofibers [125, 143, 149]. In 2007, Zhang *et al.* [125] prepared PI/Ag composite nanofibers by addition of AgTFA ((trifluoroacetylacetonoto) silver(I)) complex into PAA (PMDA-ODA) solution for electrospinning, wherein the AgTFA ((trifluoroacetylacetonoto) silver(I)) complex was prepared by dissolving AgAc (silver(I) acetate) in DMF together with TFAH (1,1,1-Trifluoro-2,4-pentanedione). Upon thermal treatment of the obtain PAA/AgTFA nanofibers, the PAA was converted into PI, while Ag nanoparticles were generated inside PI nanofibers (Fig. 13a). The X-ray diffraction results revealed that such Ag nanoparticles had the average size of ~20.2 nm with face-centered-cubic structure. Serbezeanu *et al.* [150] prepared PI/Au composite nanofibers by mixing $HAuCl_4$ salt into a soluble PI for electrospinning followed by thermally treated at 200 °C. The generated gold particles had diameters in the range of 9–22 nm. Cheng *et al.* [143] reported the fabrication of PI/silica hybrid nanofibrous mats/fabrics *via* combination of electrospinning and *in-situ* sol-gel synthesis; in specific, tetraethoxysilane (TEOS) was first added in PAA (PMDA-ODA) solution, which was then electrospun into nanofibers; after a high temperature treatment, the PI nanofibers containing silica nanoparticles (Fig. 13b) were acquired. The decomposition temperature of such PI/silica (6.58 wt.% of SiO_2) nanofibers was 133 °C higher than neat PI nanofibers.

1.5.2. Post treatment after electrospinning

Post treatment and/or surface modification of electrospun PI nanofibers can also lead to hierarchically structured composite nanofibers. Some nanoparticles/nanorods can be decorated onto the surfaces of nanofibers by physical/chemical interactions (*e.g.*, hydrogen bonding, electrostatic force, and other interactions among functional groups) [151].

ACCEPTED MANUSCRIPT

The dianhydride component in imide ring can be opened in alkaline aqueous solution, during which the hydrolysis occurs and carboxyl groups are generated on the surface of PI fibers; note that carboxyl groups would facilitate the ion-exchange reaction. For example, Carlberg *et al.* [152] immersed PI (BTDA-AAPTMI) nanofibers in KOH aqueous solution, due to hydrolysis of imide ring, a thin layer of potassium polyamate was generated on the surface of nanofibers; subsequently, the nanofiber mat was immersed in $AgNO_3$ aqueous solution, and Ag^+ ions were introduced to the surface-modified layer through ion exchange with K^+ ions. Finally, the Ag^+ ions were reduced into Ag nanoparticles and coated on nanofibers by two routes: (1) thermal reduction and (2) chemical reduction (Fig. 14). For thermal reduction, the sample was heated at 350 °C for 40 min, during which Ag^+ ions were reduced to Ag nanoparticles; while the broken imide rings were simultaneously re-formed. The resulting Ag nanoparticles with the average diameter of ~5.2 nm were uniformly distributed in the surface layers of re-imidized nanofibers, while the core parts of electrospun PI nanofibers were not distinguishably affected. For chemical reduction, the sample was immersed in dimethylamine borane (DMAB) for reduction; different to thermal reduction, the Ag nanoparticles were coated/attached on the surface of nanofibers, leading to PI-PAA-Ag core-shell composite nanofibers.

Nevertheless, to use KOH solution for hydrolysis of imide structure is difficult to control the thickness of surface layer; and it may considerably deteriorate the properties (especially the mechanical properties) of electrospun PI nanofibers. On the other hand, the PAA precursor also contains carboxyl group and thus can be used directly for ion exchange. Han *et al.* [153] reported the direct use of PAA nanofibers for ion exchange to prepare PI/Ag composite nanofibers. Electrospun PAA (PMDA-ODA) nanofibers were first immersed in 0.01 M $[Ag(NH_3)_2]^+$ aqueous solution for a short time period (*i.e.*, 10–20 s) to complete the ion exchange. Thereafter, the thermal imidization of PAA and reduction of Ag^+ could occur simultaneously upon a one-step heat treatment. Ding *et al.* [154] also prepared PI/ZnO composite nanofibers by a similar process. In specific, the PAA (PMDA-ODA) nanofibers were first immersed into $ZnCl_2$ solution, and Zn^{2+} ions would then attach onto the nanofiber surface through the ion-exchange process; and ZnO nanoparticles were finally generated during one-step thermal imidization of PAA. The obtained PI/ZnO composite nanofibrous membrane had excellent photocatalytic performance towards degradation of organic dyes in water. Li *et al*. [155] prepared PI/Fe_2O_3 composite nanofibers by immersing PAA (PMDA-ODA) nanofibers in $FeCl_3$ solution for 2 h followed by the thermal treatment at 300 °C. The obtained PI/Fe_2O_3 composite nanofibers could be further converted to PI/Fe_3O_4 composite nanofibers upon hydrogen reduction at 300 °C, and the resulting PI/Fe_3O_4 nanofibers exhibited the magnetic response capability.

More intriguingly, Chang [156] produced firecracker-shaped PI/ZnO nanofibers *via* combination of electrospinning and hydrothermal treatment. As shown in Fig. 15, the ZnO seeds (Fig. 15c) are generated on PI nanofibers (Fig. 15b) by using a dip-coating technique; ZnO nanorods are then grown on the nanofiber surface through a

ACCEPTED MANUSCRIPT

hydrothermal process (at 90 °C for 6 h). The firecracker-shaped PI/ZnO hybrid nanofibers (Fig. 15d) had very high photocatalytic performance. Later, they also prepared core-shell PI/Cu-BTC hierarchical nanofibers through the similar method of combining electrospinning and hydrothermal treatment, wherein the Cu-BTC was a well-studied metal organic frameworks (MOFs) [157]. In specific, the PI/Cu-BTC nanofibers were prepared by the following four steps: (1) electrospinning of PAA (PMDA-ODA) nanofibers, (2) immobilization of Cu–BTC seeds onto PAA nanofibers by repeatedly (*i.e.*, 16 cycles) immersing PAA nanofibers into a $Cu(CH_3COO)_2 \cdot H_2O$ ethanol solution for 30 min and a BTC ethanol solution for 60 min, (3) thermal imidization of the PAA/Cu–BTC seeds nanofiber, and (4) hydrothermal growth of Cu–BTC. The prepared hierarchical nanofibers showed excellent performance of separating CO_2 from CO_2/N_2 mixtures, and they also exhibited high adsorption capability of methylene blue from its aqueous solutions.

Polyaniline (PANi) nanoparticles/nanowires decorated on carbon nanofibers or other conductive substrates possess good electrochemical properties and can be used as electrode materials for energy storage/conversion devices (*e.g.*, supercapacitors) [59, 62]. Electrospun PI nanofibers surface-decorated with PANi have been reported recently [158, 159]. Since the PI nanofibers are mostly hydrophobic, Chen *et al*. [158] first treated the PI (PMDA-ODA) nanofibers with H_2SO_4/H_2O_2 (3/1 by v/v) solution to improve the hydrophilicity; the PANi nanoparticles were then deposited on the surface of PI nanofibers by *in situ* polymerization of aniline in an ice-water medium. The prepared PI/PANi composite nanofibers had improved electrical conductivity, *p*H sensitivity, and electromagnetic impedance; hence, it would be a promising material for the applications related to electronics (*e.g.*, sensor). Ye *et al*. [159] improved the hydrophilicity of electrospun PI (HQDPA-BPA-ODA) nanofibers through the treatment with 1 wt.% sodium dodecyl-benzenesulfonate aqueous solution; as a result, rod-like PANi nanoparticles were covered on the nanofibers after *in situ* polymerization of aniline in an ice-water medium. The hierarchical PI/PANi composite nanofibers were studied for the application of high performance lithium-ion battery separator.

In 2009, Chang *et al.* [160] reported an interesting method for the preparation of PI nanofibers grafted with PMMA (PI-g-PMMA) *via* the combination of electrospinning and "click chemistry". The PI (PMDA-ODA) nanofibers were first prepared by electrospinning PAA solution followed by thermal imidization; the PI nanofibers were then treated with typical chloromethylation to prepare the chloromethylated PI nanofibers (PI-Cl), which subsequently reacted with an excess amount of NaN_3 at room temperature in DMF to yield azide-decorated polyimide (PI-N_3) nanofibers. Finally, alkyne-terminated PMMA chains made by atom transfer radical polymerization (ATRP) were surface-grafted onto the azide-decorated PI nanofibers through the click coupling reaction. This study provided a versatile approach for surface-decoration of electrospun PI nanofibers with various polymers.

ACCEPTED MANUSCRIPT

3. *Properties of electrospun polyimide nanofibers*

3.1. *Mechanical properties*

Fibers with high mechanical properties (*e.g.*, strength and modulus) are crucial for making structural composites [161-165]. Conventional high-performance fibers include carbon, Kevlar®, Nomex®, polybenzimidazole (PBI), PBO (Zylon®), aromatic PI, poly(hydroquinone-diimidazopyridine) (M-5), and ultra-high molecular weight polyethylene (UHMWPE) fibers [103, 166, 167]. For example, the tensile strength value of conventional PI fibers after the stretching process can reach 2.6–3.2 GPa [19, 168, 169].

In general, the mechanical strength of fibers increases with decrease of diameters. Electrospun nanofibers are orders of magnitude thinner than conventional fibers, thus they could possess extremely high mechanical strength [163, 165, 170-172]. However, the reported mechanical strength values of electrospun nanofibers are substantially lower than those of their conventional counterparts [89, 105, 163, 173]; and the reasons include: (1) there are numerous structural imperfections within electrospun nanofibers [170], and (2) macromolecular chains in nanofibers are not well aligned along the fiber axes [90, 171]. Note that the macromolecular chains are expected to be highly oriented during electrospinning (particularly during bending instability); however, the oriented chains would undergo the relaxation, especially if electrospun filaments/nanofibers still contain relatively large amounts of solvent.

Recently, ultrafine nanofibers with high strength and modulus have been prepared by electrospinning [88, 93, 96, 99, 115, 163, 166, 174]. Hou *et al*. reported that their electrospun PI nanofibers had the tensile strength of 0.66–1.3 GPa and the elastic modulus of 6.2–15.3 GPa [88, 91, 96, 99]. The high tensile strength and elastic modulus could be attributed to the rigid rod-like molecular chains of PIs, the enhanced macromolecular orientation within the nanofibers, and the high crystallinity of aligned nanofibers [172].

3.1.1. *Mechanical properties of individual electrospun PI nanofibers*

In previously reported studies, the mechanical properties of electrospun nanofibers were usually measured from nanofiber mats/yarns with hundreds/thousands of individual nanofibers. It is well known that the mechanical properties acquired from tensile test of nanofiber mat/yarn are substantially affected by fiber diameters (*i.e.*, size effect) and their distribution, alignment of fibers, and fiber conglutination/entanglement [90]. To accurately measure the mechanical properties of nanofibers, individual nanofibers have to be tested. To date, several testing methods have been developed to measure the mechanical properties of individual nanofibers, and the typical ones include the AFM-based three-point bending test [175-180] and the nano-indentation test [181, 182]. Nevertheless, both testing methods are specifically designed to measure the values of modulus and hardness, while the strength value is acquired indirectly through calculation.

ACCEPTED MANUSCRIPT

In 2008, Hou's group developed a micro-tension tester (Fig. 16a) to directly measure the ultimate tensile strength and strain of individual nanofibers, and they first reported the mechanical properties of individual BPDA-PDA PI nanofibers [90]. In specific, the testing nanofibers were first collected by swinging a stainless steel frame through the gap between spinneret and collector; after thermal imidization, an individual nanofiber was taken from the frame and then placed onto a paper frame (Fig. 16c) by using electrically conductive adhesive tape and super glue. The micro-tension tester (Fig. 16a) consisted of a micro-load sensor, a high-magnification optical microscope, a digital camera, the software for data acquisition and processing, and a computerized control system. The acquired values of tensile strength, elastic modulus, and ultimate strain of individual PAA nanofibers (with diameters of ~300 nm) were 766 ± 41 MPa, 13 ± 0.39 GPa, and ~43%, respectively; upon imidization at 430 °C, the resulting individual PI nanofibers exhibited the respective values at 1.7 ± 0.12 GPa, 76 ± 12.6 GPa, and ~40%. The typical stress-strain curves of individual electrospun PAA and PI nanofibers are shown in Figs. 17a and 17b, respectively. WAXD results indicated that the excellent mechanical properties of individual PI nanofibers could be attributed to high alignment degree of macromolecular chains along nanofiber axes (Fig. 17c). Due to rigid rod-like chains of BPDA-PDA PI macromolecules, the tensile failure showed a brittle fracture and there was no identifiable necking near the fractured surfaces (Fig. 17d**)**. Later, Hou's group synthesized a co-polyimide (BPDA-BPA-ODA) consisting of both rigid and flexible segments in its macromolecules; and the ultimate tensile strength of aligned nanofiber belt was ~1.1 GPa [91]. Moreover, they also measured the mechanical properties of such individual nanofibers, and the acquired values of tensile strength, elastic modulus, and strain at break were 1666 ± 450 MPa, 37.01 ± 10.4 GPa, and 7.5 ± 1.7%, respectively [69]. Recently, they have investigated the mechanical properties of another co-PI (BPDA-PRM-ODA) synthesized from a pyrimidine-containing diamine monomer of 2,5-bis(4-aminophenyl)pyrimidine (PRM) [99]. When the molar ratio of PRM/ODA was 5/5, the individual BPDA-PRM-ODA co-PAA nanofibers (with diameters of 500–600 nm) exhibited the highest tensile strength of 568 MPa; upon imidization at 330 °C, the resulting individual co-PI nanofibers showed the tensile strength of 1.77 GPa and modulus of 59 GPa.

3.1.2. Mechanical properties of aligned PI nanofiber belts (high-strength PI nanofibers)

As described in ***Section 1.2.2***, there are several methods to prepare well aligned (*i.e.*, highly oriented) nanofibers. The tensile strength of aligned/oriented nanofiber belts is much higher than that of randomly overlaid nanofiber mats. The mechanical properties of aligned/oriented nanofiber belts are anisotropic, and the tensile strength along the fiber direction is orders of magnitude higher than the strength along the perpendicular direction. Many electrospun PI nanofibers with high mechanical properties have been reported by Hou's group; as summarized in Table 1, those well-aligned PI nanofibers possessed excellent tensile strength, high modulus and toughness, as well as good thermal stability.

ACCEPTED MANUSCRIPT

In 2006, Huang *et al.* prepared high-strength electrospun BPDA-PDA PI (Fig. 18a) nanofiber mats/belts by electrospinning a PAA solution with inherent viscosity of 5.17 dL/g (*i.e.*, the PAA molecular weight was relatively high) followed by imidization treatment [88]. The alignment degree of the obtained PI nanofiber belts was ~80%, and the fiber diameters were in the range from 50 to 300 nm with the average diameter of ~180 nm. The tensile strength and elastic modulus of those PI nanofiber mats/belts (after thermal imidization at 430 °C) reached 663.7 MPa and 15.3 GPa, respectively. This report demonstrated for the first time that electrospun polymer nanofiber mats/belts could possess high values of tensile strength and modulus.

The high strength of electrospun PI nanofiber mats/belts is partially attributed to the alignment of nanofibers and high molecular weight of PAA precursor [89]; additionally, the high strength is also resulted from the rigid-rod-like structure of BPDA-PDA macromolecule and its orientation along the nanofiber axis [88]. Compared to the nanofibers thermally imidized at 430 °C, the BPDA-PDA PI nanofibers imidized at 300 °C had lower tensile strength and modulus of 367.3 MPa and 9.1 GPa, respectively. However, according to the IR spectra (Fig. 18b), both samples were completely converted into PI. The large difference on tensile strength could be explained as follows: the rigid-rod-like chains of BPDA-PDA PI macromolecules would be rearranged/oriented along the fiber axes at 430 °C (but not at 300 °C, which was lower than the T_g of this PI), leading to the improved tensile strength. Fig. 18a illustrates the different chain orientations of PI macromolecules in electrospun nanofibers, and such chain orientations could be verified by XRD spectra (Fig. 18c). Because the macromolecules were aligned along the nanofiber axes, the (200) peak of orthorhombic BPDA-PDA PI almost disappeared in the aligned nanofibers; additionally, the (210) peak was weakened, and the (110) peak was strengthened [88]. Note that the high strength of individual BPDA-PDA nanofibers was described/discussed in previous section.

Although the BPDA-PDA PI nanofibers exhibited very high tensile strength, the nanofibers with rigid-rod-like chains of BPDA-PDA macromolecules had low elongation at break (*i.e.*, <5%); in other words, the nanofibrous material was brittle with low toughness and impact resistance. In 2009, Hou *et al.* synthesized a high strength and high toughness PI (BPDA-6FBAPP, 6F-PI) from the monomers of BPDA and 2,2-bis[4-(4-aminophenoxy) phenyl]-hexafluoro-propane (6FBAPP) [93]. Note that 6FBAPP is a diamine with flexible ether bond, thus the macromolecular flexibility of the resulting PI can be improved. The 6F-PI nanofibers exhibited a large elongation at break of >200%, a tensile strength of 308 ± 14 MPa, an elastic modulus of 2.08 ± 0.25 GPa; and the large elongation and relatively high tensile strength further resulted in excellent toughness of 365 ± 20 MPa.

Neither the nanofibers of rigid-rod-like BPDA-PDA PI nor the nanofibers of flexible 6F-PI could possess high tensile strength and strain simultaneously. To improve the tensile

ACCEPTED MANUSCRIPT

strength, elongation at break, and toughness concurrently, Hou's group introduced the flexible groups/bonds into rigid molecular chains. For example, they prepared a series of co-PIs (BPDA-BPA-ODA) contains different ratios of rigid BPA and flexible ODA components [91]. As expected, the elongation at break of co-PI nanofibers were increased with the addition of flexible components in the macromolecular chain of PI. The elongation at break value of BPDA-BPA nanofibers was ~3.9%, while the value increased to 22.2% when half amount of flexible (BDPA-ODA) component was introduced; upon the amount of BDPA-ODA component was further increased to 90%, the corresponding value of elongation at break reached 44.5%. Besides the improvement of elongation at break, it was intriguing that the tensile strength value of co-PI nanofiber belts was higher than the values of both homo-PI nanofiber belts of rigid (BPDA-BPA) and flexible (BPDA-ODA). The highest tensile strength of aligned co-PI nanofiber belts was 1.1 ± 0.1 GPa, when the BPA/ODA ratio was 4/6; and the corresponding elastic modulus and elongation at break were 6.2 ± 0.7 GPa and ~21%, respectively. Fig. 19 depicts the typical stress-strain curves of the co-PI nanofiber belts (Fig. 19a) and relationships between mechanical properties (*i.e.*, tensile strength, elastic modulus, and strain) *versus* BPA amount in co-PI (Fig. 19b). As shown in Fig. 20, a high-strength co-PI nanofiber belt (with width of 7.5 mm and thickness of 12 μm) could hang 10 kg load.

Similar to BPDA-PDA PI, the homo-PI of BPDA-BPA also has a rigid-rod-like macromolecular structure; whereas the homo-PI of BPDA-ODA is more flexible. The BPDA-ODA PI nanofiber belt merely exhibited the tensile strength of ~459 MPa, tensile modulus of ~2.1 GPa, and elongation at break of ~41.3% [91]. The improvement on tensile strength of electrospun BPDA-BPA-ODA co-PI nanofiber belt was primarily due to the uniform distribution of rigid and flexible regions in the co-PI nanofibers at super-molecular level (Fig. 21). Such a super-molecular structure is a mesomorphic structure, in which the co-PI macromolecules can readily occupy several micro-blocks. The smooth transition among different blocks is resulted from the identical chemical nature of these micro-blocks and their similar transverse dimensions. This type of super-molecular structure with smooth transition among different micro-blocks further leads to the effective load transfer from one micro-block to another throughout the entire fiber. Therefore, a local concentration of load, which is one of the main factors causing the fibers to break, is much less likely to occur when the fiber sample is under tension. In consequence, the BPDA-BPA-ODA co-PI nanofibers exhibit excellent mechanical properties.

In 2015, Yao *et al.* [115] also reported the preparation of high-strength co-PI nanofibers of BPDA-PDA-ODA under the guidance of the principle of introducing flexible component PI into rigid PI; in specific, the BPDA-PDA was the rigid component while the BPDA-ODA was the flexible component. With the molar ratio of PDA/ODA being 1/1, the prepared co-PI nanofiber belt exhibited high strength and modulus of 1040 MPa and 10 GPa, respectively; while the respective elongation at break and toughness were

ACCEPTED MANUSCRIPT

13.5% and 77 MPa. Hou's group [99] investigated another co-PI (BPDA-PRM-ODA) nanofibers with the rigid component being BPDA-PRM. The mechanical properties of this co-PI showed the similar enhancement behavior to the BPDA-BPA-ODA co-PI nanofiber belt; *i.e.*, the tensile strength value of the BPDA-PRM-ODA co-PI nanofiber belt was higher than the values of both homo-PI nanofiber belts of rigid (BPDA-PRM) and flexible (BPDA-ODA). When the PRM/ODA molar ratio was 1/1, the resulting co-PI nanofiber belt had the highest tensile strength of 1161 MPa, and the corresponding modulus and elongation at break was 6.3 GPa and 21%, respectively.

As described in ***Section 2.3***, it is facile and straightforward to prepare blend-PIs by directly mixing existing/available PAAs. Recently, Hou's group has also investigated the mechanical properties of blend-PI nanofibers [96]. It was observed that the mechanical properties of some blend-PI nanofiber belts were even higher than those of the co-PI nanofiber belts. Upon blending rigid-rod-like BPDA-BPA PAA and flexible BPDA-ODA PAA at the molar ratio of 4/6, the resulting aligned blend-PI (BPDA-BPA/BPDA-ODA) nanofiber belt exhibited excellent tensile strength of 1299.43 MPa, approximately 200 MPa higher than that of the corresponding co-PI; and the elongation at break, elastic modulus, and toughness of blend-PI (BPDA-BPA/BPDA-ODA) nanofiber belts reached 15.8%, 7.68 GPa, and 81.79 J/g, respectively. The following were the proposed explanations: during blending of two PAAs, there could be re-equilibration and recombination of different molecular fragments, which might result in the formation of block co-PAA structure that would be converted into co-PI; additionally, there could be molecular alignment of rigid molecules (BPDA-BPA) along the nanofiber axis during electrospinning. Hence, there might be micro-block structures, as well as inter-lamellar and inter-fibrillar segregations of BPDA-BPA PI in the blend-PI nanofibers (Fig. 22). Such structures were expected to be uniformly distributed along the nanofibers, leading to the strong intermolecular interaction, *i.e.*, a state of aggregation of the polymer chains *via* charge-transfer complex formation. Therefore, the blend-PI nanofibers showed the abnormally high strength and toughness.

In summary, mechanical properties of PI nanofibers may be significantly affected by macromolecular structures. Rigid chains would contribute to high tensile strength and modulus but low elongation, while flexible chains would contribute to high elongation at break but low tensile strength. The electrospinning process can result in macromolecular chains oriented along nanofiber axes, and high temperature can improve the orientation of rigid macromolecular chains *via* rearrangement; note that oriented macromolecules would generally lead to high mechanical properties. Therefore, electrospun PI nanofibers with desired strength, modulus, strain, and toughness can be prepared by selecting the monomers with appropriate molecular flexibility, controlling the ratio of rigid and flexible components/moieties, and adopting the effective blending strategy.

It is known that the additions of carbon nanotubes and graphene can considerably improve mechanical properties of the resulting composite nanofibers. For example, Chen *et al.* [92] prepared PI (ODPA-ODA) composite nanofibers containing varied amounts of

ACCEPTED MANUSCRIPT

multi-wall carbon nanotubes (MWNTs). In their reported study, MWNTs were first treated/activated with concentrated HNO_3, PAA/MWNTs solutions were then prepared by *in-situ* polymerization; subsequently, the solutions were used for electrospinning followed by thermal imidization. It was observed that the MWNTs were highly aligned along the nanofibers due to the large shearing force during the electrospinning process and nanoscale confinement effect [183]. The highest tensile strength of 239.7 MPa was acquired when the amount of MWNTs in the PI/MWNTs composite nanofibers was at 3.5 wt.%; for comparison, the tensile strength of neat PI nanofibers was merely 128.2 MPa. The above PI/MWNTs composite nanofibers had the yield strength, elastic modulus, and elongation at break of 200.9 MPa, 2.56 GPa, and 90.5%, respectively. Furthermore, the thermal stability was also improved upon the addition of MWNTs, the 5% weight-loss temperature of the PI composite nanofibers with 3.5 wt.% of MWNTs was ~20 °C higher than that of the neat PI nanofibers.

3.1.3. Thermo-mechanical properties

PIs are high-performance polymers with excellent mechanical properties and thermal stabilities. For the practical applications in high-temperature environment, it is essential to study the ultimate mechanical properties of PIs at high temperature. Recently, Jiang *et al.* have investigated the thermo-mechanical properties of electrospun aligned PI (BPDA-BPA) nanofibers as well as PAA-derived PI-co-PBO and PBO nanofibers [100, 102, 118]; the mechanical properties at high temperature are summarized in Table 2. It is evident that the temperature of thermal imidization has important impact on the mechanical properties of PI nanofibers. The aligned BPDA-BPA PI nanofibers, which were thermally imidized at 370 and 450 °C, had the respective tensile strength values of 421 and 641 MPa at the room temperature. At the testing temperature of 250 °C, the aligned BPDA-BPA PI nanofibers (imidized at 450 °C) exhibited a high strength of 603 MPa; when the testing temperature was 300 °C, these nanofibers still had the strength of 510 MPa (80% retention) and the modulus of 12.41 GPa (95% retention). Even at 400 °C, the strength and modulus still remained at 330 MPa (52% retention) and 9.38 GPa (72% retention) [100]. As shown in Table 2, the MeO-PAA-derived PI-co-PBO nanofibers [102] and OH-PAA-derived PBO nanofibers [118] also possessed high thermo-mechanical properties.

3.2. Thermal stability

In general, PIs possess excellent thermal stability due to heterocyclic imide rings and aromatic benzene rings in their macromolecular backbones. As shown in Table 1, the glass transition temperature (T_g) and 5% decomposition temperature (T_d) of many PI nanofibers are higher than 250 °C and 450 °C, respectively. For example, the rigid-rod-like BPDA-PDA PI nanofibers have the T_g value of 310.2 °C and 5% weight loss temperature ($T_{5\%}$) of 508.8 °C; while the flexible BPDA-ODA PI nanofibers have the T_g and $T_{5\%}$ values of 275.7 and 463.9 °C, respectively. By studying the thermal properties of co-PI nanofibers, Chen *et al.* [91] revealed that the T_g and T_d values had a dependence on

ACCEPTED MANUSCRIPT

the ratio of rigid and flexible moieties/components in their macromolecular chains; and more rigid moieties/components would generally lead to higher T_g and T_d.

4. Applications

4.1. Reinforcement of composites

Some electrospun nanofibers with small diameters and the concomitant large specific surface areas possess high mechanical properties, good stability/resistance against heat and chemicals, and other advantageous properties, making them suitable for the reinforcement of composites [161, 162] including high-performance composites [69, 71, 72, 184-194] and self-healing composites [195-198]. In 2012, Chen *et al.* [69] prepared two types of high-strength co-PI (BPDA-BPA-ODA) nanofibers (*i.e.*, the randomly overlaid nanofibers and the highly aligned nanofibers); both types of co-PI nanofibers were studied for the reinforcement of PA6 polymer/matrix, and the composites were fabricated by using the technique of polymer melt infiltration lamination (PMIL). The tensile strength and elastic modulus of PI/PA6 nanocomposites increased with the increase of weight ratio of PI nanofibers. When the loading amount/content of PI nanofibers was 50 wt.%, the composites reinforced with aligned nanofibers exhibited the tensile strength of 447 MPa and the elastic modulus of 3.0 GPa (along the longitudinal direction), representing the respective improvements of ~700% and ~500% over neat PA6; whereas the composites reinforced with randomly overlaid nanofibers had the tensile strength and elastic modulus of 206 MPa and 1.09 GPa, and both values were ~270% higher than those of neat PA6.

Chen *et al.* [72] prepared PI self-reinforced nanocomposites (*i.e.*, PI polymer/matrix reinforced with electrospun PI nanofibers). In specific, they first made aligned electrospun PI nanofibers containing CNTs; subsequently, these nanofibers were immersed into a PAA solution. Upon evaporation of solvent followed by thermal imidization, the nanofiber self-reinforced nanocomposite was prepared. Note that different CNTs/PI composite nanofibers with varied amounts of CNTs were studied for the reinforcement. The results indicated that the PI composite nanofibers with 2 wt.% CNTs had the best reinforcement performance, and the resulting PI composite exhibited the tensile strength of 210.4 MPa and elastic modulus of 1.26 GPa, which were respectively improved by 138% and 104% than the values of neat PI. Furthermore, the composite also exhibited an 80.8% improvement of elongation at break as compared to the neat PI.

In another research, PI self-reinforced composites were fabricated by using shortened electrospun PI nanofibers as the reinforcement agent [187]. The shortened electrospun PI (PMDA-ODA) nanofibers were made by cutting electrospun PI nanofibers in liquid nitrogen with blades rotating at fast speed. Aspect ratios of the acquired shortened nanofibers were in the range of 100–200; *i.e.*, these nanofibers had the lengths of ~50–500 μm and the diameters of ~200–500 nm. The shortened PI nanofibers were then dispersed in PAA (PMDA-ODA) solution followed by being cast into films; thereafter, the films were thermally imidized at high temperature. Their results indicated that small

ACCEPTED MANUSCRIPT

amounts of shortened PI nanofibers could significantly improve mechanical properties of the resulting PI films. For example, with incorporation of 2 wt.% shortened PI nanofibers into a PI film, the tensile strength and elastic modulus were improved by 53% and 78%, respectively.

4.2. Lithium ion battery separators

Lithium ion batteries (LIBs) possess the attractive properties of high energy density, high power density, long service life, and environmental friendliness, thus they have been widely used in consumer electronics (*e.g.*, mobile phones, laptop computers, and digital cameras); and it is also promising that LIBs might be used in electric vehicles [199-201]. In a LIB device, the separator between positive and negative electrodes is an important component; it functions to prevent the electrical short circuit while to allow the electrolyte/ions to penetrate [202, 203]. The conventional LIB separators are micro-porous films of polyolefins such as polyethylene (PE), polypropylene (PP), and their composite (*e.g.*, PP/PE/PP); however, these separators have some problems/limitations such as low porosity, poor thermal stability, poor wettability, and high cell resistance, which considerably deteriorate the electrochemical performance of LIBs. Electrospun PI nanofiber mats/membranes with excellent mechanical properties, high porosity, good wettability, and superior thermal stability could be an innovative type of LIB separators [204, 205].

Miao *et al.* first studied electrospun PI (PMDA-ODA) nanofiber nonwovens/mats as LIB separators [95]. These separators showed the high degradation temperature of ~500 °C, which was over 200 °C higher than that of conventional Celgard membrane. As shown in Fig. 23a, PI nanofiber based separators had neither color change nor thermal shrinkage after the treatment at 150 °C. Furthermore, because the polarity/hydrophobicity of PI was similar to that of liquid electrolyte, the PI nanofiber mats/membranes exhibited excellent electrolyte wettability; and such a situation would greatly facilitate the high uptake of electrolyte. Electrochemical tests indicated that the PI nanofiber separators had higher initial discharge capacity (160 mAh/g at 0.2 C rate), lower resistance, and higher rate capability than the Celgard separator. As shown in Fig. 23b, the capacity retention ratio of PI nanofiber separators was higher than that of the Celgard separator at the discharge rate from 0.2 to 10 C, and the nanofiber separators also had the capacity retention of almost 100% after 100 cycles under 0.2 C. The superior performance in broad current range and long cycle stability make PI nanofiber separators suitable/ideal for high-rate LIBs. Cao *et al*. [206] further studied the feasibility of PI (PMDA-ODA) nanofiber separators for commercial application *(i.e.*, high power LIBs), in which the electrochemical performances of LIBs with PI nanofiber separators were evaluated under industrial operation conditions. In their studies, the rate capacity of a LIB device was examined at a wide rate range of 0.5–28.8 C; and the storage performance was examined at room temperature for 28 days and at 60 °C for 7 days. The results indicated that the capacity retention ratio was 69.28% at the high discharge rate up to 16 C; and the device could still work at a super-high discharge rate of 28.8 C with capacity retention ratio of 33.6%, whereas the LIB device with conventional PE separator could not work at the

ACCEPTED MANUSCRIPT

discharge rate higher than 16 C. The capacity retention ratio of the battery was 85.35% after being stored at room temperature for 28 days and was 71.22% after being stored at 60 °C for 7 days. The PI nanofiber separator also exhibited the capacity retention of 99.66% after 320 cycles at 5 C rate. Moreover, a comparison study between PI nanofiber and conventional PE separators was carried out by Kim *et al.* [207], and the results also showed that the LIB with PI nanofiber separator had higher performance than the LIB with PE separator. In addition, Jiang *et al.* [208] also prepared electrospun PI (PMDA-ODA) nanofiber mats/membranes and mechanically pressed them to reduce their (apparent/equivalent) pore sizes. The post-treated PI nanofiber mats/membranes were tested as LIB separators at high temperature. Their results showed that the capacity retention ratio of PI nanofiber separators could be retained at 86% after 50 cycles at 120 °C. Note that the conventional polyolefin membrane separators would undergo substantial thermal shrinkages upon being charged to 4.0 V even during the first cycle.

In another reported research [129], PI/PET layered composite separators were prepared by using PET nonwovens as support to collect electrospun PI nanofibers. As shown in Fig. 24a, diameters of the supporting PET fibers and the collected PI nanofibers were approximately 10 μm and 200 nm, respectively. The highly porous PI nanofiber layers/mats in the composite separators would be advantageous for the uptake of electrolyte; even though the porosity, electrolyte uptake, and ionic conductivity of composite separators were lower than those of neat PI nanofiber separators, the tensile strength of these composite separators was ~400% higher than that of neat PI nanofiber separators. Moreover, the PI/PET layered composite separators had merely ~2% of thermal shrinkage at 180 °C in air; while the charge-discharge testing results indicated that discharge capacities of composite separators were at ~88.3% of initial discharge capacities under a high current rate of 10 C, and the capacity retention ratio was 87.5% after 50 cycles.

In 2014, a sandwiched Al_2O_3-coated PI nanofiber mat was reported as LIB separator [209]. This separator was prepared by dip-coating thin layers of Al_2O_3 nanoparticles on both sides of electrospun PI nanofiber mat (Fig. 24b). Compared to neat PI nanofiber separators, the Al_2O_3-coated PI nanofiber separators exhibited the enhanced capacity, rate capability (78.91% at 10 C), and cyclability (95.53% retention after 200 cycles at 1 C). In 2015, Liang *et al*. [210] also reported the preparation of Al_2O_3/SiO_2-PI composite nanofiber mat by dip-coating Al_2O_3 and SiO_2 nanoparticles on both sides of electrospun PI nanofiber mat. In addition, Shayapat *et al*. [146] prepared PI-Al_2O_3 and PI-SiO_2 composite nanofiber mats for LIB separator by directly adding Al_2O_3 or SiO_2 nanoparticles in PAA solution for electrospinning followed by thermal imidization. In summary, the above PI composite nanofiber separators containing inorganic nanoparticles showed the improved electrolyte uptake capability and ionic conductivity, because the incorporation of hydrophilic Al_2O_3 and SiO_2 would improve the wettability of nanofiber mat and facilitate the electrolyte absorption.

ACCEPTED MANUSCRIPT

Research endeavors have also been devoted to make electrospun PI composite nanofibers with other polymers such as PVdF-HFP. In 2012, Liu *et al*. [211] prepared the core-sheath PI@PVdF-HFP composite nanofiber mats/membranes *via* the coaxial electrospinning method; note that the PI as core material could provide the superior thermal and mechanical properties, while the PVDF-HFP as sheath material could improve the ion conductivity. Chen *et al.* [212] also prepared PVdF-HFP/PI composite nanofiber mats/membranes *via* the cross-electrospinning method (*i.e.*, the electrospinning setup contained four needles/spinnerets, two of which were for spinning the PVdF-HFP solution while the other two were for spinning the PI solution). The obtained composite nanofiber mat/membrane was further treated by using the thermal calendaring process, which would result in the fusion of PVdF-HFP nanofibers thus improve the tensile strength of composite mat/membrane. Compared to the Celgard 2400 separator, the PVdF-HFP/PI composite nanofiber separator had higher mechanical properties and safety; and the ionic conductivity of PVdF-HFP/PI composite nanofiber separator (1.46×10^{-3} S/cm) was also better than that of Celgard 2400 separator (0.4×10^{-3} S/cm). In addition, they prepared TiO_2@PI/PVdF-HFP composite nanofibers by addition of TiO_2 nanoparticles in the PI spin dope [213]. The incorporation of TiO_2 nanoparticles not only improved the physical property of electrospun mats/membranes including porosity, liquid electrolyte uptake, wettability, mechanical property, and thermal dimensional stability, but also provided superior ionic conductivity and electrochemical stability as well as excellent electrochemical cycling performance.

The good thermal stability and low dimensional shrinkage at high temperature are important for a LIB separator; meantime, the shutdown behavior is also essential since electric shorting could happen in occasional accidents. The short circuit usually causes the thermal runaway of a LIB device, and it might eventually lead to fire/explosion. Hence, a shutdown separator would play a crucial role of separating the electrodes and/or stopping the electrochemical reactions. In the conventional Celgard (PP/PE/PP) separators, the PE layer with low melting point of ~130 °C could melt thus block the ion conduction pathway at high temperature. For an electrospun PI nanofiber separator, it has excellent thermal stability thus could not shrink/melt even at the temperature as high as 500 °C; as a result, it may not be safe when the electric shorting occurs because it cannot terminate the electrochemical reactions. Recently, research endeavors have been devoted to improve the shutdown behavior of PI nanofibers through coating them with low melting point polymers. For example, Shi *et al*. [214] coated a layer of PE microparticles on electrospun PI nanofibers; Liang *et al.* [215] prepared a polyethylene oxide (PEO)-coated PI nanofiber mat/membrane by the dip-coating method, while Wu *et al.* [216] reported a sandwiched PI/PVDF/PI composited nanofiber separator. As shown in Fig. 25, a middle layer of PVDF nanofibers was sandwiched between two PI nanofiber mats; at high temperature, the PVDF nanofibers can melt and form a pore-free film, thus the battery operation is shut down. The results indicated that the PI/PVDF/PI separators would shut down the battery operation within 10 min, when the device temperature was above 170 °C.

ACCEPTED MANUSCRIPT

Furthermore, gel polymer electrolytes [217] have recently been applied in LIBs due to their high ionic conductivity and good stability with electrode materials, and they are generally made through incorporation of liquid electrolytes into polymer matrices (with good absorption property toward liquid electrolytes). Wang *et al.* [218] investigated electrospun PI nanofiber mat/membrane as the polymer matrix, in which the electrolyte solution (1 mol/L $LiPF_6$/ethylene carbonate/ethylmethyl carbonate/dimethyl carbonate) was incorporated to prepare the polymer electrolyte. Their results indicated that the prepared polymer electrolyte had superior thermal stability and excellent flame retardant property, as well as high porosity and large uptake to liquid electrolyte. The electrochemical test revealed that the PI electrolytes had a high ionic conductivity up to 2.0×10^{-3} S/cm at 25 °C, and exhibited a high electrochemical stability (*i.e.*, more than 5.0 V *versus* Li/Li^+). The excellent charge/discharge performance and capacity retention suggested that electrospun PI nanofiber based polymer electrolytes would be promising for LIBs. Later, they incorporated another gel electrolyte (*i.e.*, triethylene glycol diacetate-2-propenoic acid butyl ester, TEGDA-BA) into electrospun PI (PMDA-ODA) nanofibers to prepare PI-gel electrolytes [219]. Such PI-gel electrolytes exhibited ionic conductivity of 2.79×10^{-3} S/cm at 25 °C, electrochemical stability up to 5.0 V (*versus* Li/Li+), and appropriate tensile strength of 7.22 MPa.

4.3. Fuel cell proton exchange membranes

Fuel cells are promising electrochemical devices that can convert chemical energy directly into electrical energy with high efficiency and low emission of pollutants [220], and proton exchange membranes in fuel cells have to possess high proton conductivity, low gas permeability, and excellent thermal and chemical stabilities. Presently, perfluorosulfonated aliphatic polymer membranes (*e.g.*, Nafion®) have been widely used due to high proton conductivity and good chemical stability [221, 222]; however, these membranes also have some problems including high gas permeability, low thermal stability, poor mechanical strength, and dimensional variation during operation/application. Recently, the composite membranes reinforced with porous substrates have attracted growing attention to mitigate these problems. For example, Lee *et al.* [223] developed the SiO_2/PEI-coated PI nanofiber nonwoven/mat as a new porous substrate for the reinforcement of Nafion®-impregnated composite membrane. This electrospun substrate had low thickness, high porosity, and strong affinity with hydrophilic Nafion®; furthermore, the SiO_2 nanoparticles considerably improved the mechanical strength and hydrophilicity. The reported composite membrane could chemically adsorb water, thus the dimensional stability was appreciably improved; as a result, the sharp drop of proton conductivity under low humidity condition (*e.g.*, the relative humidity of 10%) was effectively mitigated.

ACCEPTED MANUSCRIPT

Polymer electrolyte membranes based on sulfonated aromatic PIs have been developed as novel proton exchange membranes, in which the sulfonic acid groups would substantially improve the proton conductivity. In 2010, Takemori and Kawakami [224] reported the blend membranes of sulfonated PI (NTDA-BDSA) impregnated with sulfonated electrospun PI (NTDA-BDSA-r-APPF) nanofibers, and chemical structures of NTDA-BDSA and NTDA-BDSA-r-APPF are shown in Fig. 26. Compared to neat films made from the conventional solution-casting method, the proton conductivity values of blend membranes were significantly increased upon the addition of electrospun nanofibers; the oxidative and hydrolytic stabilities of blend membranes were also significantly improved. Moreover, the gas permeability of the blend membrane was reduced considerably as compared to the neat membrane. Later, Takemori and Kawakami also prepared and studied the blend membranes with the sulfonated PI nanofibers unidirectionally aligned [75, 76, 130]; and their results indicated that the proton conductivity of blend membranes with aligned electrospun nanofibers was improved on both parallel and perpendicular directions as compared to the casting film, while the proton conductivity along parallel direction was much higher than that along perpendicular direction. The proton conductivity along the parallel direction for the blend membrane with 10 wt.% nanofibers was similar to that of Nafion®. Additionally, the proton conductivity could be increased upon increasing the nanofiber amount; and the nanofibers with smaller diameters would generally lead to higher proton conductivity. Therefore, it was expected that the blend membranes (containing sulfonated PI nanofibers) with high proton conductivity, excellent shape stability, and low gas permeability would be promising as efficient proton exchange membranes of fuel cells.

4.4. Sensors

The properties of PIs can be tailored by judiciously synthesizing monomers (*i.e.*, diamines and dianhydrides) with varied functional groups, and there are several diamines and dianhydrides specifically designed/synthesized to make functional electrospun PI nanofibers, which can be used for different applications related to sensors [127, 131, 225-228].

Kim *et al.* [131] synthesized a diamine with an isocyanate group for the preparation of molecularly imprinted PI nanofibers. Isocyanate group in diamine component of PI would react with phenol group in template molecules (*i.e.*, estrone) to form urethane bond, while the formed urethane bond could be thermally reversible. After the PI nanofibers were obtained, the estrone molecules would then be removed by refluxing the PI nanofiber mats in 1,4-dioxane in the presence of water, and the urethane bonds could be converted into amino groups upon reaction with water. The resulting estrone imprinted electrospun PI nanofibers exhibited good recognition and fast response to estrone, note that these nanofibers could specifically adsorb estrone in solution. The amount of adsorbed estrone was determined by measuring the residual estrone in the filtrate *via* the reverse phase HPLC analysis.

ACCEPTED MANUSCRIPT

In 2008, by introducing porphyrin rings into PI backbones, Lv *et al.* [225] prepared a series of co-PI nanofibers from diaminotetraphenylporphyrin (DATPP), oxidianiline (ODA), and pyromellitic dianhydride (PMDA). Two types of DATPP (*i.e.*, *trans*-DATPP and *cis*-DATPP) were studied for synthesizing the porphyrinated co-PIs, and the chemical schemes are shown in Fig. 27. Both types of the prepared co-PAA and co-PI nanofibers possessed luminescence properties (*i.e.*, emitting red light uniformly), while the fluorescence intensity of co-PI nanofibers was weaker than that of co-PAA nanofibers, suggesting that fluorescence quenching might have occurred. Upon thermal imidization, the formed diimide ring is an electron acceptor, while the porphyrin is an electron donor; therefore, the photo-induced electrons would transfer from excited porphyrin units to diimide units. These porphyrinated PI nanofibers with unique photoelectric properties could potentially be used for optical switch, catalysis, nonlinear optics, and molecular wire.

In another reported research, Lv *et al.* prepared electrospun PI nanofibers containing zinc porphyrin (Fig. 28a) for ultra-sensitive detection of 2,4,6-trinitrotoluene trinitrotoluene (TNT) [127]. Fluorescence analysis results showed that the zinc porphyrin-containing PI nanofibers (Fig. 28b) possessed distinct luminescent property and could emit red light under confocal laser scanning microscopy (CLSM) (Fig. 28c). As these nanofibers were exposed to TNT vapor (10 ppb) at room temperature, the fluorescence quench would occur (Fig. 28d). The porphyrinated PI nanofibers could also be fluorescently quenched by 2,4-dinitrotoluene (DNT), 2,4,6-trinitrophenol (PA), and nitrobenzene (NB), whereas the quenching efficiencies were much lower than TNT. Hence, the porphyrinated PI nanofibers could be a promising material for detecting the trace amount of TNT.

Yen *et al.* [226] prepared an aggregation-induced emission (AIE) active PI by using cyano triphenylamine (CN-TPA). Both cast films and electrospun nanofibers were prepared and studied, and the UV-vis absorption showed that the electrospun PI nanofibers had higher photoluminescence quantum efficiency than the cast PI films. In electrospun nanofibers, there were more PI macromolecular chains oriented along the fiber axes, resulting in stronger fluorescent emission. Additionally, CN-TPA was also used for making polyamide film and electrospun nanofibers; whereas both showed lower photoluminescence efficiencies than PI.

As compared to introducing functional groups with luminescent property into monomers, the direct mixing of luminescent substances into PI matrices is a simpler approach. For example, Qin *et al.* [227] blended the DHEASPI-C1 (*i.e.*, a hemicyanine dye with good fluorescent property) into a PAA (PMDA-ODA) solution to prepare electrospun composite PI nanofiber mat, which also exhibited good photo-fluorescence properties.

ACCEPTED MANUSCRIPT

4.5. Microelectronics

In addition to excellent mechanical and thermal properties, PI materials also possess high chemical resistance, low thermal expansion, and great dielectric properties. Hence, PI materials can be used for microelectronic packaging, flexible display, and advanced dielectric materials [229-235]. Lingaiah *et al.* [236] prepared a high-temperature PI nanopaper by electrospinning a commercial P84 NT polyimide followed by heat-fusing the electrospun PI nanofibers at 330 °C. The prepared PI nanopaper exhibited good mechanical and thermal properties, and could be used for making flexible antennas. As shown in Fig. 29, the antenna grid was deposited on the PI nanopaper *via* a standard deposition process, and the resulting PI nanopaper based antenna could be used without any distortion.

In 2015, Xia *et al*. [235] made core-shell Al_2O_3@PI composite nanofibers *via* the coaxial electrospinning technique, wherein the PAA solution was used as the inner spin dope while PVP solution dispersed with Al_2O_3 nanoparticles was used as the outer spin dope. The obtained PVP-Al_2O_3@PAA nanofibers were heat-treated at 300 °C, during which the PAA was converted into PI while the PVP was almost burnt/removed, leading to the formation of Al_2O_3 nanoparticles on the surface of PI nanofibers. The obtained Al_2O_3@PI composite nanofibers had improved mechanical and thermal properties as well as excellent thermal conductivity of 9.66 W m^{-1} K^{-1}. This composite nanofiber mat/membrane was used as the thermal dissipation material in LED packaging, and the results indicated that it could disperse heat more effectively and rapidly than the neat PI nanofiber mat/membrane. Later, they also prepared Al_2O_3@PI-BT composite by using the above Al_2O_3@PI nanofibers as reinforcement filler and bismaleimide-triazine (BT) resin as matrix [237]. The resulting Al_2O_3@PI-BT composite exhibited good mechanical properties (*e.g.*, elastic modulus of 4.06 GPa), low dielectric constant (3.38–3.50 @100 kHz) and loss (0.0102–0.0107 @100 kHz), as well as high in-plane thermal conductivity (4.86 W m^{-1} K^{-1}). Moreover, it was demonstrated a practical application in printed circuit board (PCB), of which it was used as a substrate to fabricate a frequency ‘‘flasher” circuit by bonding discrete electronic components.

Due to low dielectric constants, PIs have been used for making insulators in the microelectronic industry. In 2007, Liu *et al.* [238] prepared PI (PMDA-ODA) fibers with an ultra-low dielectric constant of 1.53–1.56, and Liu *et al*. [149] made PI/SiO_2 composite nanofiber membranes through the combination of sol-gel and electrospinning techniques. Such PI/SiO_2 membranes exhibited ultra-low dielectric constants ranging from 1.78 to 1.32 upon the increase of SiO_2 content. Chen *et al.* [239] studied the relationship of dielectric properties with different electrospun PI nanofibers by using a laboratory-synthesized diamine of 4,4-bis[3’-trifluoromethyl-4’(4’-amino benzoxy) benzyl] biphenyl (denoted as Q) polymerized with various fluorinated and non-fluorinated dianhydrides (*e.g.*, PMDA, BPDA, BTDA, and 6FDA). The dielectric constants of electrospun Q-PMDA, Q-BPDA, Q-BTDA and Q-6FDA nanofibers at 1 MHz were 1.739, 1.607, 1.765, and 1.430, respectively; while the dielectric constants of the corresponding cast films at 1 MHz were 2.901, 2.861, 2.957, and 2.787, respectively.

ACCEPTED MANUSCRIPT

Therefore, the electrospun PI nanofibers generally possessed lower dielectric constants than the corresponding PI films. Li *et al*. [240] also investigated the relationship of dielectric properties with different PI nanofibers by using a diamine of ODA with three different dianhydrides of PMDA, 6FDA and 1,2,4,5-cyclohexanetetracarboxylic dianhydride (HPMDA). The prepared electrospun PMDA-ODA, 6FDA-ODA and HPMDA PI nanofiber membranes showed the dielectric constants of 1.91, 1.21 and 1.44, respectively at the testing frequency of 1 KHz, while the 6FDA-ODA PI nanofiber membrane exhibited he lowest dielectric constant due to the coupling effect of fluorine-containing groups with flexible structural units.

Because of good mechanical and thermal properties, PIs have also been utilized as matrix polymers for the fabrication of high dielectric composites. For example, Xu *et al.* prepared a series of high dielectric PI-matrix composites by using $BaTiO_3$, CNTs, and $BaTiO_3$/CNTs as fillers [104, 134, 135]. The composite nanofibers were made by mixing the fillers in PAA (HQDA-ODA) solution followed by electrospinning and then thermal imidization; thereafter, the composite nanofibers were hot-pressed into films/membranes. Their results indicated that the $BaTiO_3$ nanoparticles and/or CNTs could be well incorporated into PI nanofibers and finally dispersed in PI matrix uniformly; in consequence, these composites had stable dielectric properties, high dielectric constant, and low dielectric loss. Ding *et al.* [94] also made high dielectric PI/$BaTiO_3$ composite through combination of electrospinning and electrospraying techniques. In specific, the PAA/$BaTiO_3$ composite nanofibers were first prepared by simultaneously electrospinning PAA (HQDA-ODA) solution and electrospraying $BaTiO_3$ suspension. After thermal imidization, the PI/$BaTiO_3$ nanofibers were hot-pressed into film/membrane. The resulting composite film/membrane exhibited high dielectric constant of 28.93 (with 50 vol.% $BaTiO_3$) under 1 kHz at room temperature.

4.6. High temperature filtration media

Nowadays, air pollution has become a major environmental concern, particularly in the countries such as China. The developments of efficient personal and industrial filtration media are of great importance. Electrospun PI nanofiber mats/membranes have attracted growing interests for air filtration/purification applications, especially for the removal of micron-sized particles (*e.g.*, particulate matter 2.5, $PM_{2.5}$) at elevated temperatures (*e.g.*, industrial exhaust, coal combustion, and vehicle exhaust), because electrospun PI nanofiber mats/membranes possess small pore size, high porosity, good mechanical properties, and superior thermal stability [241-243].

Zhang *et al*. [241] studied the filtration performance of electrospun PI nanofibers for removal of $PM_{2.5}$ form pollution sources at high temperature. As shown in Fig. 30, they prepared a transparent air filter of PI nanofibers supported on a copper mesh (Fig. 30c). The PI nanofibers were smooth and with diameter of ~300 nm (Fig. 30e-g). These PI nanofibers had good capability to catch/adsorb PM particles, as shown in the images of Fig. 30h–i; after filtration, the PI nanofibers would be covered with PM particles. The authors studied the $PM_{2.5}$ removal efficiency of PI nanofibers in the temperature range of

ACCEPTED MANUSCRIPT

25–370 °C. The results indicated that the filtration performance would be almost the same at temperatures below 350 °C; and the $PM_{2.5}$ removal efficiency of the prepared PI nanofiber filter (with optical transmittance of ~60%) was higher than 95%. If the PI nanofiber filter had the optical transmittance of ~45%, the $PM_{2.5}$ removal efficiency was higher than 99.98%. The long-term test showed that the PI nanofiber filters (with optical transmittance of ~55%) could be used continuingly for more than 120 h at the $PM_{2.5}$ index of >300; as shown in Fig. 31a, the $PM_{2.5}$ and $PM_{2.5-10}$ removal efficiency values were retained at 97−99% and 99−100%, respectively. Another practical application of car exhaust filtration was also investigated by using the PI nanofiber filters (Fig. 31b–c), and these filters could effectively remove all kinds of particles with sizes from <0.3 μm to >10 μm (Fig. 31d).

4.7. Super-hydrophobic PI nanofibers

Although PIs are generally hydrophobic, their intrinsic hydrophobicity is relatively weak; such a situation hinders some applications (*e.g.*, water-proofing products); to improve the hydrophobicity, low surface energy and rough surface morphology are two important factors [244, 245]. It has been demonstrated that the electrospinning technique is effective towards producing rough surface, which can further lead to super-hydrophobicity [246-249]. Zhao *et al.* [183] prepared a soluble fluorinated aromatic PI with naphthalene pendant groups, and then electrospun this PI into nanofibers with controlled morphological structure. During electrospinning, the diameter, shape, and structure of nanofibers could be tailored by using different solvents including mixture solvents (*e.g.*, chloroform/ethanol and chloroform/DMF) and solvent with salt (*e.g.*, chloroform/CTAB). Upon adjusting the solvent ratios and controlling the vapor pressures of mixture solvents, the bead-free, rough, and ribbon-shaped nanofibers were obtained, and the water contact angles of such PI nanofiber mats/membranes were in the range from137.6° to 144.5°. Liu *et al.* [250] studied the effects of using different solvents (*e.g.*, DMF and NMP) and different spin solution concentrations on the morphology and hydrophobicity of electrospun PI nanofibers, and they made a hydrophobic PI nanofiber mat with the maximum contact angle of 140.78°.

Despite that the electrospinning technique can result in the increase of surface roughness, many electrospun nanofiber mats/membranes still cannot be considered as super-hydrophobic, since the commonly accepted definition of super-hydrophobicity is that the water contact angle has to be greater than 150° [251]. Hence, chemical/morphological modifications are often necessary to further improve the hydrophobicity. Fluorine-based chemicals and/or functional groups possess low surface energy, thus could be used to further improve the hydrophobicity. In 2012, Gong *et al.* [252] reported a new type of fluorinated polyimide (ODPA-6FBAPP). By adjusting the concentration of solutions and the ratio of mixture solvents, the highly porous beaded nanofibers were prepared *via* electrospinning. Since $–CF_3$ groups in ODPA-6FBAPP PI improved the water repellency, the fluorinated PI nanofiber mats exhibited the large water contact angle of 157.8°, showed the "Petal Effect" [252], and possessed the strong adhesive force up to 98.3 μN. Later, they synthesized another fluorinated PI (6FDA-6FBAPP) from 4,4'-

ACCEPTED MANUSCRIPT

(hexafluoroisopropylidene) diphthalicanhydride (6FDA) and 2,2-bis[4-(4-aminophenoxy) phenyl] hexafluoropropane (6FBAPP) [253]. This fluorinated PI contained more $–CF_3$ groups than ODPA-6FBAPP PI, and the resulting 6FDA-6FBAPP PI nanofiber mats (with bowl-like microstructure) had further enhanced hydrophobicity, as evidenced by higher adhesive force of 127 μN. Oktay *et al*. [254] synthesized segmented polyimide-siloxane copolymers by using the monomers of BTDA, ODA, and aminopropyl terminated polydimethylsiloxane (APPS). Upon varying the loading amount and molecular weight of APPS, a super-hydrophobic co-PI nanofiber mat with the contact angle of 167° was prepared, wherein the PI nanofibers had rough surfaces and the bead-on-string morphology.

Through direct incorporation of nanoparticles into polymer nanofibers, the surface roughness and hydrophobicity of the resulting nanocomposite nanofibers can also be increased. Gong *et al.* [144] added hydrophobic SiO_2 nanoparticles (with average diameter of 40 nm and specific surface area of 200 m^2/g) into PAA (PMDA-ODA) solution to prepare PI/SiO_2 composite nanofiber mats, which exhibited super-hydrophobicity with water contact angle of 157 ± 0.7° when the SiO_2 content was 30 wt.%; note that the water contact angle of neat PI nanofiber mats was merely 137 ± 1.1°. Additionally, the composite nanofiber mats had excellent thermal stability and mechanical properties as well as good anti-abrasion and thermal insulation characteristics. Hence, such super-hydrophobic and heat-resistant electrospun PI composite nanofiber mats are promising as self-cleaning materials for the applications in the environment with elevated temperature.

Recently, smart surfaces with reversible wettability (especially being able to switch between super-hydrophobic and super-hydrophilic) have been of great interests [255]. In 2011, Weng *et al.* [256] reported an electrospun PI nanofiber mat with reversible wettability. This PI was intrinsically electro-active, and the switchable wettability was attributed to the conjugated segments in its macromolecular backbone. A special electro-active diamine of amino-capped aniline trimer (*i.e.*, *N,N'*-bis(4'-aminophenyl)-1,4-quinonenediimine (ACAT)) was used for making this PI with conjugated segments (Fig. 32). Similar to polyaniline, the prepared PI also possessed the electrochemical activity and dopable properties, and these properties could be adjusted by varying the ACAT content. If ACAT alone was used as diamine, the electro-active PI nanofiber (EPF) mat had excellent reversible wettability between super-hydrophobic and super-hydrophilic upon doped with perfluorooctanesulfonic acid (PFOS) and de-doped with ammonia gas (Fig. 33). If ACAT was used together with other diamines, the resulting co-PI nanofiber (ECPF) mat was also electro-active; whereas the water contact angle of ECPF mat was smaller than that of EPF mat. Note that the water contact angle of non-electroactive PI nanofiber (NEPF) mat was only 106°, and the NEPF mat could not be doped with PFOS to possess the switchable wettability.

4.8. Polyimide-based carbon nanofibers

ACCEPTED MANUSCRIPT

Electrospun carbon nanofibers (ECNFs) with high porosity, large specific surface area, as well as good electrical and thermal conductivities, have potential applications in supercapacitors, Li-ion batteries, sensors, fuel cells, and catalyst supports [257-263]. To date, many polymers have been studied as precursors for making carbon fibers; while polyacrylonitrile (PAN) is one of the most commonly adopted precursors [264-266]. Note that many literatures also reported the conversion of PIs into carbon, and the advantages of using PIs as carbon precursor include well-defined molecular structure, high carbon yield, and relatively simple process of carbonization [267].

In 2003, Yang *et al.* [87] first reported the preparation of PI-based ECNFs; such carbon nanofibers were obtained by first electrospinning PMDA-ODA PAA solution into nanofibers followed by thermal imidization and then carbonization. Their results indicated that, with the increase of carbonization temperature, the carbon yield decreased while the electrical conductivity increased. At the carbonization temperature of 1000 °C, the carbon yield was ~53% and the electrical conductivity was ~2.5 S/cm. When the carbonization temperature was increased to 2200 °C, the electrical conductivity increased to 5.26 S/cm, which was significantly higher than the value (1.96 S/cm) of PAN-based ECNFs prepared under the same conditions; whereas the tensile strength and elastic modulus of the PI-based carbon nanofiber mats were merely 5.0 and 73.9 MPa, respectively. Subsequently, the PI-based carbon nanofibers were further activated with steam in the temperature range of 650–850 °C; and specific surface areas of the activated ECNFs were in the range of 940–2100 m^2/g. The prepared carbon nanofiber mats were then investigated as electrodes of electrical double layer capacitors (EDLCs) [268]; and the resulting EDLCs had the large specific capacitance of 175 F/g at the high current density of 1000 mA/g.

Yan *et al.* revealed [269] that the graphitic structures, as well as the electrical and thermal conductivities, of ECNFs could be distinguishably improved through addition of mesophase pitch into electrospun PI nanofibers. Mani *et al*. [138] improved the electrical conductivity of PI-based ECNFs by incorporating a small amount (<2 wt.%) of CNTs in the PAA solution for electrospinning. In another research, Xuyen *et al.* [270] indicated that the electrical and thermal conductivities of PI-based carbon nanofiber mats would increase with the decrease of nanofiber diameters. According to their explanation, the higher conductivity of smaller diameter nanofibers was due to the formation of more cross-junctions among nanofibers. Upon optimizations of PAA structures and carbonization conditions, ECNFs with diameters of ~80 nm and conductivity of ~16 S/cm were acquired.

ECNFs were also reported to be prepared by electrospinning a blend solution of PAN and PAA [271]. The results indicated that the diameters of ECNFs would decrease with the increase of PAN amount in the blend solution, and it appeared that the addition of PAN would make the blend solution easier to be electrospun than PAA solution. The smaller nanofiber diameters and the improved nanofiber-to-nanofiber contacts (in the nanofiber mats) were attributed to the higher electrical conductivity; nevertheless, the carbon yield would decrease with the increase of PAN amount in the blend solution, confirming that the carbon yield of PI was higher than that of PAN. In another reported research, Chung

ACCEPTED MANUSCRIPT

et al. [272] prepared ECNFs from electrospun soluble thermotropic PI (Matrimid® 5218) nanofibers. To facilitate carbonization and further increase the carbon yield, $[CH_3COCH{=}C(O\text{-})CH_3]_3Fe$ (AAI) was added into the PI solution. The XRD results revealed that the sizes of crystallites in nanofibers were increased from 1.06 to 4.18 nm with addition of 3 wt.% AAI.

An interesting approach for making ECNFs from PI precursor nanofibers is through combination of electrospinning and ion-beam irradiation [273]. Upon ion-beam irradiation, the surface of electrospun PI nanofibers would possess carbonaceous structure, while the core of nanofibers would still remain as polymeric structure. Seki *et al.* reported that ion species and ion fluencies would have important impacts on surface carbonaceous structure, and their results suggested that the electrical conductivity of nanofibers would be primarily determined by the ion-beam irradiation conditions. They indicated that the electrical conductivity of ion-irradiated PI nanofibers increased in the order of $He^+ < Ne^+ < Ar^+$, and the electrical conductivity of PI (6FDA-6FAP) nanofibers irradiated at 1×10^{16} ions/cm^2 of Ar^+ was 0.18 S/cm. Another research revealed that, through combination of electrospinning and ion-beam irradiation, the electrical conductivity of ECNFs derived from PI (6FDA-6FAP) was much higher than that of ECNFs derived from PI (6FDA-APPS), polysulfone (PSF), and polyacrylonitrile (PAN) [274]. Upon varying the ion-beam irradiation conditions, it would be easy to control the carbonaceous structure on nanofiber surface; and the obtained ECNFs were flexible because the core of nanofibers was polymeric.

Jung *et al.* [275] studied the electrochemical properties of ECNFs prepared from the blends of polybenzimidazole (PBI) and PI (Matrimid® 5218). The specific surface area and porosity of ECNFs would be increased with the increase of PI content in nanofibers. The ECNFs made from PBI/PI (75/25) blend exhibited low electrochemical impedance; moreover, the specific capacitance, energy density, and power density were 111 F/g, 24 kW/kg, and 6 kW/kg, respectively. The performance of PBI/PI derived ECNFs could be further improved *via* the steam activation, and the resulting ECNFs showed specific capacitance of 126 F/g, energy density of 49 kW/kg, and power density of 7 kW/kg.

Nan *et al.* [260] prepared highly porous electrospun carbon nanofibers (PECNFs) from hybrid PI/SiO_2 nanofibers; thereafter, the PECNFs were studied as anode for lithium-ion batteries. An etching treatment was adopted to introduce micro-porous structure in PECNFs, in which HF acid was used to remove the SiO_2 nanoparticles in ECNFs; and the obtained PECNFs had the specific surface area of 950 m^2/g. The electrochemical performance measurements indicated that the PECNFs could be freestanding anodes with large capacity of 730 mAh/g in the first cycle; furthermore, the cycling retention and rate capability were also excellent. Additionally, Kang's group proposed several strategies for the preparation of highly porous PI-based ECNFs: (1) activating at 700 °C under steam/N_2 flow (1:3 v/v), by which they made porous ECNFs with specific surface area of 995 m^2/g [276]; (2) adding high temperature decomposable polymer (*e.g.*, PVP) as pore inducer for electrospinning, and the resulting ECNFs had the specific surface area in the range of 456–804 m^2/g [277]; (3) combining coaxial electrospinning and addition of pore inducer polymer for the preparation of porous hollow ECNFs, which had the specific

ACCEPTED MANUSCRIPT

surface of 456–603 m^2/g [278]. The above porous ECNFs were studied as the electrode materials for high-performance supercapacitors and lithium-sulfur batteries [276-278].

In 2009, Xuyen *et al.* [279] reported the PI-based ECNFs surface-decorated with Pt nanoparticles having sizes of ~3 nm. The decoration of Pt nanoparticles on ECNFs were accomplished by immobilization of $Pt(acac)_2$ on hydrolyzed PI nanofibers followed by carbonization. The prepared Pt/ECNFs exhibited superior electrocatalytic performance. Recently, Liu's group reported several different types of PI-based ECNFs surface-decorated with Ni nanoparticles, $Ni(OH)_2$ nanoplatelets, or PANi, which were respectively prepared by incorporating precursor salt ($Ni(NO_3)_2 \cdot 6H_2O$) in PAA solution for electrospinning followed by carbonization, or by treating the ECNFs *via* hydrothermal growth or *in situ* polymerization [280-282]. After the surface-decorations, the resulting nanofiber mats showed excellent performances for different applications including hydrogen evolution reaction, double layer supercapacitor, and flexible all-solid-state supercapacitor [280-282].

Nitrogen-doping of carbon materials can effectively tailor their electronic properties, leading to the improvements on electrochemical performances of energy-storage devices such as supercapacitors and lithium-ion batteries [283, 284]. Recently, research endeavors have suggested that the PI-based ECNFs could be nitrogen-doped carbon materials. It is because PIs are heterocyclic polymers containing imide rings, and the excellent thermal stability of PIs may result in the remaining of nitrogen atoms in heterocyclic rings during the high temperature carbonization, further leading to the formation of ECNFs with high nitrogen content. The PI-based nitrogen-doped ECNFs have been studied as the electrode materials for high performance flexible supercapacitors [283], lithium-ion batteries [284], sodium-ion batteries (SIBs) [285], and Zn-air batteries [286]. As shown in Fig. 34, Li *et al*. [283] prepared flexible nitrogen-doped ECNFs by carbonization of electrospun PI nanofibers at 1000 °C. The obtained ECNFs had a high nitrogen content of 5.8%, and it exhibited high electrical conductivity of 2500 S/m and large specific surface area of 442 m^2/g. Moreover, the assembled supercapacitors (by using the nitrogen-doped ECNFs) demonstrated excellent volumetric capacitance of 159.3 F/cm^3 (at 1 A/g), high rate capability of 127.5 F/cm^3 (at 7 A/g), and a long cycling life/stability (*i.e.*, over 100,000 cycles).

5. *Conclusions and Perspectives*

Electrospun PI nanofibers are high-performance materials with excellent physical and chemical properties; additionally, the chemical and morphological structures of electrospun PI nanofibers can be readily tailored by using different monomers and/or adjusting electrospinning conditions. The mechanical and thermal properties of PI nanofibers are related to the rigidity/flexibility and orientation of PI macromolecules in the nanofibers. PI composite nanofibers can be prepared by electrospinning PAA solutions containing different polymers/fillers followed by imidization. In general, electrospun PI nanofibers, PI composite nanofibers, and PI-based carbon nanofibers possess large specific surface area, high mechanical properties, and superior thermal

ACCEPTED MANUSCRIPT

stability; hence, they can be utilized for various applications including reinforcement of composites, energy storage and conversion, microelectronics, filtration/separation, environmental protection, and biomedical engineering. Nevertheless, because the preparation of electrospun PI nanofibers typically contains two steps and the second step of imidization is usually carried out at an elevated temperature, the development and application of electrospun PI nanofibers have not been widely investigated until the recent years.

From our perspective, future research endeavors on electrospun PI nanofibers would be primarily focused on (1) optimization of preparation conditions/procedures and (2) practical and high-value applications. To date, numerous electrospun PI (including homo-PI, co-PI, and blend-PI nanofibers) nanofibers have been successfully prepared; and several explanations/mechanisms have been proposed to address high mechanical properties and thermal stability: (1) the rigid components/moieties in PI macromolecules contribute to high strength and modulus, while the flexible components/moieties contribute to great flexibility; (2) the formation of micro-blocks between rigid and flexible components/moieties of co-PIs and/or blend-PIs further improves their mechanical properties; and (3) during the thermal imidization, high temperature can lead to the enhanced orientation of PI macromolecules in electrospun nanofibers.

The above explanations provide general guidance for the design and preparation of high-performance PI nanofibers; however, the mechanical properties of most electrospun PI nanofibers are still considerably lower than conventional high-performance fibers (*e.g.*, PI fibers, Kevlar fibers, and carbon fibers). Presumably, there are two reasons including (1) the reported mechanical properties are usually measured from nanofiber mats/bundles instead of individual nanofibers; (2) the preparation procedures/conditions need to be optimized. It is necessary to note that the technique/equipment for accurately measuring mechanical and electrical properties of individual electrospun nanofibers is still upon further development. Additionally, a comprehensive strategy/approach needs to be established for developing high-performance electrospun PI nanofibers; and this includes (1) the synthesis of novel PAAs with high molecular weights, (2) the control of morphological and structural properties of electrospun PAA precursor nanofibers, and (3) the optimization of imidization process.

For practical and high-value applications, it appears that electrospun PI nanofiber mats/membranes would be particularly useful for filtration/separation and Li-ion battery separator. Although it has been reported that electrospun PI nanofiber mats/membranes are excellent microfiltration media [287, 288], the potential filtration/purification applications need to be further investigated, especially those with the application temperatures being high such as high-temperature filters for vehicle exhausts and industrial dusts/wastes. Arguably, the most high-value application of electrospun PI nanofiber mats/membranes might be the separators for Li-ion batteries in electric vehicles, since excellent mechanical properties and superior thermal stability are both important for battery safety. It is noteworthy that the scale-up of electrospun nanofibers is still a technological challenge, even though some techniques (*e.g.*, needless electrospinning) have been developed for large-scale-production of electrospun

ACCEPTED MANUSCRIPT

nanofibers [38, 289, 290]; additionally, to align electrospun nanofibers is another technological challenge [291]. Nevertheless, it is envisioned that electrospun PI nanofibers with excellent mechanical properties and thermal stability would be utilized for various high-value applications.

Acknowledgments

This work was supported by the National Natural Science Foundation of China (Grant Numbers: 21174058 and 21374044). H. Fong would like to acknowledge the "Thousands of People Plan of the Shanghai City" in China. The authors would also like to acknowledge the Biomedical Engineering Program at the South Dakota School of Mines and Technology.

References

[1] Sroog CE. Polyimides. J Polym Sci Macromol Rev 1976;11:161-208.

[2] Sroog CE. Polyimides. Prog Polym Sci 1991;16:561-694.

[3] Liaw DJ, Wang KL, Huang YC, Lee KR, Lai JY, Ha CS. Advanced polyimide materials: Syntheses, physical properties and applications. Prog Polym Sci 2012;37:907-74.

[4] Ding M. Polyimides: Monomers, polymerization and materials. Beijing: Science Press, 2011. 983 pp.

[5] Ding M. Isomeric polyimides. Prog Polym Sci 2007;32:623-68.

[6] Ding M. Polyimides: Chemistry, relationship between structure and properties and materials. Beijing: Science Press, 2006. 913 pp.

[7] Bogert MT, Renshaw RR. 4-amino-0-phthalic acid and some of its derivatives. J Am Chem Soc 1908;30:1135-44.

[8] Ghosh M. History of the invention and development of the polyimides. In: Ghosh MK, L. MK, editors. Polyimides: Fundamentals and applications. New York: CRC press 1996. p. 1-6.

[9] Edwards WM, Robinson IM. Polyimides of pyromellitic acid. US 2710853, 1955.

[10] Robinson IM, Edwards WM. Polyimide composition. US 2900369, 1959.

[11] Edwards WM. Polyamide-acids, compositions thereof, and process for their preparation. US 3179614, 1965.

ACCEPTED MANUSCRIPT

[12] Gay FP. Stretching process for polyimide film. US 3619461, 1971.

[13] Farrissey J, William J, Onder BK. Polyimide fiber having a serrated surface and a process of producing same. US 3985934, 1976.

[14] Gagliani J. Polyimide fibers. US 4255488, 1981.

[15] St Clair TL, Fay CC, Working DC. Polyimide fibers. US 5840828, 1998.

[16] Gagliani J. Melt spinning polyimide fibers. US 4299787, 1981.

[17] Irwin RS, Sweeny W. Polyimide fibers. J Polym Sci C Polym Symp 1967;19:41-8.

[18] Park SK, Farris RJ. Dry-jet wet spinning of aromatic polyamic acid fiber using chemical imidization. Polymer 2001;42:10087-93.

[19] Cheng SZD, Wu Z, Mark E, Steven LCH, Frank WH. A high-performance aromatic polyimide fibre: 1. Structure, properties and mechanical-history dependence. Polymer 1991;32:1803-10.

[20] Weinrotter K, Seidl S, Lenzing AG. High-performance polyimide fibres. In: Handbook of fiber science and technology Volume 2: high technology fibers: Part C, London: CRC Press, 1993. p. 179-205.

[21] Krol JJ, Boerrigter M, Koops GH. Polyimide hollow fiber gas separation membranes: preparation and the suppression of plasticization in propane/propylene environments. J Membr Sci 2001;184:275-86.

[22] Chung TS, Kafchinski ER, Foley P. Development of asymmetric hollow fibers from polyimides for air separation. J Membr Sci 1992;75:181-95.

[23] Gong G, Wu J, Jiang L. Novel polyimide materials produced by electrospinning. Prog Chem 2011;23:750-9.

[24] Gong G, Wu J. Novel Polyimide materials produced by electrospinning. In: Abadie M, editor. High performance polymers-polyimides based-from chemistry to applications, Rijeka: InTech, 2012. p. 127-144.

[25] Huang ZM, Zhang YZ, Kotaki M, Ramakrishna S. A review on polymer nanofibers by electrospinning and their applications in nanocomposites. Compos Sci Technol 2003;63:2223-53.

[26] Li D, Xia Y. Electrospinning of nanofibers: Reinventing the wheel? Adv Mater 2004;16:1151-70.

Accepted Manuscript

ACCEPTED MANUSCRIPT

[27] Greiner A, Wendorff JH. Electrospinning: a fascinating method for the preparation of ultrathin fibers. Angew Chem Int Ed 2007;46:5670-703.

[28] Doshi J, Reneker DH. Electrospinning process and applications of electrospun fibers. J Electrostat 1995;35:151-60.

[29] Reneker DH, Chun I. Nanometre diameter fibres of polymer, produced by electrospinning. Nanotechnology 1996;7:216-23.

[30] Srinivasan G, Reneker DH. Structure and morphology of small diameter electrospun aramid fibers. Polym Int 1995;36:195-201.

[31] Fong H, Chun I, Reneker DH. Beaded nanofibers formed during electrospinning. Polymer 1999;40:4585-92.

[32] Spivak AF, Dzenis YA, Reneker DH. A model of steady state jet in the electrospinning process. Mech Res Commun 2000;27:37-42.

[33] Koombhongse S, Liu W, Reneker DH. Flat polymer ribbons and other shapes by electrospinning. J Polym Sci B Polym Phys 2001;39:2598-606.

[34] Yarin AL, Koombhongse S, Reneker DH. Bending instability in electrospinning of nanofibers. J Appl Phys 2001;89:3018-26.

[35] Yarin AL, Koombhongse S, Reneker DH. Taylor cone and jetting from liquid droplets in electrospinning of nanofibers. J Appl Phys 2001;90:4836-46.

[36] Reneker DH, Yarin AL, Fong H, Koombhongse S. Bending instability of electrically charged liquid jets of polymer solutions in electrospinning. J Appl Phys 2000;87:4531-47.

[37] Reneker DH, Yarin AL. Electrospinning jets and polymer nanofibers. Polymer 2008;49:2387-425.

[38] Persano L, Camposeo A, Tekmen C, Pisignano D. Industrial upscaling of electrospinning and applications of polymer nanofibers: A review. Macromol Mater Eng 2013;298:504-20.

[39] Anonymous. Naficate Nanofibers Gateway. http://www.nafigate.com/en. 2106;Accessed June 2016.

[40] Anonymous. Jiangxi Xian Cai Nanofibers Technology Co., Ltd. http://www.hinanofiber.com/. 2016;Accessed June 2016.

Accepted Manuscript

ACCEPTED MANUSCRIPT

[41] Anonymous. Elmarco Nano for Life. http://www.elmarco.com/. 2016;Accessed June 2016.

[42] Hou H, Cheng C, Chen S, Zhou X, Lv X, He P, Kuang X, Ren J. Copolyimide nano-fiber non-woven fabric, process for producing the same and the use thereof. US 20130196562, 2013.

[43] Taylor G. Electrically driven jets. Proc R Soc Lond Ser A 1969;313:453-75.

[44] Huang C, Chen S, Lai C, Reneker DH, Qiu H, Ye Y, Hou H. Electrospun polymer nanofibres with small diameters. Nanotechnology 2006;17:1558-63.

[45] Zhou Z, Lai C, Zhang L, Qian Y, Hou H, Reneker DH, Fong H. Development of carbon nanofibers from aligned electrospun polyacrylonitrile nanofiber bundles and characterization of their microstructural, electrical, and mechanical properties. Polymer 2009;50:2999-3006.

[46] Bognitzki M, Czado W, Frese T, Schaper A, Hellwig M, Steinhart M, Greiner A, Wendorff JH. Nanostructured fibers via electrospinning. Adv Mater 2001;13:70-2.

[47] Lin J, Ding B, Yu J, Hsieh Y. Direct fabrication of highly nanoporous polystyrene fibers via electrospinning. ACS Appl Mater Interfaces 2010;2:521-8.

[48] Li D, Xia Y. Direct fabrication of composite and ceramic hollow nanofibers by electrospinning. Nano Lett 2004;4:933-8.

[49] Di J, Chen H, Wang X, Zhao Y, Jiang L, Yu J, Xu R. Fabrication of zeolite hollow fibers by coaxial electrospinning. Chem Mater 2008;20:3543-5.

[50] Sun Z, Zussman E, Yarin AL, Wendorff JH, Greiner A. Compound core-shell polymer nanofibers by co-electrospinning. Adv Mater 2003;15:1929-32.

[51] Chen H, Wang N, Di J, Zhao Y, Song Y, Jiang L. Nanowire-in-microtube structured core/shell fibers via multifluidic coaxial electrospinning. Langmuir 2010;26:11291-6.

[52] Zhao Y, Cao X, Jiang L. Bio-mimic multichannel microtubes by a facile method. J Am Chem Soc 2007;129:764-5.

[53] Zhao T, Liu Z, Nakata K, Nishimoto S, Murakami T, Zhao Y, Jiang L, Fujishima A. Multichannel TiO_2 hollow fibers with enhanced photocatalytic activity. J Mater Chem 2010;20:5095-9.

Accepted Manuscript

ACCEPTED MANUSCRIPT

[54] Tao J, Shivkumar S. Molecular weight dependent structural regimes during the electrospinning of PVA. Mater Lett 2007;61:2325-8.

[55] Díaz JE, Barrero A, Márquez M, Loscertales IG. Controlled encapsulation of hydrophobic liquids in hydrophilic polymer nanofibers by co-electrospinning. Adv Funct Mater 2006;16:2110-6.

[56] Holzmeister A, Greiner A, Wendorff JH. "Barbed nanowires" from polymers via electrospinning. Polym Eng Sci 2009;49:148-53.

[57] Hou H, Reneker DH. Carbon nanotubes on carbon nanofibers: A novel structure based on electrospun polymer nanofibers. Adv Mater 2004;16:69-73.

[58] Ostermann R, Li D, Yin Y, McCann JT, Xia Y. V_2O_5 nanorods on TiO_2 nanofibers: A new class of hierarchical nanostructures enabled by electrospinning and calcination. Nano Lett 2006;6:1297-302.

[59] He S, Hu X, Chen S, Hu H, Hanif M, Hou H. Needle-like polyaniline nanowires on graphite nanofibers: hierarchical micro/nano-architecture for high performance supercapacitors. J Mater Chem 2012;22:5114-20.

[60] He S, Chen L, Xie C, Hu H, Chen S, Hanif M, Hou H. Supercapacitors based on 3D network of activated carbon nanowhiskers wrapped-on graphitized electrospun nanofibers. J Power Sources 2013;243:880-6.

[61] Zhang M, Shao C, Mu J, Huang X, Zhang Z, Guo Z, Zhang P, Liu Y. Hierarchical heterostructures of Bi_2MoO_6 on carbon nanofibers: controllable solvothermal fabrication and enhanced visible photocatalytic properties. J Mater Chem 2012;22:577-84.

[62] Zhou Z, Wu XF. High-performance porous electrodes for pseudosupercapacitors based on graphene-beaded carbon nanofibers surface-coated with nanostructured conducting polymers. J Power Sources 2014;262:44-9.

[63] Thavasi V, Singh G, Ramakrishna S. Electrospun nanofibers in energy and environmental applications. Energy Environ Sci 2008;1:205-21.

[64] Ramakrishna S, Fujihara K, Teo WE, Yong T, Ma Z, Ramaseshan R. Electrospun nanofibers: Solving global issues. Mater Today 2006;9:40-50.

Accepted Manuscript

ACCEPTED MANUSCRIPT

[65] Cavaliere S, Subianto S, Savych I, Jones DJ, Roziere J. Electrospinning: designed architectures for energy conversion and storage devices. Energy Environ Sci 2 0 11;4:4761-85.

[66] Feng C, Khulbe KC, Matsuura T, Tabe S, Ismail AF. Preparation and characterization of electro-spun nanofiber membranes and their possible applications in water treatment. Sep Purif Technol 2013;102:118-35.

[67] Sill TJ, von Recum HA. Electrospinning: Applications in drug delivery and tissue engineering. Biomaterials 2008;29:1989-2006.

[68] Lu W, Sun J, Jiang X. Recent advances in electrospinning technology and biomedical applications of electrospun fibers. J Mater Chem B 2014;2:2369-80.

[69] Chen Y, Han D, Ouyang W, Chen S, Hou H, Zhao Y, Fong H. Fabrication and evaluation of polyamide 6 composites with electrospun polyimide nanofibers as skeletal framework. Compos B Eng 2012;43:2382-8.

[70] Yao J, Li G, Bastiaansen CWM, Peijs T. High performance co-polyimide nanofiber reinforced composites. Polymer 2015;76:46-51.

[71] Shen Y, Chen L, Jiang S, Ding Y, Xu W, Hou H. Electrospun nanofiber reinforced all-organic PVDF/PI tough composites and their dielectric permittivity. Mater Lett 2015;160:515-7.

[72] Chen D, Wang R, Tjiu WW, Liu T. High performance polyimide composite films prepared by homogeneity reinforcement of electrospun nanofibers. Compos Sci Technol 2011;71:1556-62.

[73] Zhu Z, Zhang L, Howe JY, Liao Y, Speidel JT, Smith S, Fong H. Aligned electrospun ZnO nanofibers for simple and sensitive ultraviolet nanosensors. Chem Commun 2009 :2568-70.

[74] Persano L, Dagdeviren C, Su Y, Zhang Y, Girardo S, Pisignano D, Huang Y, Rogers JA. High performance piezoelectric devices based on aligned arrays of nanofibers of poly(vinylidenefluoride-co-trifluoroethylene). Nat Commun 2013;4:1633/1-10.

[75] Tamura T, Takemori R, Kawakami H. Proton conductive properties of composite membranes containing uniaxially aligned ultrafine electrospun polyimide nanofiber. J Power Sources 2012;217:135-41.

Accepted Manuscript

ACCEPTED MANUSCRIPT

[76] Tamura T, Kawakami H. Aligned electrospun nanofiber composite membranes for fuel cell electrolytes. Nano Lett 2010;10:1324-8.

[77] Dersch R, Liu T, Schaper AK, Greiner A, Wendorff JH. Electrospun nanofibers: Internal structure and intrinsic orientation. J Polym Sci A Polym Chem 2003;41:545-53.

[78] Li D, Wang Y, Xia Y. Electrospinning of polymeric and ceramic nanofibers as uniaxially aligned arrays. Nano Lett 2003;3:1167-71.

[79] Dalton PD, Klee D, Möller M. Electrospinning with dual collection rings. Polymer 2005;46:611-4.

[80] Pan H, Li L, Hu L, Cui X. Continuous aligned polymer fibers produced by a modified electrospinning method. Polymer 2006;47:4901-4.

[81] Yang D, Lu B, Zhao Y, Jiang X. Fabrication of aligned fibrous arrays by magnetic electrospinning. Adv Mater 2007;19:3702-6.

[82] Theron A, Zussman1 E, Yarin AL. Electrostatic field-assisted alignment of electrospun nanofibres. Nanotechnology 2001;12:384-90.

[83] Katta P, Alessandro M, Ramsier RD, Chase GG. Continuous electrospinning of aligned polymer nanofibers onto a wire drum collector. Nano Lett 2004;4:2215-8.

[84] Smit E, Bűttner U, Sanderson RD. Continuous yarns from electrospun fibers. Polymer 2005;46:2419-23.

[85] Teo WE, Gopal R, Ramaseshan R, Fujihara K, Ramakrishna S. A dynamic liquid support system for continuous electrospun yarn fabrication. Polymer 2007;48:3400-5.

[86] Nah C, Han SH, Lee MH, Kim JS, Lee DS. Characteristics of polyimide ultrafine fibers prepared through electrospinning. Polym Int 2003;52:429-32.

[87] Yang KS, Edie DD, Lim DY, Kim YM, Choi YO. Preparation of carbon fiber web from electrostatic spinning of PMDA-ODA poly(amic acid) solution. Carbon 2003;41:2039-46.

[88] Huang C, Chen S, Reneker DH, Lai C, Hou H. High-strength mats from electrospun poly(p-phenylene biphenyltetracarboximide) nanofibers. Adv Mater 2006;18:668-71.

Accepted Manuscript

ACCEPTED MANUSCRIPT

[89] Huang C, Wang S, Zhang H, Li T, Chen S, Lai C, Hou H. High strength electrospun polymer nanofibers made from BPDA-PDA polyimide. Eur Polym J 2006;42:1099-104.

[90] Chen F, Peng X, Li T, Chen S, Wu XF, Reneker DH, Hou H. Mechanical characterization of single high-strength electrospun polyimide nanofibres. J Phys D 2008;41:025308/1-8.

[91] Chen S, Hu P, Greiner A, Cheng C, Cheng H, Chen F, Hou H. Electrospun nanofiber belts made from high performance copolyimide. Nanotechnology 2008;19:015604/1-9.

[92] Chen D, Liu T, Zhou X, Tjiu WC, Hou H. Electrospinning fabrication of high strength and toughness polyimide nanofiber membranes containing multiwalled carbon nanotubes. J Phys Chem B 2009;113:9741-8.

[93] Cheng C, Chen J, Chen F, Hu P, Wu XF, Reneker DH, Hou H. High-strength and high-toughness polyimide nanofibers: Synthesis and characterization. J Appl Polym Sci 2010;116:1581-6.

[94] Ding Y, Wu Q, Zhao D, Ye W, Hanif M, Hou H. Flexible PI/$BaTiO_3$ dielectric nanocomposite fabricated by combining electrospinning and electrospraying. Eur Polym J 2013;49:2567-71.

[95] Miao YE, Zhu GN, Hou H, Xia YY, Liu T. Electrospun polyimide nanofiber-based nonwoven separators for lithium-ion batteries. J Power Sources 2013;226:82-6.

[96] He Y, Han D, Chen J, Ding Y, Jiang S, Hu C, Chen S, Hou H. Highly strong and highly tough electrospun polyimide/polyimide composite nanofibers from binary blend of polyamic acids. RSC Adv 2014;4:59936-42.

[97] Ding Y, Xie C, Zhu J, Zhu Y, Peng X, Hou H. PI/CB conductive composites with low percolation threshold prepared by electrospinning technique. Polym Mater Sci Eng 2013;29:160-3.

[98] Peng X, Wu Q, Jiang S, Hanif M, Chen S, Hou H. High dielectric constant polyimide derived from 5,5'-bis[(4-amino) phenoxy]-2,2'-bipyrimidine. J Appl Polym Sci 2014;131:40828/1-8.

Accepted Manuscript

ACCEPTED MANUSCRIPT

[99] Chen L, Jiang S, Chen J, Chen F, He Y, Zhu Y, Hou H. Single electrospun nanofiber and aligned nanofiber belts from copolyimide containing pyrimidine units. New J Chem 2015;39:8956-63.

[100] Jiang S, Duan G, Chen L, Hu X, Hou H. Mechanical performance of aligned electrospun polyimide nanofiber belt at high temperature. Mater Lett 2015;140:12-5.

[101] Peng X, Wu Q, Jiang S, Hanif M, Chen S, Hou H. High performance polyimide-Yb complex with high dielectric constant and low dielectric loss. Mater Lett 2014;133:240-2.

[102] Jiang S, Duan G, Chen L, Hu X, Ding Y, Jiang C, Hou H. Thermal, mechanical and thermomechanical properties of tough electrospun poly(imide-co-benzoxazole) nanofiber belts. New J Chem 2015;39:7797-804.

[103] Chen S, Han D, Hou H. High strength electrospun fibers. Polym Adv Technol 2011;22:295-303.

[104] Xu W, Ding Y, Jiang S, Ye W, Liao X, Hou H. High permittivity nanocomposites fabricated from electrospun polyimide/$BaTiO_3$ hybrid nanofibers. Polym Compos 2016;37:794-801.

[105] Zhang M, Wang Z, Zhang Y. Preparation of polyimide nanofibers by electrospinning. *2006 International Conference on MEMS, NANO, and Smart Systems,* Cairo, 2006. p. 58-60.

[106] Karube Y, Kawakami H. Fabrication of well-aligned electrospun nanofibrous membrane based on fluorinated polyimide. Polym Adv Technol 2010;21:861-6.

[107] Fukushima S, Karube Y, Kawakami H. Preparation of ultrafine uniform electrospun polyimide nanofiber. Polym J 2010;42:514-8.

[108] Arai T, Kawakami H. Ultrafine electrospun nanofiber created from cross-linked polyimide solution. Polymer 2012;53:2217-22.

[109] Chisca S, Barzic AI, Sava I, Olaru N, Bruma M. Morphological and rheological insights on polyimide chain entanglements for electrospinning produced fibers. J Phys Chem B 2012;116:9082-8.

Accepted Manuscript

ACCEPTED MANUSCRIPT

[110] Serbezeanu D, Butnaru I, Varganici CD, Bruma M, Fortunato G, Gaan S. Phosphorus-containing polyimide fibers and their thermal properties. RSC Adv 2016;6:38371-9.

[111] Goponenko AV, Hou H, Dzenis YA. Avoiding fusion of electrospun 3,3',4,4'-biphenyltetracarboxylic dianhydride-4,4'-oxydianiline copolymer nanofibers during conversion to polyimide. Polymer 2011;52:3776-82.

[112] Park JW, Lee M, Lee MH, Liu JW, Kim SD, Chang JY, Rhee SB. Synthesis and characterization of soluble alternating aromatic copolyimides. Macromolecules 1994;27:3459-63.

[113] Wang Y, Wang N, Yu Z, Li G, Zhang X. Novel dye-containing copolyimides: synthesis, characterization and effect of chain entanglements on developed electrospun nanofiber morphologies. J Polym Res 2015;22:1-8.

[114] Peciulyte L, Rutkaite R, Zemaitaitis A, Ignatova M, Rashkov I, Manolova N. Thermal imidization peculiarities of electrospun BPDA-PDA/ODA copolyamic acid nanofibers. Macromol Res 2013;21:419-26.

[115] Yao J, Pantano MF, Pugno NM, Bastiaansen CWM, Peijs T. High-performance electrospun co-polyimide nanofibers. Polymer 2015;76:105-12.

[116] Hsu SLC, Lin KS, Wang C. Preparation of polybenzoxazole fibers via electrospinning and postspun thermal cyclization of polyhydroxyamide. J Polym Sci A Polym Chem 2008;46:8159-69.

[117] Duan G, Jiang S, Chen S, Hou H. Heat and solvent resistant electrospun polybenzoxazole nanofibers from methoxy-containing polyaramide. J Nanomater 2010;2010: 219562/1-5.

[118] Zhang H, Jiang S, Duan G, Li J, Liu K, Zhou C, Hou H. Heat-resistant polybenzoxazole nanofibers made by electrospinning. Eur Polym J 2014;50:61-8.

[119] Sarkar A, Honkhambe PN, Avadhani CV, Wadgaonkar PP. Synthesis and characterization of poly(amideimide)s containing pendent flexible alkoxy chains. Eur Polym J 2007;43:3646-54.

[120] Sadavarte NV, Avadhani CV, Naik PV, Wadgaonkar PP. Regularly alternating poly(amideimide)s containing pendent pentadecyl chains: Synthesis and characterization. Eur Polym J 2010;46:1307-15.

Accepted Manuscript

ACCEPTED MANUSCRIPT

[121] Lee SH, Kim SY, Youn JR, Seong DG, Jee SY, Choi JI, Lee JR. Processing of continuous poly(amide-imide) nanofibers by electrospinning. Polym Int 2 0 10;59:212-7.

[122] Yokota R, Horiuchi R, Kochi M, Soma H, Mita I. High strength and high modulus aromatic polyimide/polyimide molecular composite films. J Polym Sci C Polym Lett 1988;26:215-23.

[123] Hasegawa M, Mita I, Kochi M, Yokota R. Miscibility of polyimide/polyimide blends and charge-transfer fluorescence spectra. Polymer 1991;32:3225-32.

[124] Tong YJ, Huang XD, Chung TS. A new strategy to prepare rodlike/flexible polyimide blends through poly(amic acid) amine salt precursors. Macromolecules 2001;34:5748-51.

[125] Zhang Q, Wu D, Qi S, Wu Z, Yang X, Jin R. Preparation of ultra-fine polyimide fibers containing silver nanoparticles via in situ technique. Mater Lett 2007;61:4027-30.

[126] Maceiras A, Martins P, Sebastián MS, Lasheras A, Silva M, Laza JM, Vilas JL, Gutierrez J, Lanceros-Mendez S, Barandiarán JM, León LM. Synthesis and characterization of novel piezoelectric nitrile copolyimide films for high temperature sensor applications. Smart Mater Struct 2014;23:105015/1-15.

[127] Lv YY, Xu W, Lin FW, Wu J, Xu ZK. Electrospun nanofibers of porphyrinated polyimide for the ultra-sensitive detection of trace TNT. Sens Actuators B 2 0 13;184:205-11.

[128] Yang Y, Wang Z, Ding Y, Lu Z, Sun H, Li Y, Wei J, Xiong R, Shi J, Liu Z, Lei Q. Research update: polyimide/$CaCu_3Ti_4O_{12}$ nanofiber functional hybrid films with improved dielectric properties. APL Mater 2013;1:050701/1-13.

[129] Ding J, Kong Y, Li P, Yang J. Polyimide/Poly(ethylene terephthalate) composite membrane by electrospinning for nonwoven separator for lithium-ion battery. J Electrochem Soc 2012;159:A1474-80.

[130] Takemori R, Ito G, Tanaka M, Kawakami H. Ultra-high proton conduction in electrospun sulfonated polyimide nanofibers. RSC Adv 2014;4:20005-9.

[131] Kim WJ, Chang JY. Molecularly imprinted polyimide nanofibers prepared by electrospinning. Mater Lett 2011;65:1388-91.

Accepted Manuscript

ACCEPTED MANUSCRIPT

[132] Lijo F, Marsano E, Vijila C, Barhate RS, Vijay VK, Ramakrishna S, Thavasi V. Electrospun polyimide/titanium dioxide composite nanofibrous membrane by electrospinning and electrospraying. J Nanosci Nanotechnol 2011;11:1154-9.

[133] Zhang T, Xu XL, Jin YN, Wu J, Xu ZK. Immobilization of horseradish peroxidase (HRP) on polyimide nanofibers blending with carbon nanotubes. J Mol Catal B 2014;106:56-62.

[134] Xu W, Ding Y, Jiang S, Zhu J, Ye W, Shen Y, Hou H. Mechanical flexible PI/MWCNTs nanocomposites with high dielectric permittivity by electrospinning. Eur Polym J 2014;59:129-35.

[135] Xu W, Ding Y, Jiang S, Chen L, Liao X, Hou H. Polyimide/$BaTiO_3$/MWCNTs three-phase nanocomposites fabricated by electrospinning with enhanced dielectric properties. Mater Lett 2014;135:158-61.

[136] Dhakshnamoorthy M, Ramakrishnan S, Vikram S, Kothurkar NK, Rangarajan M, Vasanthakumari R. In-situ preparation and characterization of acid functionalized single walled carbon nanotubes with polyimide nanofibers. J Nanosci Nanotechnol 2014;14:5011-8.

[137] Zha JW, Sun F, Wang SJ, Wang D, Lin X, Chen G, Dang ZM. Improved mechanical and electrical properties in electrospun polyimide/multiwalled carbon nanotubes nanofibrous composites. J Appl Phys 2014;116:134104/1-5.

[138] Mani D, Shanmugam R, Srinivasan V, Kothurkar NK, Rangarajan M, Raju V. Carbonization of electrospun polyimide/f-multiwalled carbon nanotubes nanofiber webs by RF-induction heating. Nanosci Nanotechnol Lett 2015;7:521-8.

[139] Liu M, Du Y, Miao YE, Ding Q, He S, Tjiu WW, Pan J, Liu T. Anisotropic conductive films based on highly aligned polyimide fibers containing hybrid materials of graphene nanoribbons and carbon nanotubes. Nanoscale 2015;7:1037-46.

[140] Ramakrishnan S, Dhakshnamoorthy M, Jelmy EJ, Vasanthakumari R, Kothurkar NK. Synthesis and characterization of graphene oxide-polyimide nanofiber composites. RSC Adv 2014;4:9743-9.

Accepted Manuscript

ACCEPTED MANUSCRIPT

[141] Wang C, Lan Y, Li X, Yu W, Qian Y. Improving the mechanical, electrical, and thermal properties of polyimide by incorporating functionalized graphene oxide. High Perform Polym 2015;5:1-9

[142] Yan H, Mahanta NK, Majerus LJ, Abramson AR, Cakmak M. Thermal conductivities of electrospun polyimide-mesophase pitch nanofibers and mats. Polym Eng Sci 2014;54:977-83.

[143] Cheng S, Shen D, Zhu X, Tian X, Zhou D, Fan LJ. Preparation of nonwoven polyimide/silica hybrid nanofiberous fabrics by combining electrospinning and controlled in situ sol-gel techniques. Eur Polym J 2009;45:2767-78.

[144] Gong G, Gao K, Wu J, Sun N, Zhou C, Zhao Y, Jiang L. A highly durable silica/polyimide superhydrophobic nanocomposite film with excellent thermal stability and abrasion-resistant performance. J Mater Chem A 2015;3:713-8.

[145] Ma W, Zhang Q, Samal SK, Wang F, Gao B, Pan H, Xu H, Yao J, Zhan X, De Smedt SC, Huang C. Core-sheath structured electrospun nanofibrous membranes for oil-water separation. RSC Adv 2016;6:41861-70.

[146] Shayapat J, Chung OH, Park JS. Electrospun polyimide-composite separator for lithium-ion batteries. Electrochim Acta 2015;170:110-21.

[147] Li XJ, Wei Q, Wang X. Preparation of magnetic polyimide/maghemite nanocomposite fibers by electrospinning. High Perform Polym 2014;26:810-6.

[148] Zhu J, Wei S, Chen X, Karki AB, Rutman D, Young DP, Guo Z. Electrospun polyimide nanocomposite fibers reinforced with core-shell Fe-FeO nanoparticles. J Phys Chem C 2010;114:8844-50.

[149] Liu L, Lv F, Li P, Ding L, Tong W, Chu PK, Zhang Y. Preparation of ultra-low dielectric constant silica/polyimide nanofiber membranes by electrospinning. Compos A Appl Sci Manuf 2016;84:292-8.

[150] Serbezeanu D, Popa AM, Sava I, Carja ID, Amberg M, Rossi RM, Fortunato G. Design and synthesis of polyimide–Gold nanofibers with tunable optical properties. Eur Polym J 2015;64:10-20.

[151] Zhang CL, Yu SH. Nanoparticles meet electrospinning: recent advances and future prospects. Chem Soc Rev 2014;43:4423-48.

Accepted Manuscript

ACCEPTED MANUSCRIPT

[152] Carlberg B, Ye LL, Liu J. Surface-confined synthesis of silver nanoparticle composite coating on electrospun polyimide nanofibers. Small 2011;7:3057-66.

[153] Han E, Wu D, Qi S, Tian G, Niu H, Shang G, Yan X, Yang X. Incorporation of silver nanoparticles into the bulk of the electrospun ultrafine polyimide nanofibers via a direct ion exchange self-metallization process. ACS Appl Mater Interfaces 2012;4:2583-90.

[154] Ding Q, Miao YE, Liu T. Morphology and photocatalytic property of hierarchical polyimide/ZnO fibers prepared via a direct ion-exchange process. ACS Appl Mater Interfaces 2013;5:5617-22.

[155] Li P, Lv F, Liu L, Ding L, Zhang Y. Transformation of iron oxides on PI electrospun membranes. J Magn Magn Mater 2016;414:105-10.

[156] Chang Z. "Firecracker-shaped" ZnO/polyimide hybrid nanofibers via electrospinning and hydrothermal process. Chem Commun 2011;47:4427-9.

[157] Chang Z, Zeng J. Immobilization seeding layers using precursor for fabricating core–shell polyimide/Cu–BTC hierarchical nanofibers with high gas separation and adsorption of methylene blue from aqueous solution. Macromol Chem Phys 2016;217:1007-13.

[158] Chen D, Miao YE, Liu T. Electrically conductive polyaniline/polyimide nanofiber membranes prepared via a combination of electrospinning and subsequent in situ polymerization growth. ACS Appl Mater Interfaces 2013;5:1206-12.

[159] Ye W, Zhu J, Liao X, Jiang S, Li Y, Fang H, Hou H. Hierarchical three-dimensional micro/nano-architecture of polyaniline nanowires wrapped-on polyimide nanofibers for high performance lithium-ion battery separators. J Power Sources 2015;299:417-24.

[160] Chang Z, Xu Y, Zhao X, Zhang Q, Chen D. Grafting poly(methyl methacrylate) onto polyimide nanofibers via "Click" reaction. ACS Appl Mater Interfaces 2009;1:2804-11.

[161] Dzenis YA. Structural nanocomposites. Science 2008;319:419-20.

[162] Dzenis YA. Spinning continuous fibers for nanotechnology. Science 2004;304:1917-9.

Accepted Manuscript

ACCEPTED MANUSCRIPT

[163] Papkov D, Zou Y, Andalib MN, Goponenko A, Cheng SZD, Dzenis YA. Simultaneously strong and tough ultrafine continuous nanofibers. ACS Nano 2013;7:3324-31.

[164] Mohammadzadehmoghadam S, Dong Y, Davies IJ. Recent progress in electrospun nanofibers: Reinforcement effect and mechanical performance. J Polym Sci B Polym Phys 2015;53:1171-212.

[165] Dzenis YC, Stephen Z, Harris F. Advanced single-polymer nanofiber-reinforced composite-towards next generation ultralight superstrong/tough structural material. Department of Mechanical and Materials Engineering, University of Nebraska-Lincoln, http://oai.dtic.mil/oai/oai?verb=getRecord&metadataPrefix=html&identifier=ADA618612, 2015. 39 pp

[166] Yao J, Bastiaansen CWM, Peijs T. High strength and high modulus electrospun nanofibers. Fibers 2014;2:158-86.

[167] Preston J. High-strength/high-modulus organic fibers. Polym Eng Sci 1975;15:199-206.

[168] Niu H, Qi S, Han E, Tian G, Wang X, Wu D. Fabrication of high-performance copolyimide fibers from 3,3',4,4'-biphenyltetracarboxylic dianhydride, p-phenylenediamine and 2-(4-aminophenyl)-6-amino-4(3H)-quinazolinone. Mater Lett 2012;89:63-5.

[169] Kaneda T, Katsura T, Nakagawa K, Makino H, Horio M. High-strength-high-modulus polyimide fibers II. Spinning and properties of fibers. J Appl Polym Sci 1986;32:3151-76.

[170] Liu J, Yue Z, Fong H. Continuous nanoscale carbon fibers with superior mechanical strength. Small 2009;5:536-42.

[171] Baji A, Mai YW, Wong SC, Abtahi M, Chen P. Electrospinning of polymer nanofibers: Effects on oriented morphology, structures and tensile properties. Compos Sci Technol 2010;70:703-18.

[172] Richard-Lacroix M, Pellerin C. Molecular orientation in electrospun fibers: From mats to single fibers. Macromolecules 2013;46:9473-93.

Accepted Manuscript

ACCEPTED MANUSCRIPT

[173] Hou H, Ge JJ, Zeng J, Li Q, Reneker DH, Greiner A, Cheng SZD. Electrospun polyacrylonitrile nanofibers containing a high concentration of well-aligned multiwall carbon nanotubes. Chem Mater 2005;17:967-73.

[174] Chen K, Zhang S, Liu B, Mao X, Sun G, Yu J, Al-Deyab SS, Ding B. Large-scale fabrication of highly aligned poly(m-phenylene isophthalamide) nanofibers with robust mechanical strength. RSC Adv 2014;4:45760-7.

[175] Tan EPS, Lim CT. Mechanical characterization of nanofibers - A review. Compos Sci Technol 2006;66:1102-11.

[176] Tan EPS, Lim CT. Novel approach to tensile testing of micro- and nanoscale fibers. Rev Sci Instrum 2004;75:2581-5.

[177] Wang M, Jin HJ, Kaplan DL, Rutledge GC. Mechanical properties of electrospun silk fibers. Macromolecules 2004;37:6856-64.

[178] Guhados G, Wan W, Hutter JL. Measurement of the elastic modulus of single bacterial cellulose fibers using atomic force microscopy. Langmuir 2005;21:6642-6.

[179] Gu SY, Wu QL, Ren J, Vancso GJ. Mechanical properties of a single electrospun fiber and its structures. Macromol Rapid Commun 2005;26:716-20.

[180] Tan EPS, Ng SY, Lim CT. Tensile testing of a single ultrafine polymeric fiber. Biomaterials 2005;26:1453-6.

[181] Li X, Gao H, Murphy CJ, Caswell KK. Nanoindentation of silver nanowires. Nano Lett 2003;3:1495-8.

[182] Tan EPS, Lim CT. Nanoindentation study of nanofibers. Appl Phys Lett 2005;87:123106/1-3.

[183] Zhao X, Wang C, Ji J, Sun Z. The controllable surface morphology of polyimide (PI) electrospun fibers. J Macromol Sci B Phys 2012;52:364-72.

[184] Fong H. Electrospun nylon 6 nanofiber reinforced Bis-GMA/TEGDMA dental restorative composite resins. Polymer 2004;45:2427-32.

[185] Fong H, Liu W, Wang CS, Vaia RA. Generation of electrospun fibers of nylon 6 and nylon 6-montmorillonite nanocomposite. Polymer 2002;43:775-80.

[186] Jiang S, Duan G, Hou H, Greiner A, Agarwal S. Novel layer-by-layer procedure for making nylon-6 nanofiber reinforced high strength, tough, and transparent

Accepted Manuscript

ACCEPTED MANUSCRIPT

thermoplastic polyurethane composites. ACS Appl Mater Interfaces 2012;4:4366-72.

[187] Jiang S, Duan G, Schöbel J, Agarwal S, Greiner A. Short electrospun polymeric nanofibers reinforced polyimide nanocomposites. Compos Sci Technol 2013;88:57-61.

[188] Jiang S, Greiner A, Agarwal S. Short nylon-6 nanofiber reinforced transparent and high modulus thermoplastic polymeric composites. Compos Sci Technol 2013;87:164-9.

[189] Jiang S, Hou H, Greiner A, Agarwal S. Tough and transparent nylon-6 electrospun nanofiber reinforced melamine-formaldehyde composites. ACS Appl Mater Interfaces 2012;4:2597-603.

[190] Xu W, Feng Y, Ding Y, Jiang S, Fang H, Hou H. Short electrospun carbon nanofiber reinforced polyimide composite with high dielectric permittivity. Mater Lett 2015;161:431-4.

[191] Tian M, Gao Y, Liu Y, Liao Y, Xu R, Hedin NE, Fong H. Bis-GMA/TEGDMA dental composites reinforced with electrospun nylon 6 nanocomposite nanofibers containing highly aligned fibrillar silicate single crystals. Polymer 2007;48:2720-8.

[192] Tian M, Gao Y, Liu Y, Liao Y, Hedin NE, Fong H. Fabrication and evaluation of Bis-GMA/TEGDMA dental resins/composites containing nano fibrillar silicate. Dent Mater 2008;24:235-43.

[193] Gao Y, Sagi S, Zhang L, Liao Y, Cowles DM, Sun Y, Fong H. Electrospun nano-scaled glass fiber reinforcement of bis-GMA/TEGDMA dental composites. J Appl Polym Sci 2008;110:2063-70.

[194] Chen Q, Zhao Y, Zhou Z, Rahman A, Wu XF, Wu W, Xu T, Fong H. Fabrication and mechanical properties of hybrid multi-scale epoxy composites reinforced with conventional carbon fiber fabrics surface-attached with electrospun carbon nanofiber mats. Compos B Eng 2013;44:1-7.

[195] Wu XF, Rahman A, Zhou Z, Pelot DD, Sinha-Ray S, Chen B, Payne S, Yarin AL. Electrospinning core-shell nanofibers for interfacial toughening and self-healing of carbon-fiber/epoxy composites. J Appl Polym Sci 2013;129:1383-93.

Accepted Manuscript

ACCEPTED MANUSCRIPT

[196] Sinha-Ray S, Pelot DD, Zhou ZP, Rahman A, Wu XF, Yarin AL. Encapsulation of self-healing materials by coelectrospinning, emulsion electrospinning, solution blowing and intercalation. J Mater Chem 2012;22:9138-46.

[197] Lee MW, An S, Lee C, Liou M, Yarin AL, Yoon SS. Self-healing transparent core-shell nanofiber coatings for anti-corrosive protection. J Mater Chem A 2014;2:7045-53.

[198] Lee MW, An S, Lee C, Liou M, Yarin AL, Yoon SS. Hybrid self-healing matrix using core-shell nanofibers and capsuleless microdroplets. ACS Appl Mater Interfaces 2014;6:10461-8.

[199] Yoshino A. The birth of the lithium-ion battery. Angew Chem Int Ed 2012;51:5798-800.

[200] Jansen AN, Kahaian AJ, Kepler KD, Nelson PA, Amine K, Dees DW, Vissers DR, Thackeray MM. Development of a high-power lithium-ion battery. J Power Sources 1999;81-82:902-5.

[201] Lu L, Han X, Li J, Hua J, Ouyang M. A review on the key issues for lithium-ion battery management in electric vehicles. J Power Sources 2013;226:272-88.

[202] Arora P, Zhang Z. Battery separators. Chem Rev 2004;104:4419-62.

[203] Huang X. Separator technologies for lithium-ion batteries. J Solid State Electrochem 2011;15:649-62.

[204] Hou H, Cheng C, Chen S, Zhou X, Lv X, He P, Kuang X, Ren J. Polymide blend nanofiber and its use in battery separator. US 9209444, 2015.

[205] Chen S, Ye W, Hou H. Electrospun fibrous membranes as separators of lithium-ion batteries. In: Ding B, Yu J, editors. Electrospun nanofibers for energy and environmental applications, New York: Springer, 2014. p. 91-110.

[206] Cao L, An P, Xu Z, Huang J. Performance evaluation of electrospun polyimide non-woven separators for high power lithium-ion batteries. J Electroanal Chem 2016;767:34-9.

[207] Kim YJ, Lee SM, Kim SH, Kim HS. Electrochemical and safety performances of polyimide nano fiber-based nonwoven separators for Li-ion batteries. J Electrochem Sci Technol 2015;6:26-33.

Accepted Manuscript

ACCEPTED MANUSCRIPT

[208] Jiang W, Liu Z, Kong Q, Yao J, Zhang C, Han P, Cui G. A high temperature operating nanofibrous polyimide separator in Li-ion battery. Solid State Ionics 2013;232:44-8.

[209] Lee J, Lee CL, Park K, Kim ID. Synthesis of an Al_2O_3-coated polyimide nanofiber mat and its electrochemical characteristics as a separator for lithium ion batteries. J Power Sources 2014;248:1211-7.

[210] Liang X, Yang Y, Jin X, Huang Z, Kang F. The high performances of SiO_2/Al_2O_3-coated electrospun polyimide fibrous separator for lithium-ion battery. J Membr Sci 2015;493:1-7.

[211] Liu Z, Jiang W, Kong Q, Zhang C, Han P, Wang X, Yao J, Cui G. A core@sheath nanofibrous separator for lithium ion batteries obtained by coaxial electrospinning. Macromol Mater Eng 2013;298:806-13.

[212] Chen W, Liu Y, Ma Y, Liu J, Liu X. Improved performance of PVdF-HFP/PI nanofiber membrane for lithium ion battery separator prepared by a bicomponent cross-electrospinning method. Mater Lett 2014;133:67-70.

[213] Chen W, Liu Y, Ma Y, Yang W. Improved performance of lithium ion battery separator enabled by co-electrospinning polyimide/poly(vinylidene fluoride-co-hexafluoropropylene) and the incorporation of TiO_2-(2-hydroxyethyl methacrylate). J Power Sources 2015;273:1127-35.

[214] Shi C, Zhang P, Huang S, He X, Yang P, Wu D, Sun D, Zhao J. Functional separator consisted of polyimide nonwoven fabrics and polyethylene coating layer for lithium-ion batteries. J Power Sources 2015;298:158-65.

[215] Liang X, Yang Y, Jin X, Cheng J. Polyethylene Oxide-coated electrospun polyimide fibrous separator for high-performance lithium-ion battery. J Mater Sci Technol 2016;32:200-6.

[216] Wu D, Shi C, Huang S, Qiu X, Wang H, Zhan Z, Zhang P, Zhao J, Sun D, Lin L. Electrospun nanofibers for sandwiched polyimide/poly (vinylidene fluoride)/polyimide separators with the thermal shutdown function. Electrochim Acta 2015;176:727-34.

[217] Stephan AM. Review on gel polymer electrolytes for lithium batteries. Eur Polym J 2006;42:21-42.

Accepted Manuscript

ACCEPTED MANUSCRIPT

[218] Wang Q, Song WL, Wang L, Song Y, Shi Q, Fan LZ. Electrospun polyimide-based fiber membranes as polymer electrolytes for lithium-ion batteries. Electrochim Acta 2014;132:538-44.

[219] Wang Q, Jian Z, Song WL, Zhang S, Fan LZ. Facile fabrication of safe and robust polyimide fibrous membrane based on triethylene glycol diacetate-2-propenoic acid butyl ester gel electrolytes for lithium-ion batteries. Electrochim Acta 2014;149:176-85.

[220] Borup R, Meyers J, Pivovar B, Kim YS, Mukundan R, Garland N, Myers D, Wilson M, Garzon F, Wood D, Zelenay P, More K, Stroh K, Zawodzinski T, Boncella J, McGrath JE, Inaba M, Miyatake K, Hori M, Ota K, Ogumi Z, Miyata S, Nishikata A, Siroma Z, Uchimoto Y, Yasuda K, Kimijima K, Iwashita N. Scientific aspects of polymer electrolyte fuel cell durability and degradation. Chem Rev 2007;107:3904-51.

[221] Diat O, Gebel G. Fuel cells: Proton channels. Nat Mater 2008;7:13-4.

[222] Schmidt-Rohr K, Chen Q. Parallel cylindrical water nanochannels in Nafion fuel-cell membranes. Nat Mater 2008;7:75-83.

[223] Lee JR, Kim NY, Lee MS, Lee SY. SiO_2-coated polyimide nonwoven/Nafion composite membranes for proton exchange membrane fuel cells. J Membr Sci 2011;367:265-72.

[224] Takemori R, Kawakami H. Electrospun nanofibrous blend membranes for fuel cell electrolytes. J Power Sources 2010;195:5957-61.

[225] Lv YY, Wu J, Wan LS, Xu ZK. Novel porphyrinated polyimide nanofibers by electrospinning. J Phys Chem C 2008;112:10609-15.

[226] Yen HJ, Chen CJ, Liou GS. Novel high-efficiency PL polyimide nanofiber containing aggregation-induced emission (AIE)-active cyanotriphenylamine luminogen. Chem Commun 2013;49:630-2.

[227] Qin C, Wang J, Cheng S, Wang X, Dai L, Chen G. Fluorescent performance of electrospun polyimide web mixed with hemicyanine dye. Mater Lett 2009;63:1239-41.

Accepted Manuscript

ACCEPTED MANUSCRIPT

[228] Wu JH, Liou GS. High-efficiency fluorescent polyimides based on locally excited triarylamine-containing dianhydride moieties. Polym Chem 2015;6:5225-32.

[229] Kurosawa T, Higashihara T, Ueda M. Polyimide memory: a pithy guideline for future applications. Polym Chem 2013;4:16-30.

[230] Ruh D, Reith P, Sherman S, Theodor M, Ruhhammer J, Seifert A, Zappe H. Stretchable optoelectronic circuits embedded in a polymer network. Adv Mater 2014;26:1706-10.

[231] Xu H, Yang H, Tao L, Liu J, Fan L, Yang S. Preparation and properties of glass cloth-reinforced meltable thermoplastic polyimide composites for microelectronic packaging substrates. High Perform Polym 2010;22:581-97.

[232] Ree M. High performance polyimides for applications in microelectronics and flat panel displays. Macromol Res 2006;14:1-33.

[233] Kuntman A, Kuntman H. A study on dielectric properties of a new polyimide film suitable for interlayer dielectric material in microelectronics applications. Microelectron J 2000;31:629-34.

[234] Jiang LY, Leu CM, Wei KH. Layered Silicates/fluorinated polyimide nanocomposites for advanced dielectric materials applications. Adv Mater 2002;14:426-9.

[235] Xia J, Zhang G, Deng L, Yang H, Sun R, Wong C-P. Flexible and enhanced thermal conductivity of a Al_2O_3@polyimide hybrid film via coaxial electrospinning. RSC Adv 2015;5:19315-20.

[236] Lingaiah S, Shivakumar K. Electrospun high temperature polyimide nanopaper. Eur Polym J 2013;49:2101-8.

[237] Xia J, Li J, Zhang G, Zeng X, Niu F, Yang H, Sun R, Wong C. Highly mechanical strength and thermally conductive bismaleimide–triazine composites reinforced by Al_2O_3@polyimide hybrid fiber. Compos A Appl Sci Manuf 2016;80:21-7.

[238] Liu J, Min Y, Chen J, Zhou H, Wang C. Preparation of the ultra-low dielectric constant polyimide fiber membranes enabled by electrospinning. Macromol Rapid Commun 2007;28:215-9.

Accepted Manuscript

ACCEPTED MANUSCRIPT

[239] Chen F, Bera D, Banerjee S, Agarwal S. Low dielectric constant polyimide nanomats by electrospinning. Polym Adv Technol 2012;23:951-7.

[240] Li P, Liu L, Ding L, Lv F, Zhang Y. Thermal and dielectric properties of electrospun fiber membranes from polyimides with different structural units. J Appl Polym Sci 2016;133:43081/1-7.

[241] Zhang R, Liu C, Hsu PC, Zhang C, Liu N, Zhang J, Lee HR, Lu Y, Qiu Y, Chu S, Cui Y. Nanofiber air filters with high-temperature stability for efficient $PM_{2.5}$ removal from the pollution sources. Nano Lett 2016;16:3642-9.

[242] Wang Q, Bai Y, Xie J, Jiang Q, Qiu Y. Synthesis and filtration properties of polyimide nanofiber membrane/carbon woven fabric sandwiched hot gas filters for removal of PM 2.5 particles. Powder Technol 2016;292:54-63.

[243] Wang Q, Bai Y, Xie J, Qiu Y, Jiang Q. Multi-scale polyimide/carbon fibers hybrid filters for hot gas filtration. Mater Sci Forum 2015;814:464-9.

[244] Feng XJ, Jiang L. Design and creation of superwetting/antiwetting surfaces. Adv Mater 2006;18:3063-78.

[245] Liu M, Zheng Y, Zhai J, Jiang L. Bioinspired super-antiwetting interfaces with special liquid−solid adhesion. Acc Chem Res 2009;43:368-77.

[246] Nuraje N, Khan WS, Lei Y, Ceylan M, Asmatulu R. Superhydrophobic electrospun nanofibers. J Mater Chem A 2013;1:1929-46.

[247] Acatay K, Simsek E, Ow-Yang C, Menceloglu YZ. Tunable, superhydrophobically stable polymeric surfaces by electrospinning. Angew Chem Int Ed 2004;43:5210-3.

[248] Ma M, Hill RM, Lowery JL, Fridrikh SV, Rutledge GC. Electrospun poly(styrene-block-dimethylsiloxane) block copolymer fibers exhibiting superhydrophobicity. Langmuir 2005;21:5549-54.

[249] Lin J, Cai Y, Wang X, Ding B, Yu J, Wang M. Fabrication of biomimetic superhydrophobic surfaces inspired by lotus leaf and silver ragwort leaf. Nanoscale 2011;3:1258-62.

[250] Liu J, Huang J, Wujcik EK, Qiu B, Rutman D, Zhang X, Salazard E, Wei S, Guo Z. Hydrophobic electrospun polyimide nanofibers for self-cleaning materials. Macromol Mater Eng 2015;300:358-68.

Accepted Manuscript

ACCEPTED MANUSCRIPT

[251] Li XM, Reinhoudt D, Crego-Calama M. What do we need for a superhydrophobic surface? A review on the recent progress in the preparation of superhydrophobic surfaces. Chem Soc Rev 2007;36:1350-68.

[252] Gong G, Wu J, Liu J, Sun N, Zhao Y, Jiang L. Bio-inspired adhesive superhydrophobic polyimide mat with high thermal stability. J Mater Chem 2 0 12;22:8257-62.

[253] Gong G, Wu J, Zhao Y, Liu J, Jin X, Jiang L. A novel fluorinated polyimide surface with petal effect produced by electrospinning. Soft Matter 2014;10:549-52.

[254] Oktay B, Toker RD, Kayaman-Apohan N. Superhydrophobic behavior of polyimide–siloxane mats produced by electrospinning. Polym Bull 2015;72:2831-42.

[255] Xin B, Hao J. Reversibly switchable wettability. Chem Soc Rev 2010;39:769-82.

[256] Weng CJ, Jhuo YS, Chang CH, Feng CF, Peng CW, Dai CF, Yeh JM, Wei Y. A smart surface prepared using the switchable superhydrophobicity of neat electrospun intrinsically electroactive polyimide fiber mats. Soft Matter 2011;7:10313-8.

[257] Kim C, Yang KS. Electrochemical properties of carbon nanofiber web as an electrode for supercapacitor prepared by electrospinning. Appl Phys Lett 2003;83:1216-8.

[258] Guo Q, Zhou X, Li X, Chen S, Seema A, Greiner A, Hou H. Supercapacitors based on hybrid carbon nanofibers containing multiwalled carbon nanotubes. J Mater Chem 2009;19:2810-6.

[259] Kim C, Yang KS, Kojima M, Yoshida K, Kim YJ, Kim YA, Endo M. Fabrication of electrospinning-derived carbon nanofiber webs for the anode material of lithium-ion secondary batteries. Adv Funct Mater 2006;16:2393-7.

[260] Nan D, Wang JG, Huang ZH, Wang L, Shen W, Kang F. Highly porous carbon nanofibers from electrospun polyimide/SiO_2 hybrids as an improved anode for lithium-ion batteries. Electrochem Commun 2013;34:52-5.

Accepted Manuscript

ACCEPTED MANUSCRIPT

[261] Huang J, Liu Y, Hou H, You T. Simultaneous electrochemical determination of dopamine, uric acid and ascorbic acid using palladium nanoparticle-loaded carbon nanofibers modified electrode. Biosens Bioelectron 2008;24:632-7.

[262] Chen S, Hou H, Harnisch F, Patil SA, Carmona-Martinez AA, Agarwal S, Zhang Y, Sinha-Ray S, Yarin AL, Greiner A, Schroder U. Electrospun and solution blown three-dimensional carbon fiber nonwovens for application as electrodes in microbial fuel cells. Energy Environ Sci 2011;4:1417-21.

[263] Huang J, Wang D, Hou H, You T. Electrospun palladium nanoparticle-loaded carbon nanofibers and their electrocatalytic activities towards hydrogen peroxide and NADH. Adv Funct Mater 2008;18:441-8.

[264] Rahaman MSA, Ismail AF, Mustafa A. A review of heat treatment on polyacrylonitrile fiber. Polym Degrad Stab 2007;92:1421-32.

[265] Nataraj SK, Yang KS, Aminabhavi TM. Polyacrylonitrile-based nanofibers-A state-of-the-art review. Prog Polym Sci 2012;37:487-513.

[266] Zhang L, Aboagye A, Kelkar A, Lai C, Fong H. A review: carbon nanofibers from electrospun polyacrylonitrile and their applications. J Mater Sci 2013;49:463-80.

[267] Inagaki M, Ohta N, Hishiyama Y. Aromatic polyimides as carbon precursors. Carbon 2013;61:1-21.

[268] Kim C, Choi YO, Lee WJ, Yang KS. Supercapacitor performances of activated carbon fiber webs prepared by electrospinning of PMDA-ODA poly(amic acid) solutions. Electrochim Acta 2004;50:883-7.

[269] Yan H, Mahanta NK, Wang B, Wang S, Abramson AR, Cakmak M. Structural evolution in graphitization of nanofibers and mats from electrospun polyimide-mesophase pitch blends. Carbon 2014;71:303-18.

[270] Xuyen NT, Ra EJ, Geng HZ, Kim KK, An KH, Lee YH. Enhancement of conductivity by diameter control of polyimide-based electrospun carbon nanofibers. J Phys Chem B 2007;111:11350-3.

[271] Kim C, Cho YJ, Yun WY, Ngoc BTN, Yang KS, Chang DR, Lee JW, Kojima M, Kim YA, Endo M. Fabrications and structural characterization of ultra-fine

ACCEPTED MANUSCRIPT

carbon fibres by electrospinning of polymer blends. Solid State Commun 2007;142:20-3.

[272] Chung GS, Jo SM, Kim BC. Properties of carbon nanofibers prepared from electrospun polyimide. J Appl Polym Sci 2005;97:165-70.

[273] Seki N, Arai T, Suzuki Y, Kawakami H. Novel polyimide-based electrospun carbon nanofibers prepared using ion-beam irradiation. Polymer 2012;53:2062-7.

[274] Sode K, Sato T, Tanaka M, Suzuki Y, Kawakami H. Carbon nanofibers prepared from electrospun polyimide, polysulfone and polyacrylonitrile nanofibers by ion-beam irradiation. Polym J 2013;45:1210-5.

[275] Jung KH, Ferraris JP. Preparation and electrochemical properties of carbon nanofibers derived from polybenzimidazole/polyimide precursor blends. Carbon 2012;50:5309-15.

[276] Wang J, Yang Y, Kang F. Porous carbon nanofiber paper as an effective interlayer for high-performance lithium-sulfur batteries. Electrochim Acta 2015;168:271-6.

[277] Le T, Yang Y, Huang Z, Kang F. Preparation of microporous carbon nanofibers from polyimide by using polyvinyl pyrrolidone as template and their capacitive performance. J Power Sources 2015;278:683-92.

[278] Le TH, Yang Y, Yu L, Gao T, Huang Z, Kang F. Polyimide-based porous hollow carbon nanofibers for supercapacitor electrode. J Appl Polym Sci 2016;133:43397/1-7.

[279] Xuyen NT, Jeong HK, Kim G, So KP, An KH, Lee YH. Hydrolysis-induced immobilization of $Pt(acac)_2$ on polyimide-based carbon nanofiber mat and formation of Pt nanoparticles. J Mater Chem 2009;19:1283-8.

[280] Ding Q, Liu M, Miao YE, Huang Y, Liu T. Electrospun nickel-decorated carbon nanofiber membranes as efficient electrocatalysts for hydrogen evolution reaction. Electrochim Acta 2015;159:1-7.

[281] Zhang L, Ding Q, Huang Y, Gu H, Miao YE, Liu T. Flexible hybrid membranes with $Ni(OH)_2$ nanoplatelets vertically grown on electrospun carbon nanofibers for high-performance supercapacitors. ACS Appl Mater Interfaces 2015;7:22669-77.

Accepted Manuscript

ACCEPTED MANUSCRIPT

[282] Miao YE, Yan J, Huang Y, Fan W, Liu T. Electrospun polymer nanofiber membrane electrodes and an electrolyte for highly flexible and foldable all-solid-state supercapacitors. RSC Adv 2015;5:26189-96.

[283] Li Y, Dong J, Zhang J, Zhao X, Yu P, Jin L, Zhang Q. Nitrogen-doped carbon membrane derived from polyimide as free-standing electrodes for flexible supercapacitors. Small 2015;11:3476-84.

[284] Xia L, Wang S, Liu G, Ding L, Li D, Wang H, Qiao S. Flexible SnO_2/N-doped carbon nanofiber films as integrated electrodes for lithium-ion batteries with superior rate capacity and long cycle life. Small 2016;12:853-9.

[285] Wang S, Xia L, Yu L, Zhang L, Wang H, Lou XW. Free-standing nitrogen-doped carbon nanofiber films: Integrated electrodes for sodium-ion batteries with ultralong cycle life and superior rate capability. Adv Energy Mater 2016;6:201502217/1-7.

[286] Liu Q, Wang Y, Dai L, Yao J. Scalable fabrication of nanoporous carbon fiber films as bifunctional catalytic electrodes for flexible Zn-Air batteries. Adv Mater 2016;28:3000-6.

[287] Gautam AK, Lai C, Fong H, Menkhaus TJ. Electrospun polyimide nanofiber membranes for high flux and low fouling microfiltration applications. J Membr Sci 2014;466:142-50.

[288] Li S, Wu D, Yan X, Guan Y. Acetone-activated polyimide electrospun nanofiber membrane for thin-film microextraction and thermal desorption-gas chromatography–mass spectrometric analysis of phenols in environmental water. J Chromatogr A 2015;1411:1-8.

[289] Jirsak O, Sysel P, Sanetrnik F, Hruza J, Chaloupek J. Polyamic acid nanofibers produced by needleless electrospinning. J Nanomater 2010;2010: 842831/1-6.

[290] Jain N, Chakraborty J, Tripathi SK, Nasim M. Fabrication and characterization of insitu synthesized iron oxide-modified polyimide nanoweb by needleless electrospinning. J Appl Polym Sci 2014;131:40432/1-10.

[291] Carnell LS, Siochi EJ, Holloway NM, Stephens RM, Rhim C, Niklason LE, Clack RL. Aligned mats from electrospun single fibers. Macromolecules 2008;41:5345-9.

Accepted Manuscript

ACCEPTED MANUSCRIPT

Fig. 1 Illustration of two-step method for synthesizing polyimides (PIs) and chemical structures of some commonly used diamines and dianhydrides.

Fig. 2 The numbers of publications with the keywords of "polyimide fiber" (a) and "polyimide nanofiber" (b) acquired from the Web of Knowledge^{SM} on May 22, 2016.

Fig. 3 Fabrication of electrospun PI nanofiber nonwovens/fabrics in industrial scale.

Fig. 4 Schematic illustration of a laboratory setup for electrospinning.

Fig. 5 Microscopic images of electrospun nanofibers with different morphologies: a) Cylindrical PAN nanofibers [45]. Copyright 2009, Reproduced with permission from Elsevier B.V.; b) Porous PLLA nanofibers [46]. Copyright 2001, Reproduced with permission from John Wiley & Sons, Inc.; c) TiO_2/PVP hollow nanofibers [48]. Copyright 2004, Reproduced with permission from American Chemical Society; d) PDT/PEO core-shell nanofiber [50]. Copyright 2003, Reproduced with permission from John Wiley & Sons, Inc.; e) TiO_2 multi-channel nanotubes [52]. Copyright 2007, Reproduced with permission from American Chemical Society; f) Poly(ether imide) nano-ribbons [33]. Copyright 2001, Reproduced with permission from John Wiley & Sons, Inc.; g) Bead-on-string PVP-oil nanofibers [55]. Copyright 2006, Reproduced with permission from John Wiley & Sons, Inc.; h) Carbon nanotubes growth on

Accepted Manuscript

ACCEPTED MANUSCRIPT

electrospun carbon nanofibers [57]. Copyright 2004, Reproduced with permission from John Wiley & Sons, Inc.

Fig. 6 SEM images of well-aligned electrospun nanofibers and schematic setups used for collecting aligned nanofibers: a) SEM images of well-aligned PVA nanofibers [80]. Copyright 2006, Reproduced with permission from Elsevier B.V.; b) Parallel electrode collector with a gap between two conductive substrates [78]. Copyright 2003, Reproduced with permission from American Chemical Society; c) Dual rings collector [79]. Copyright 2005, Reproduced with permission from Elsevier B.V.; d) Two oppositely placed metallic needles with opposite voltages [80]. Copyright 2006, Reproduced with permission from Elsevier B.V.; e) Collection of aligned magnetized nanofibers with magnetic field [81]. Copyright 2007, Reproduced with permission from John Wiley & Sons, Inc.; f) Collector of rotating disc with high speed [82]. Copyright 2001, Reproduced with permission from IOP Publishing; g) Rotating wire drum collector [83]. Copyright 2004, Reproduced with permission from American Chemical Society; h) Yarn collection by using an electrically grounded water bath [84]. Copyright 2005, Reproduced with permission from Elsevier B.V.

Fig. 7 Chemical schemes showing the two-step method for synthesis of homo-PIs: a) PMDA-ODA PI and b) BPDA-PDA PI.

Fig. 8 SEM images of PI nanofibers after imidization. PAA precursor nanofibers were obtained from electrospinning of solutions with varied concentrations of DEDAC (left images) followed by being aged in vacuum at

Accepted Manuscript

ACCEPTED MANUSCRIPT

different temperature (top images) [111]. Copyright 2011, Reproduced with permission from Elsevier B.V.

Fig. 9 Chemical scheme showing the synthesis of BPDA-BPA-ODA co-PI through polymerization of BPDA with two diamines of ODA and BPA.

Fig. 10 Chemical schemes showing the preparation and thermal conversion of PBO nanofibers through OH-PAA (a) [118]. Copyright 2014, Reproduced with permission from Elsevier B.V.; and PI-co-PBO nanofibers through MeO-PAA (b) [102]. Copyright 2015, Reproduced with permission from Royal Society of Chemistry.

Fig. 11 Chemical scheme showing thermal imidization of PAI (a); and SEM images showing fracture surfaces of PAI nanofibers imidized at 330 °C (b) and at 400 °C under tension after the glycerol pre-treatment (c) [121]. Copyright 2010, Reproduced with permission from John Wiley & Sons, Inc.

Fig. 12 Schematic diagrams depicting the preparations of blend-PI and co-PI [96]. Copyright 2014, Reproduced with permission from Royal Society of Chemistry.

Fig. 13 a) TEM image of electrospun PI/Ag nanofiber with 2 wt.% of Ag [125]. Copyright 2007, Reproduced with permission from Elsevier B.V.; b) TEM image of electrospun PI/SiO_2 nanofiber with 6.58 wt.% of SiO_2 [143]. Copyright 2009, Reproduced with permission from Elsevier B.V.

Fig. 14 Schematic illustration showing the preparation of PI/Ag composite nanofibers by stepped processes of hydrolysis, ion-exchange, and finally

Accepted Manuscript

ACCEPTED MANUSCRIPT

reduction (thermal reduction and chemical reduction) [152]. Copyright 2011, Reproduced with permission from John Wiley & Sons, Inc.

Fig. 15 a) Schematic illustration showing the combined processes of electrospinning and hydrothermal growth to prepare ZnO nanorods on PI nanofibers; b) SEM image of pristine PI nanofibers; c) SEM image of ZnO seeds on PI nanofiber; d) SEM image of ZnO/PI hybrid nanofiber [156]. Copyright 2011, Reproduced with permission from Royal Society of Chemistry.

Fig. 16 a) Photograph of micro-tension testing machine with a paper frame carrying an individual nanofiber into the clamps for testing; b) Photograph showing the tensile stretching of an individual nanofiber; c) Schematic diagram of the paper frame holding an individual nanofiber for the test before and after the fiber is broken [90]. Copyright 2008, Reproduced with permission from IOP Publishing.

Fig. 17 Typical stress-strain curves of individual electrospun PAA nanofiber (a) and PI nanofiber (b); XRD patterns (c) of PI film (with thickness of 18 μm) and electrospun nanofiber mats (multilayer aligned and non-aligned PI nanofiber mats); d) TEM-fractographical analysis of an individual PI nanofiber after tensile failure [90]. Copyright 2008, Reproduced with permission from IOP Publishing.

Fig. 18 a) Chemical and structural conversion of electrospun BPDA-PDA PAA nanofibers into BPDA-PDA PI nanofibers; b) IR spectra of BPDA-PDA nanofiber mats cured at 300 °C and 430 °C, respectively; c) XRD patterns of

Accepted Manuscript

ACCEPTED MANUSCRIPT

PBDA-PDA PI film and electrospun nanofiber mat [88]. Copyright 2006, Reproduced with permission from John Wiley & Sons, Inc.

Fig. 19 a) Typical stress-strain curves of aligned O-PI, B-PI, co-PI nanofiber belts; b) relationships between mechanical properties and BPA moiety content in the PIs; curve (A): strain, curve (B): tensile strength, curve (C): elastic modulus [91]. Copyright 2008, Reproduced with permission from IOP Publishing.

Fig. 20 Photograph showing an electrospun co-PI nanofiber belt (with width and thickness of 7.5 mm and 12 μm, respectively) capable of hanging a weight of 10 kg [91]. Copyright 2008, Reproduced with permission from IOP Publishing.

Fig. 21 Schematic representation showing high-strength PI nanofiber composed of the ordered flexible and rigid micro-block regions [91]. Copyright 2008, Reproduced with permission from IOP Publishing.

Fig. 22 Schematic representation showing the microstructure of blend-PI nanofiber with rigid and flexible components [96]. Copyright 2014, Reproduced with permission from Royal Society of Chemistry.

Fig. 23 a) Digital images of Celgard membrane, PI nanofiber mats/membranes with the thickness values of 40 μm (b) and 100 μm (c) before (a, b, c) and after (d, e, f) the thermal test at 150 °C; b) Rate capability tests for the cells with Celgard membrane and PI nanofiber mat/membrane as separators [95]. Copyright 2013, Reproduced with permission from Elsevier B.V.

Accepted Manuscript

ACCEPTED MANUSCRIPT

Fig. 24 a) SEM image showing the cross-section of PI/PET composite membrane [129]. Copyright 2012, Reproduced with permission from The Electrochemical Society; b) SEM image showing the cross-section of Al_2O_3-PI separator [209]. Copyright 2014, Reproduced with permission from Elsevier B.V.

Fig. 25 Illustration showing the shutdown behavior of the sandwiched PI/PVDF/PI nanofiber separator [216]. Copyright 2015, Reproduced with permission from Elsevier B.V.

Fig. 26 Chemical structures of sulfonated PIs [208, 210].

Fig. 27 Chemical schemes depicting the syntheses and molecular structures of porphyrinated co-PIs made from *trans*-DATPP (a) and *cis*-DATPP (b) [225]. Copyright 2008, Reproduced with permission from American Chemical Society.

Fig. 28 (a) Molecular structure of porphyrinated PI and schematic illustration showing the porphyrinated nanofiber membrane for fluorescent detection of TNT; SEM micrograph (b), and CLSM images of the porphyrinated nanofiber membrane before (c) and after (d) exposing to 10 ppb TNT vapor (λ_{ex} = 488 nm) [127]. Copyright 2013, Reproduced with permission from Elsevier B.V.

Fig. 29 An example of using the PI nanopaper for flexible antenna [236]. Copyright 2013, Reproduced with permission from Elsevier B.V.

Fig. 30 Structure and PM removal performance of PI nanofiber air filters: (a) General molecular structure of PI; (b) Schematic representation showing the

Accepted Manuscript

ACCEPTED MANUSCRIPT

fabrication of transparent PI air filters by electrospinning; (c) Photograph of a typical transparent PI air filter with optical transmittance of 70%; (d) OM image of a transparent PI air filter; (e−g) SEM images acquired from the PI air filters with different magnifications; (h) SEM image of a PI air filter with captured PM particles; (i) OM image of a PI air filter with captured PM particles. (j) PM removal efficiencies of the PI air filter with optical transmittance of 50%; (k) Demonstration of using the PI nanofiber air filter to block the PM from the sources (left bottle) entering the environment (right bottle) [241]. Copyright 2016, Reproduced with permission from American Chemical Society.

Fig. 31 Long-term performance and practical application of PI air filters: (a) Long-term $PM_{2.5}$ and $PM_{2.5-10}$ removal efficiencies by the PI nanofiber air filter with transmittance of 50% under continuous hazardous condition of PM pollution; (b) PM number concentration measurement of vehicle exhaust gas without air filter. (c) PM number concentration measurement of vehicle exhaust gas with air filter; (d) Removal efficiencies of PM particles from vehicle exhaust gas [241]. Copyright 2016, Reproduced with permission from American Chemical Society.

Fig. 32 Scheme showing the synthesis of electro-active PAA and PI [256]. Copyright 2011, Reproduced with permission from Royal Society of Chemistry.

Fig. 33 Reversible super-hydrophobic/super-hydrophilic conversions of the EPF through doping with PFOS and de-doping by ammonia gas [256]. Copyright 2011, Reproduced with permission from Royal Society of Chemistry.

ACCEPTED MANUSCRIPT

Fig. 34 Preparation of carbon nanofiber membrane derived from PI: a) Electrospinning PI membrane; b) Carbonization of PI membrane in a furnace at 1000 °C; c) Photograph of the resulting $Carbon_{PI}$ membrane and molecular structure showing the nitrogen doping; d) Chemical structure of PI polymer [283]. Copyright 2015, Reproduced with permission from John Wiley & Sons, Inc.

Table 1 Summary of mechanical and thermal properties of electrospun PI nanofibers

	Sample	Tensile strength (MPa)	Elastic modulus (GPa)	Elongation at break (%)	Toughness (J/g or MPa)	Tg (°C)	5% weight loss temp. (°C)	Ref e
Homo-PI	BPDA-PDA	663.7	15.3	4.9	17.5	310.2	508.8	[8
	BPDA-PDA	1700*	76*	3*	–	–	–	[9
	BPDA-BPA	384 ± 18	11.5 ± 0.6	3.9 ± 0.1	–	–	523.6	[9
	BPDA-ODA	459 ± 36	2.1 ± 0.3	41.3 ± 2.2	120	275.7	463.9	[9
	BPDA-PRM	345 ± 22	10.2 ± 1.2	4 ± 1	–	288.9	598.4	[9
	BPDA-6FBAPP	308 ± 14	2.08 ± 0.25	201.9 ± 6.8	365 ± 20	265.2	450	[9
	ODPA-ODA	186.8 ± 20	2.47 ± 0.34	64.1 ± 10	–	~250	583	[9
Co-PI	BPDA-BPA-ODA (BPA/ODA = 4/6)	1103 ± 61	6.2 ± 0.7	20.8 ± 1.2	115	292.6	500.6	[9

ACCEPTED MANUSCRIPT

	BPDA-PDA-ODA (PDA/ODA = 9/1)	845	10.67	9.14	32.5	307.1	499.7	[1
	BPDA-PDA-ODA (PDA/ODA = 1/1)	1040	10	13.5	77 ± 5	–	–	[1
	BPDA-PRM-ODA (PRM/ODA = 5/5)	1161 ± 64	6.3 ± 0.5	21 ± 2	–	261.9	572.6	[9
	BPDA-PRM-ODA (PRM/ODA = 5/5)	1.77*	59*	~17.5*	–	–	–	[9
Blend-PI	BPDA-BPA/BPDA-ODA, 8/2	668.17	10.77	4.68	9.86	287	584	[9
	BPDA-BPA/BPDA-ODA, 6/4	919.44	8.31	7.84	24.53	299	555	[9
	BPDA-BPA/BPDA-ODA, 4/6	1299.43	7.68	15.80	81.79	296	545	[9
	BPDA-BPA/BPDA-ODA, 2/8	1061.95	5.50	22.62	94.25	–	536	[9
Compose PI	ODPA-ODA/CNTs (3.5 wt.%)	239.7 ± 21	2.56 ± 0.15	90.5 ± 11	–	~245	603	[9

* Mechanical properties of individual nanofibers

Table 2 Thermo-mechanical properties of electrospun PI, PI-co-PBO, and PBO nanofibers

Sample	Strength (MPa)				Modulus (GPa)				Reference
	25 °C	250 °C	300 °C	400 °C	25 °C	250 °C	300 °C	400 °C	
BPDA-BPA (370 °C)	421	393	235	92.5	8.46	7.83	4.98	3.42	[100]
BPDA-BPA (450 °C)	641	603	510	330	13.09	12.86	12.41	9.38	[100]
PI-co-PBO	518	379	303	217	8.36	7.18	6.37	5.01	[102]
PBO (BPDA-DHB)	537	533	520	444*	8.3	7.9	7.5	6.5*	[118]

* Thermo-mechanical properties of PBO nanofibers at 380 °C

ACCEPTED MANUSCRIPT

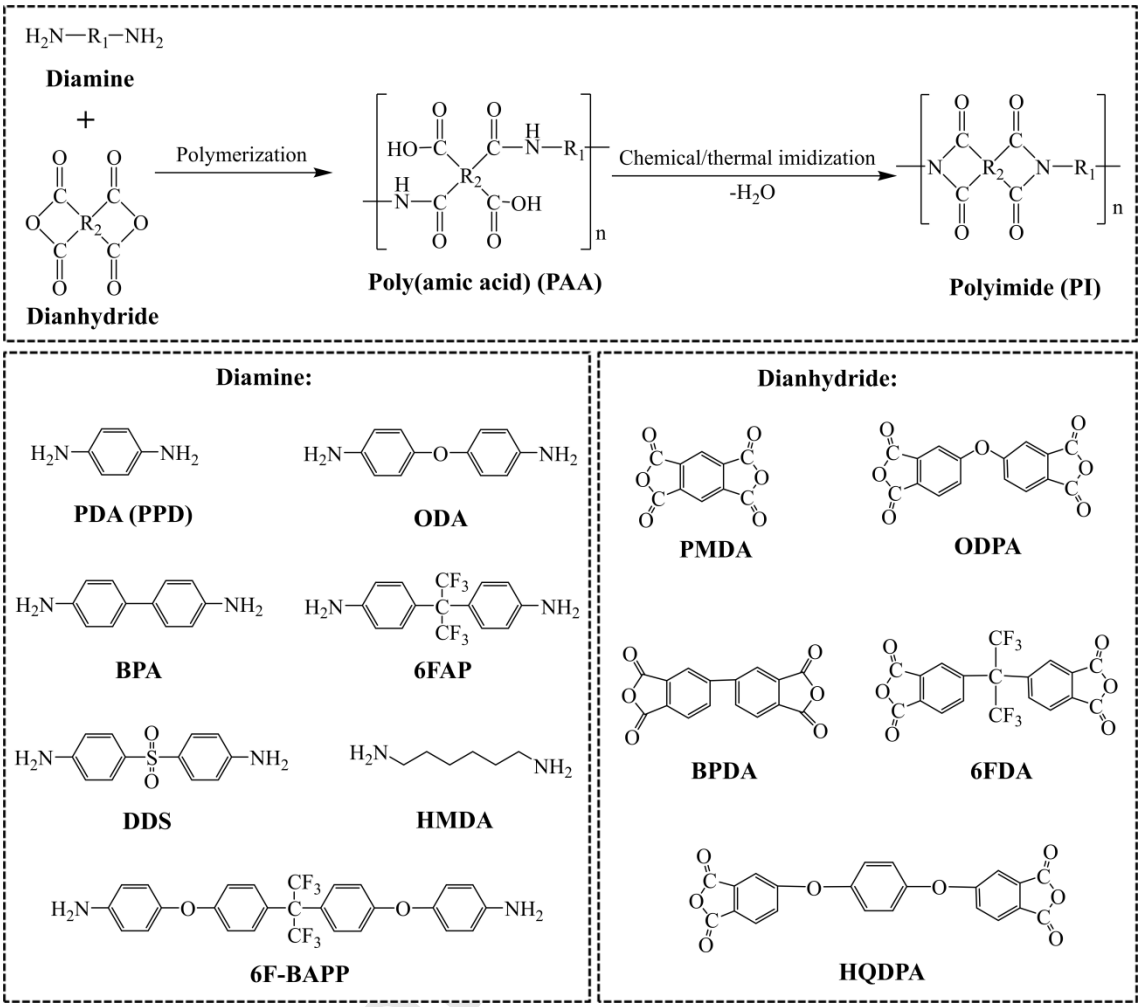

Fig 1. Illustration of two-step method for synthesizing polyimides (PIs) and chemical structures of some commonly used diamines and dianhydrides.

ACCEPTED MANUSCRIPT

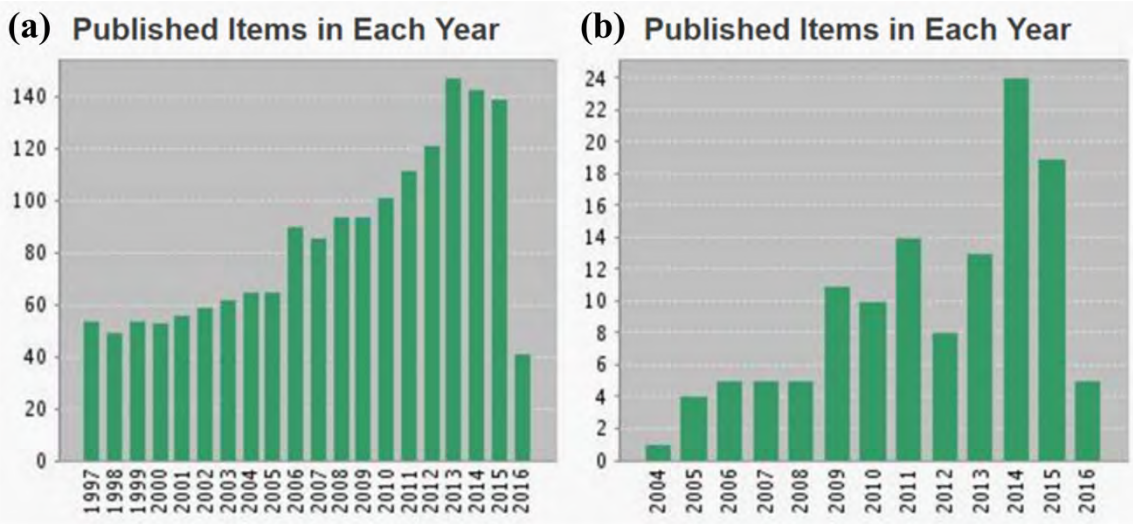

Fig 2. The numbers of publications with the keywords of "polyimide fiber" (a) and "polyimide nanofiber" (b) acquired from the Web of Knowledge^{SM} on May 22, 2016.

Accepted Manuscript

ACCEPTED MANUSCRIPT

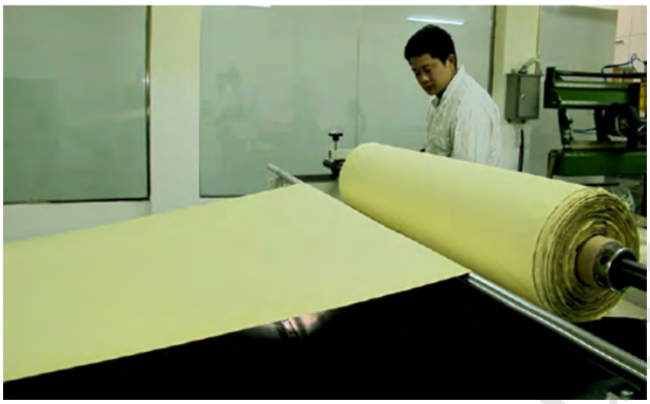

Fig 3. Fabrication of electrospun PI nanofiber nonwovens/fabrics in industrial scale.

Accepted Manuscript

ACCEPTED MANUSCRIPT

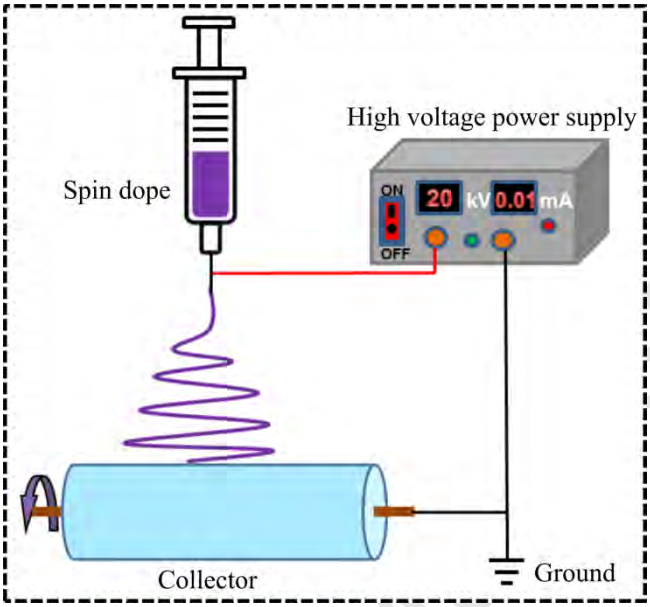

Fig 4. Schematic illustration of a laboratory setup for electrospinning.

Accepted Manuscript

ACCEPTED MANUSCRIPT

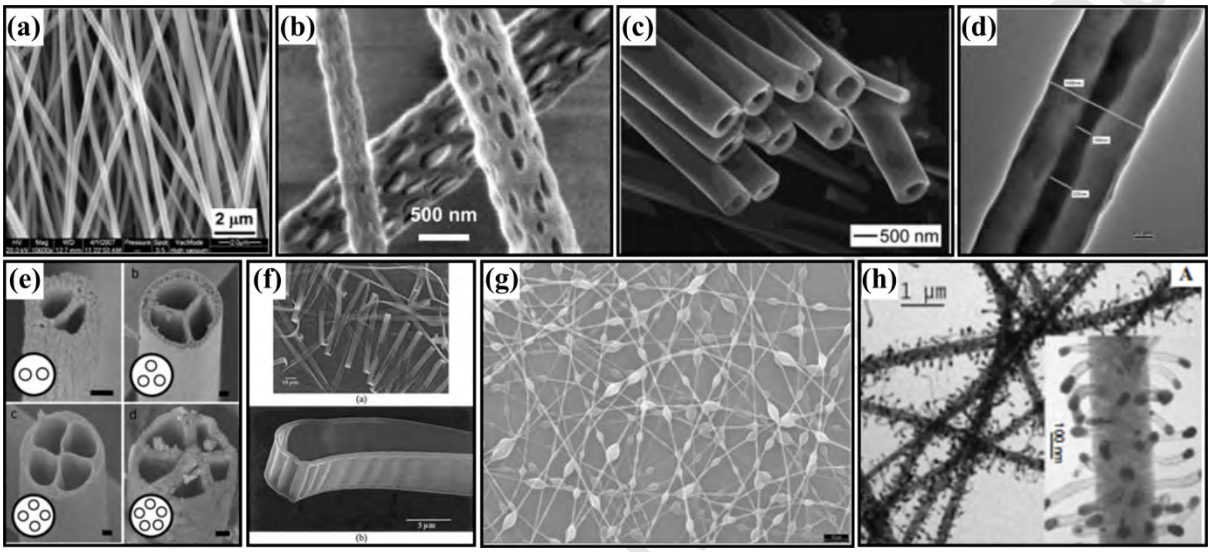

Fig 5. Microscopic images of electrospun nanofibers with different morphologies: a) Cylindrical PAN nanofibers [45]. Copyright 2009, Reproduced with permission from Elsevier B.V.; b) Porous PLLA nanofibers [46]. Copyright 2001, Reproduced with permission from John Wiley & Sons, Inc.; c) TiO_2/PVP hollow nanofibers [48]. Copyright 2004, Reproduced with permission from American Chemical Society; d) PDT/PEO core-shell nanofiber [50]. Copyright 2003, Reproduced with permission from John Wiley & Sons, Inc.; e) TiO_2 multi-channel nanotubes [52]. Copyright 2007, Reproduced with permission from American Chemical Society; f) Poly(ether imide) nano-ribbons [33]. Copyright 2001, Reproduced with permission from John Wiley & Sons, Inc.; g) Bead-on-string PVP-oil nanofibers [55]. Copyright 2006, Reproduced with permission from John Wiley & Sons, Inc.; h) Carbon nanotubes growth on electrospun carbon nanofibers [57]. Copyright 2004, Reproduced with permission from John Wiley & Sons, Inc.

ACCEPTED MANUSCRIPT

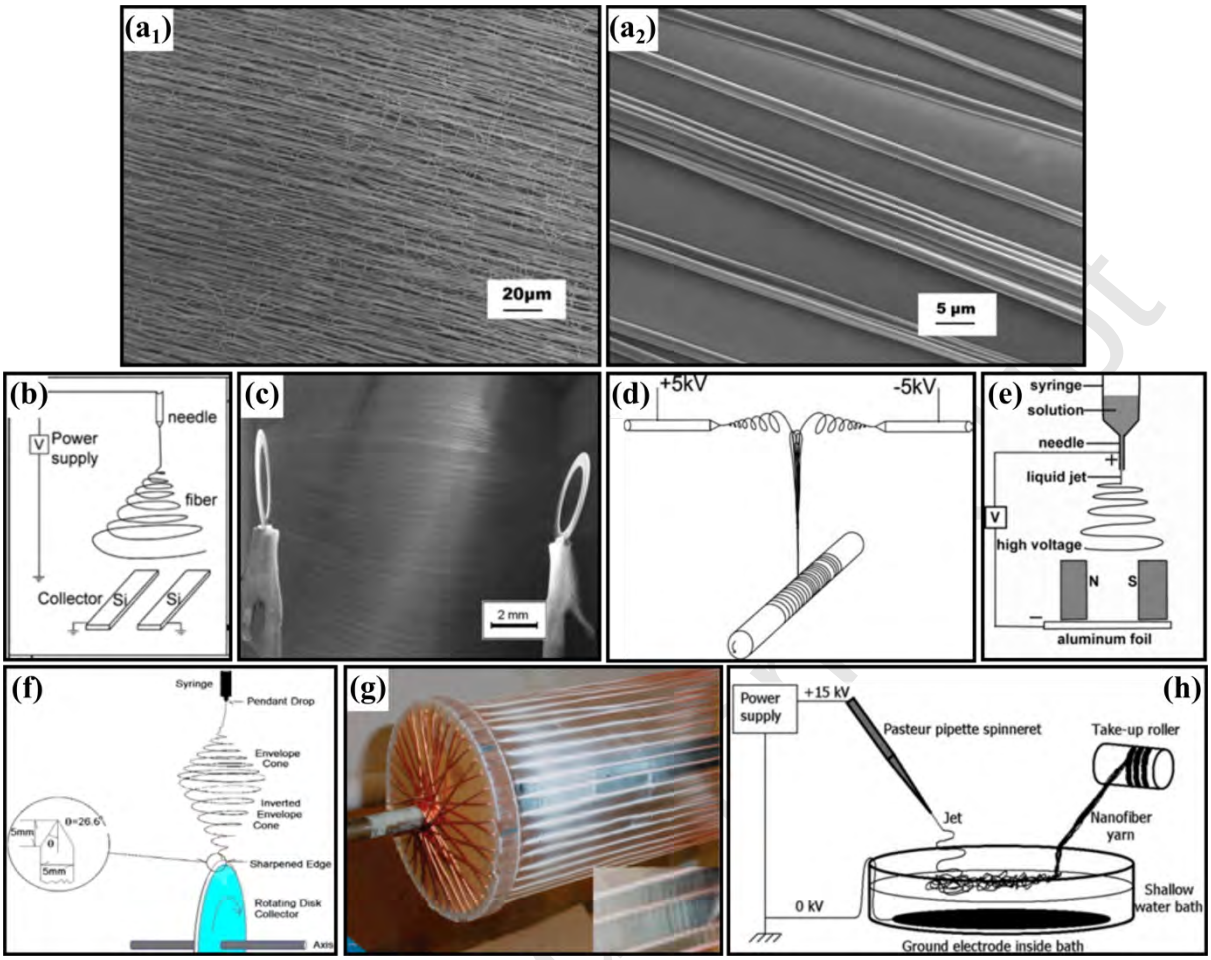

Fig 6. SEM images of well-aligned electrospun nanofibers and schematic setups used for collecting aligned nanofibers: a) SEM images of well-aligned PVA nanofibers [80]. Copyright 2006, Reproduced with permission from Elsevier B.V.; b) Parallel electrode collector with a gap between two conductive substrates [78]. Copyright 2003, Reproduced with permission from American Chemical Society; c) Dual rings collector [79]. Copyright 2005, Reproduced with permission from Elsevier B.V.; d) Two oppositely placed metallic needles with opposite voltages [80]. Copyright 2006, Reproduced with permission from Elsevier B.V.; e) Collection of aligned magnetized nanofibers with magnetic field [81]. Copyright 2007, Reproduced with permission from John Wiley & Sons, Inc.; f) Collector of rotating disc with high speed [82]. Copyright 2001, Reproduced with permission from IOP Publishing; g) Rotating wire drum collector [83]. Copyright 2004, Reproduced with permission from American Chemical Society; h) Yarn collection by using an electrically grounded water bath [84]. Copyright 2005, Reproduced with permission from Elsevier B.V.

ACCEPTED MANUSCRIPT

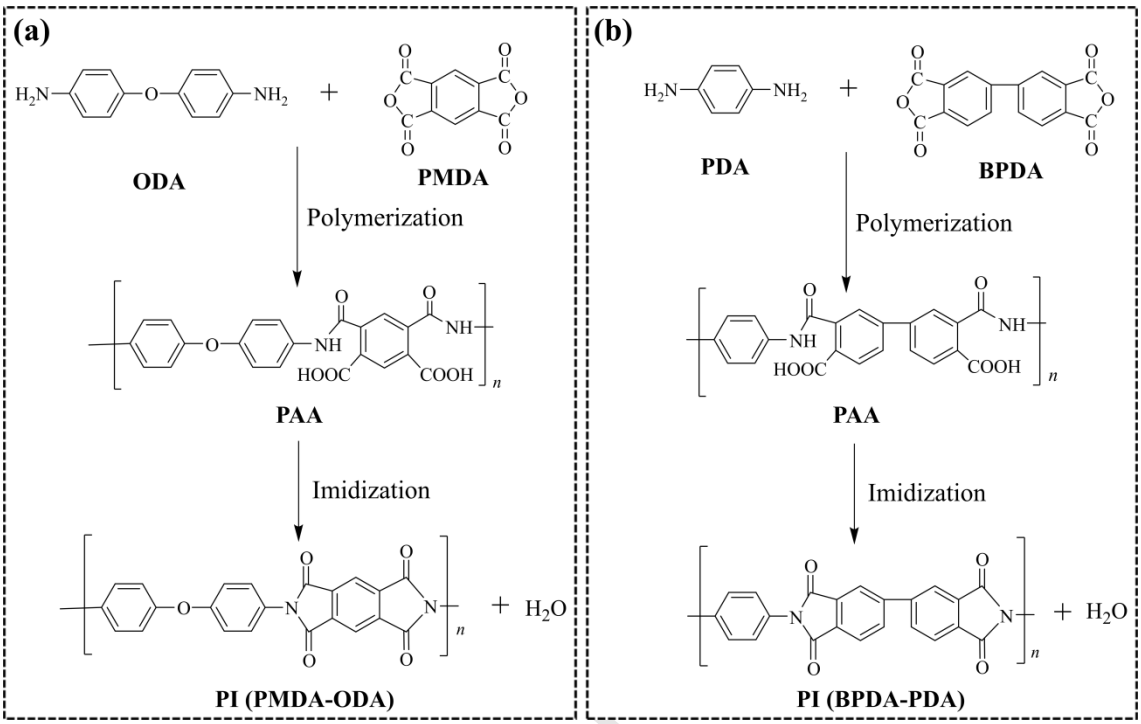

Fig 7. Chemical schemes showing the two-step method for synthesis of homo-PIs: a) PMDA-ODA PI and b) BPDA-PDA PI.

Accepted

ACCEPTED MANUSCRIPT

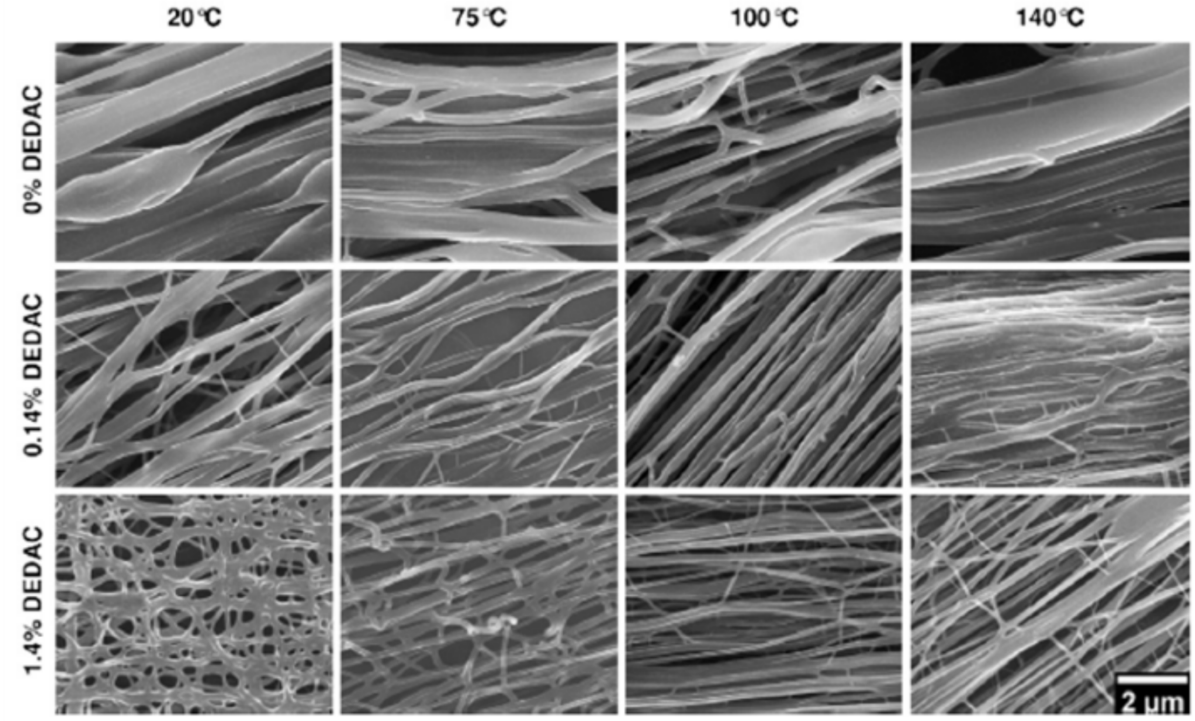

Fig 8. SEM images of PI nanofibers after imidization. PAA precursor nanofibers were obtained from electrospinning of solutions with varied concentrations of DEDAC (left images) followed by being aged in vacuum at different temperature (top images) [111]. Copyright 2011, Reproduced with permission from Elsevier B.V.

Accepted

ACCEPTED MANUSCRIPT

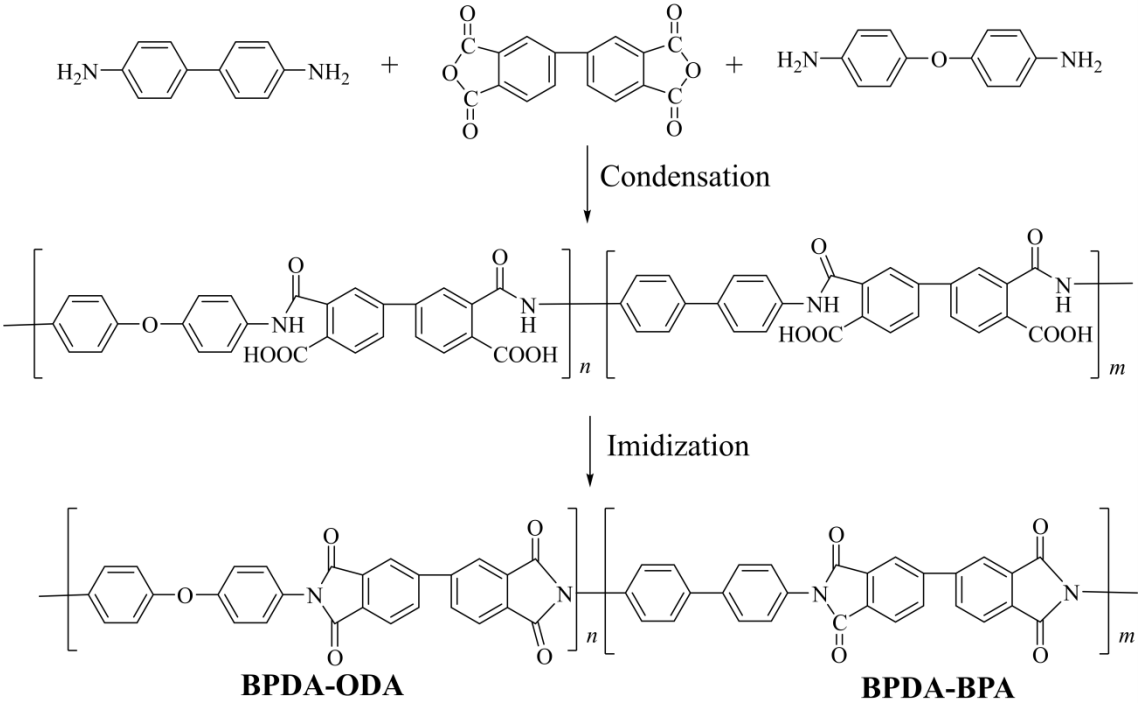

Fig 9. Chemical scheme showing the synthesis of BPDA-BPA-ODA co-PI through polymerization of BPDA with two diamines of ODA and BPA.

Accepted

ACCEPTED MANUSCRIPT

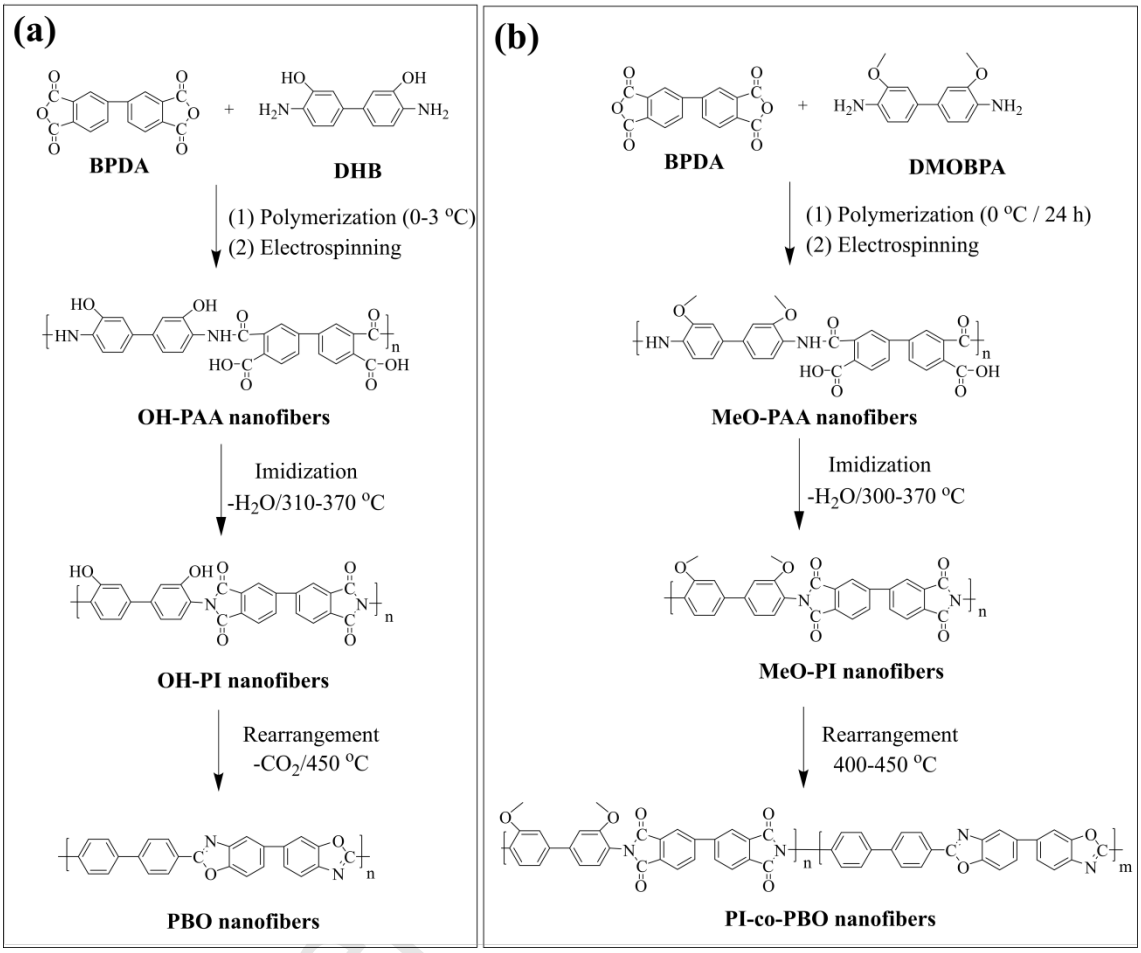

Fig 10. Chemical schemes showing the preparation and thermal conversion of PBO nanofibers through OH-PAA (a) [118]. Copyright 2014, Reproduced with permission from Elsevier B.V.; and PI-co-PBO nanofibers through MeO-PAA (b) [102]. Copyright 2015, Reproduced with permission from Royal Society of Chemistry.

ACCEPTED MANUSCRIPT

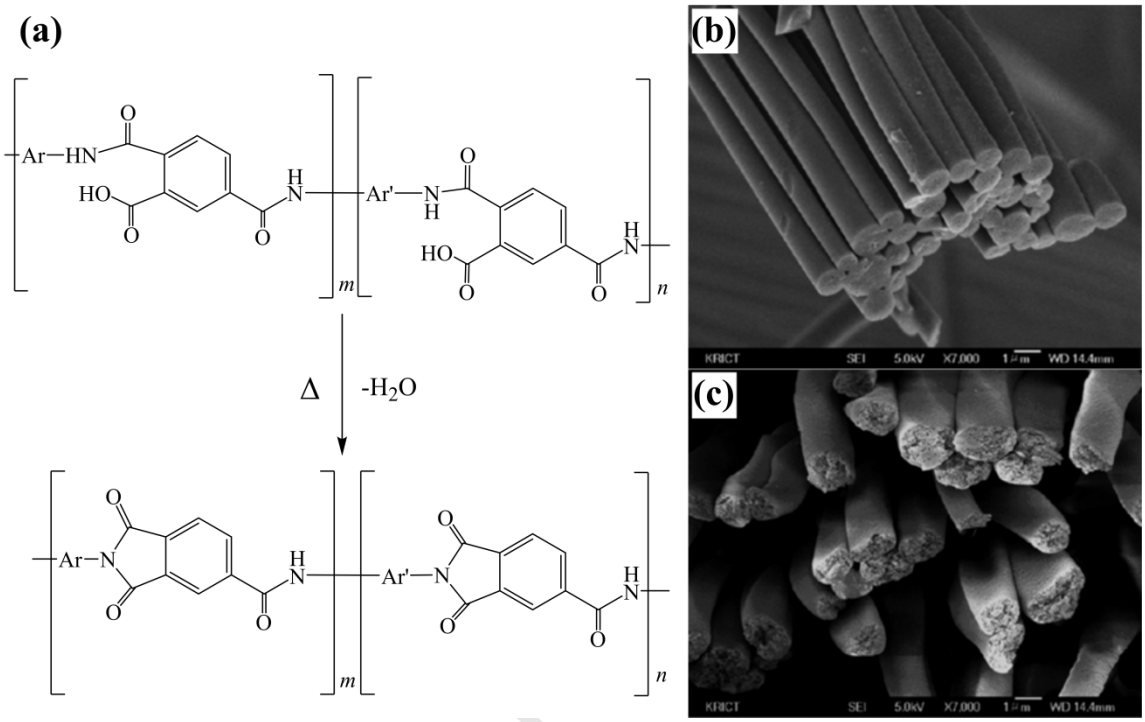

Fig 11. Chemical scheme showing thermal imidization of PAI (a); and SEM images showing fracture surfaces of PAI nanofibers imidized at 330 °C (b) and at 400 °C under tension after the glycerol pre-treatment (c) [121]. Copyright 2010, Reproduced with permission from John Wiley & Sons, Inc.

Accepted

ACCEPTED MANUSCRIPT

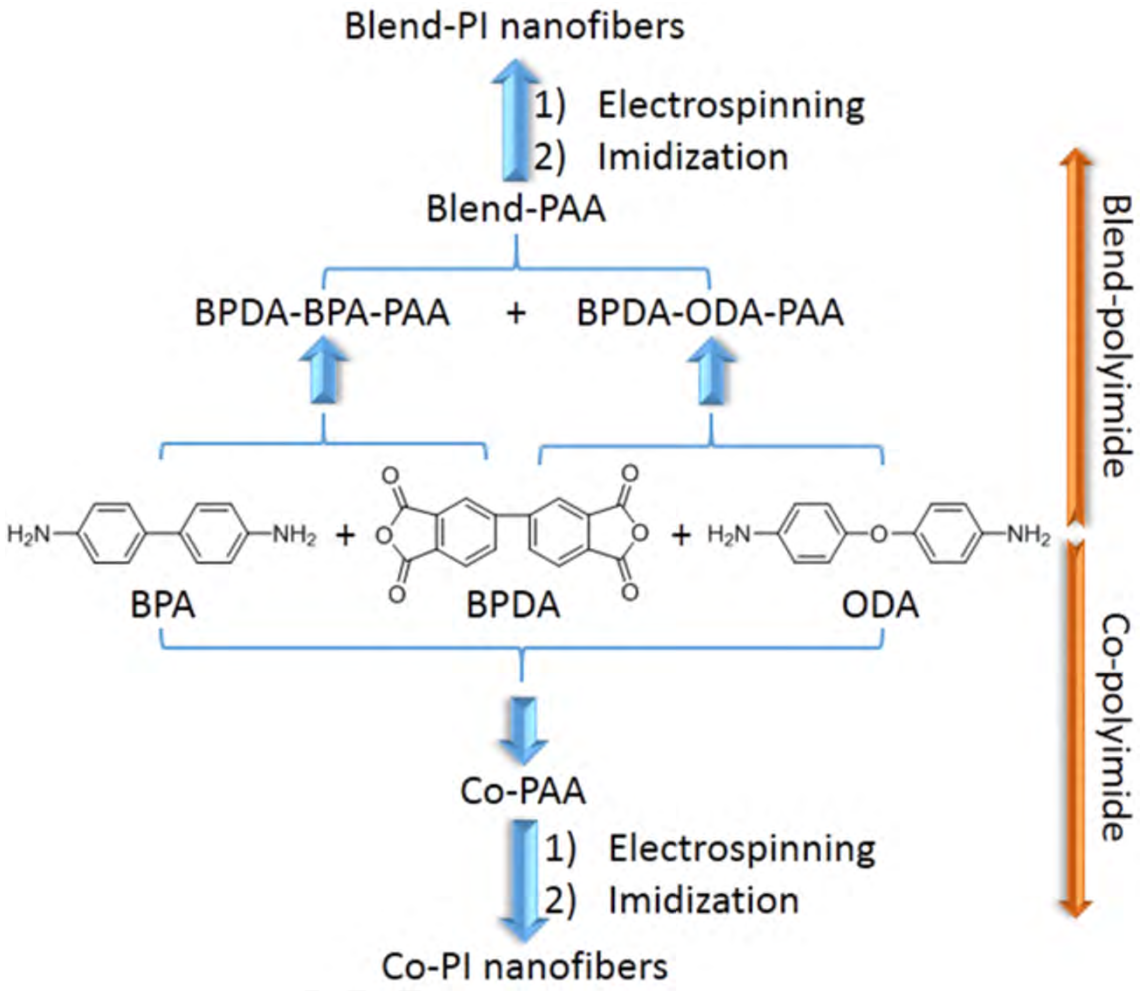

Fig 12. Schematic diagrams depicting the preparations of blend-PI and co-PI [96]. Copyright 2014, Reproduced with permission from Royal Society of Chemistry.

ACCEPTED MANUSCRIPT

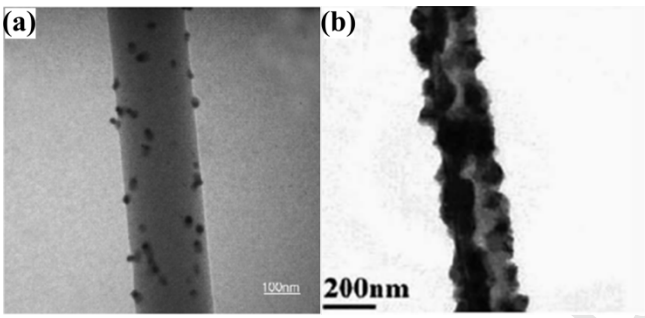

Fig 13. a) TEM image of electrospun PI/Ag nanofiber with 2 wt.% of Ag [125]. Copyright 2007, Reproduced with permission from Elsevier B.V.; b) TEM image of electrospun PI/SiO_2 nanofiber with 6.58 wt.% of SiO_2 [143]. Copyright 2009, Reproduced with permission from Elsevier B.V.

Accepted Manuscript

ACCEPTED MANUSCRIPT

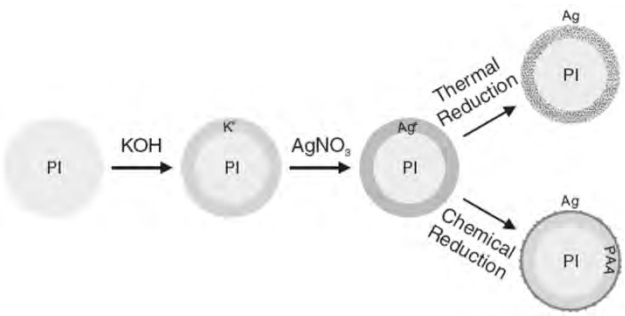

Fig 14. Schematic illustration showing the preparation of PI/Ag composite nanofibers by stepped processes of hydrolysis, ion-exchange, and finally reduction (thermal reduction and chemical reduction) [152]. Copyright 2011, Reproduced with permission from John Wiley & Sons, Inc.

Accepted Manuscript

ACCEPTED MANUSCRIPT

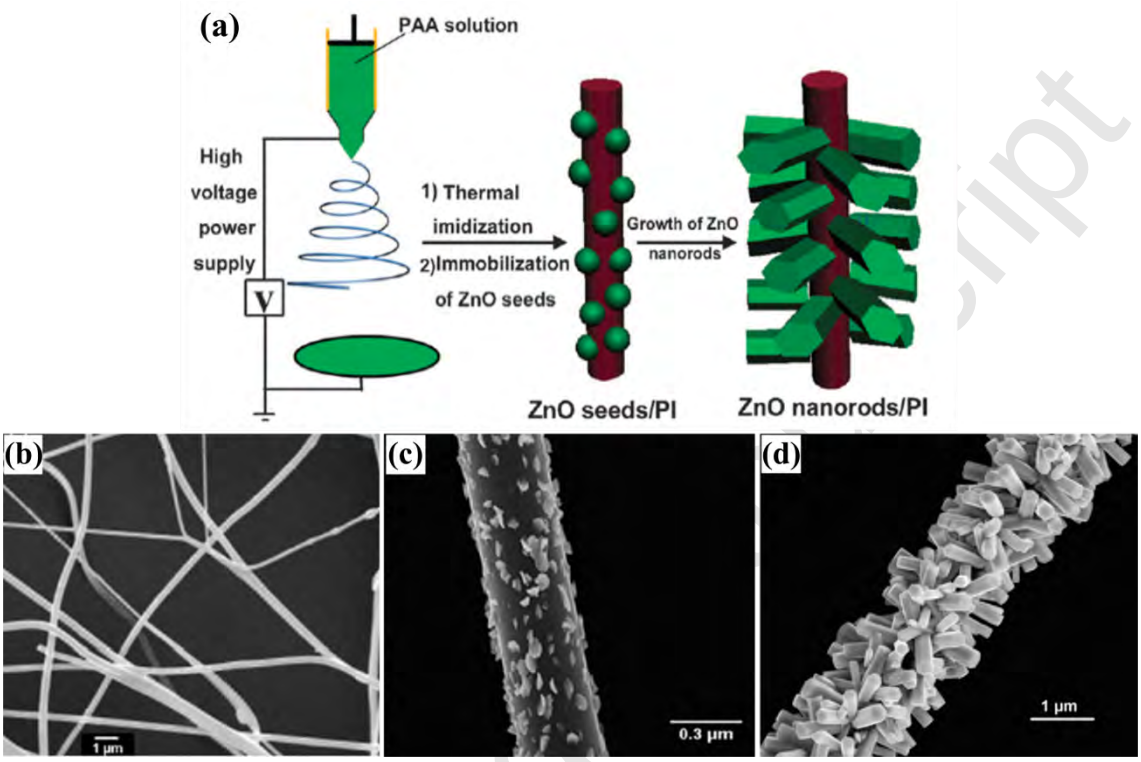

Fig 15. a) Schematic illustration showing the combined processes of electrospinning and hydrothermal growth to prepare ZnO nanorods on PI nanofibers; b) SEM image of pristine PI nanofibers; c) SEM image of ZnO seeds on PI nanofiber; d) SEM image of ZnO/PI hybrid nanofiber [156]. Copyright 2011, Reproduced with permission from Royal Society of Chemistry.

ACCEPTED MANUSCRIPT

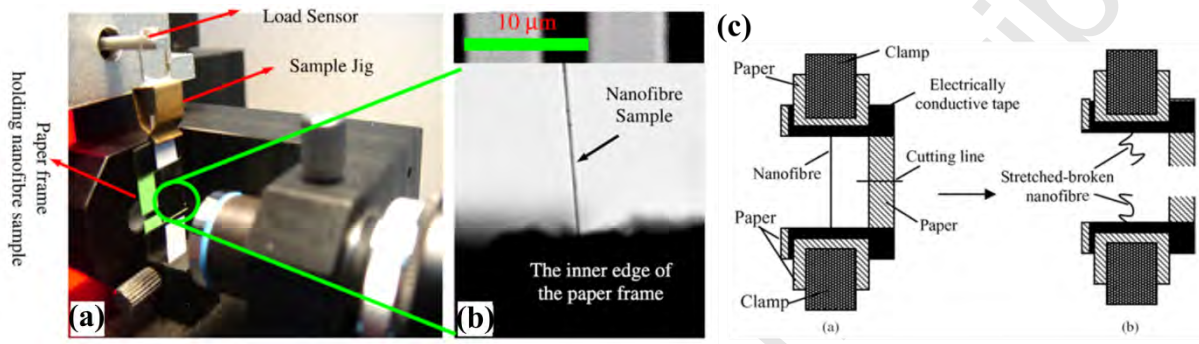

Fig 16. a) Photograph of micro-tension testing machine with a paper frame carrying an individual nanofiber into the clamps for testing; b) Photograph showing the tensile stretching of an individual nanofiber; c) Schematic diagram of the paper frame holding an individual nanofiber for the test before and after the fiber is broken [90]. Copyright 2008, Reproduced with permission from IOP Publishing.

Accepted Manuscript

ACCEPTED MANUSCRIPT

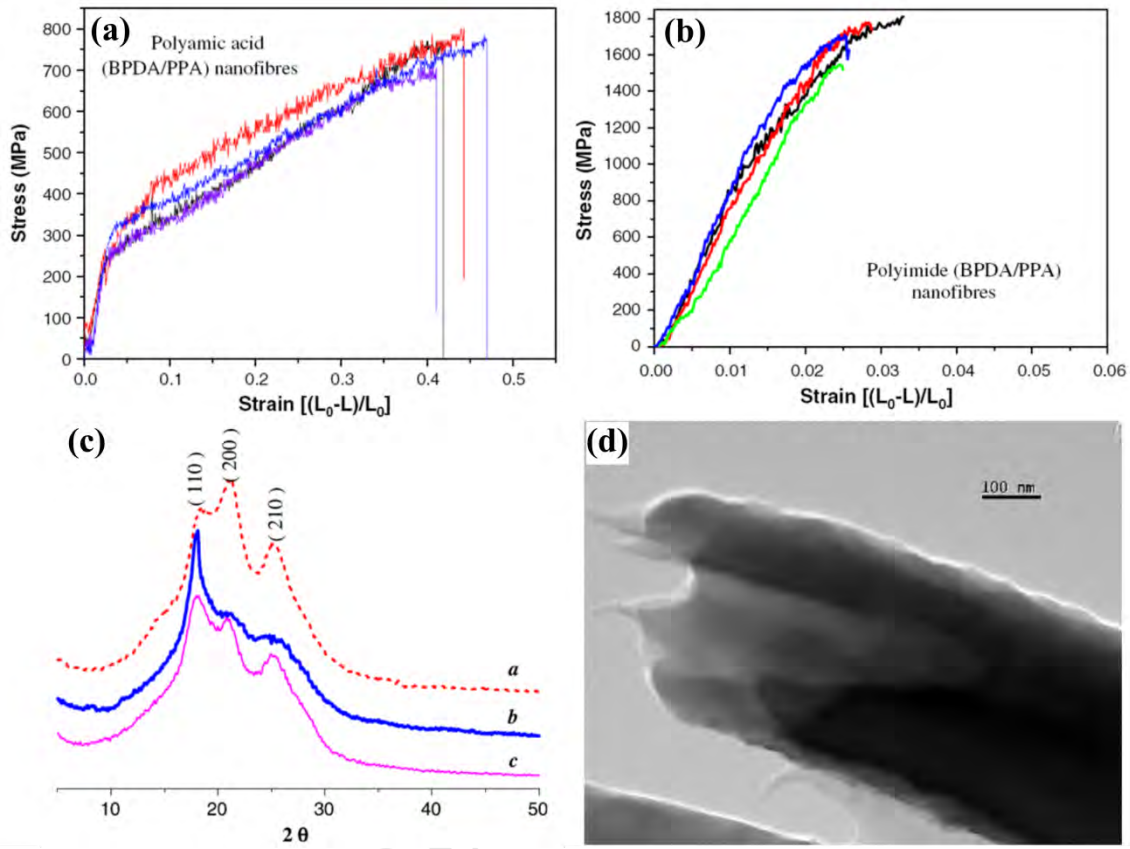

Fig 17. Typical stress-strain curves of individual electrospun PAA nanofiber (a) and PI nanofiber (b); XRD patterns (c) of PI film (with thickness of 18 μm) and electrospun nanofiber mats (multilayer aligned and non-aligned PI nanofiber mats); d) TEM-fractographical analysis of an individual PI nanofiber after tensile failure [90]. Copyright 2008, Reproduced with permission from IOP Publishing.

ACCEPTED MANUSCRIPT

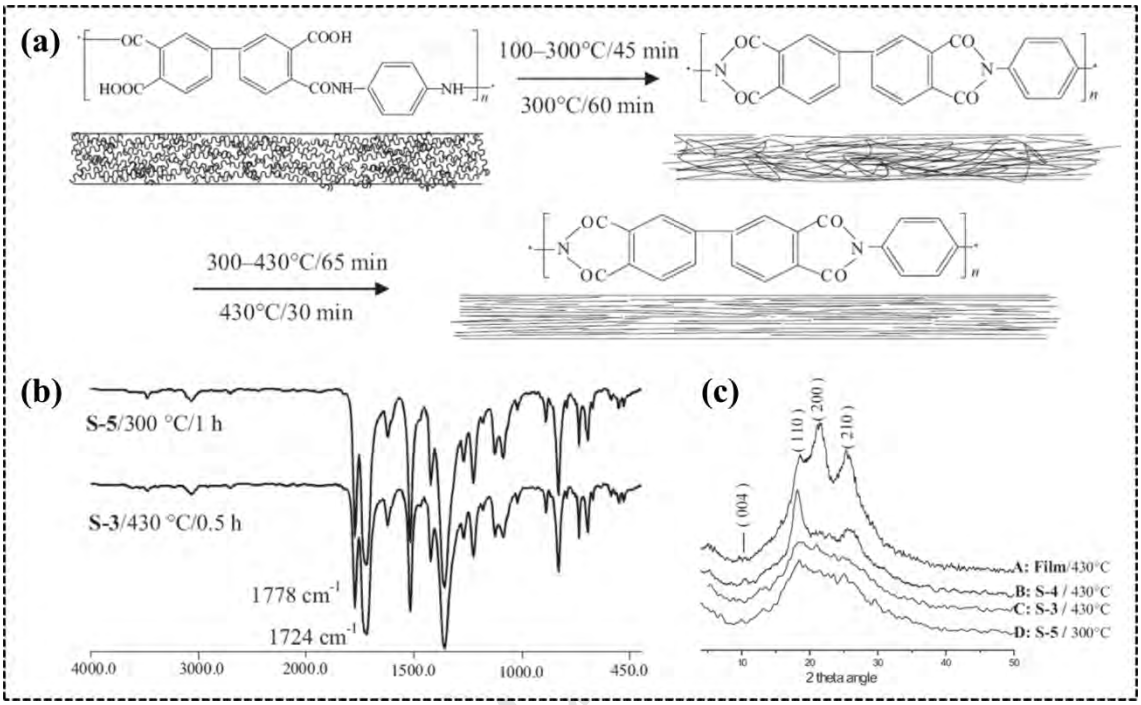

Fig 18. a) Chemical and structural conversion of electrospun BPDA-PDA PAA nanofibers into BPDA-PDA PI nanofibers; b) IR spectra of BPDA-PDA nanofiber mats cured at 300 °C and 430 °C, respectively; c) XRD patterns of PBDA-PDA PI film and electrospun nanofiber mat [88]. Copyright 2006, Reproduced with permission from John Wiley & Sons, Inc.

ACCEPTED MANUSCRIPT

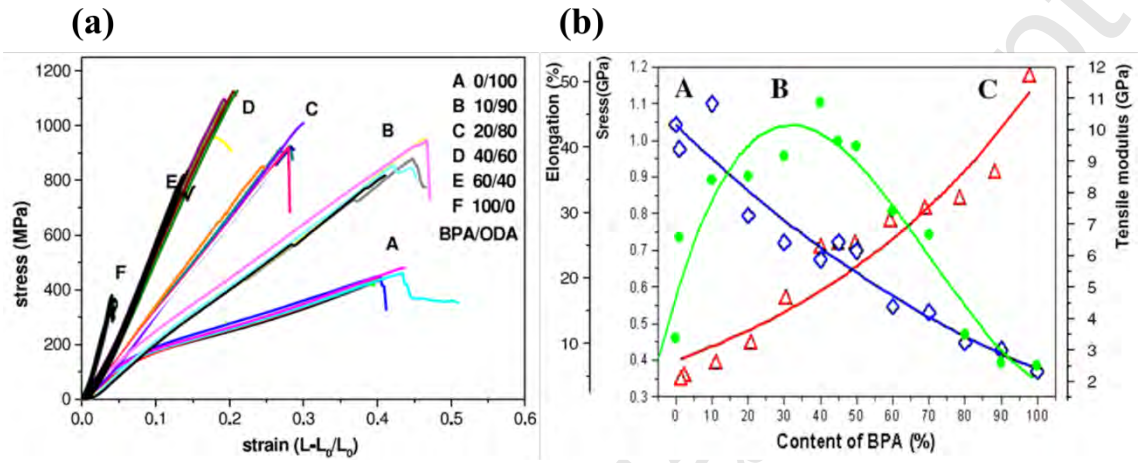

Fig 19. a) Typical stress-strain curves of aligned O-PI, B-PI, co-PI nanofiber belts; b) relationships between mechanical properties and BPA moiety content in the PIs; curve (A): strain, curve (B): tensile strength, curve (C): elastic modulus [91]. Copyright 2008, Reproduced with permission from IOP Publishing.

Accepted Manuscript

ACCEPTED MANUSCRIPT

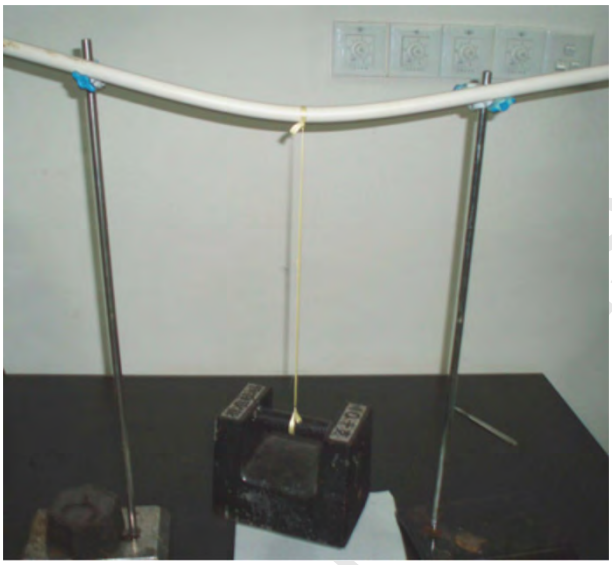

Fig 20. Photograph showing an electrospun co-PI nanofiber belt (with width and thickness of 7.5 mm and 12 μm, respectively) capable of hanging a weight of 10 kg [91]. Copyright 2008, Reproduced with permission from IOP Publishing.

Accepted Manuscript

ACCEPTED MANUSCRIPT

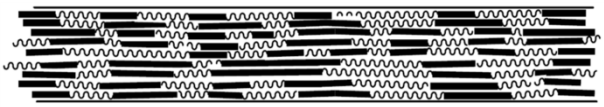

Fig 21. Schematic representation showing high-strength PI nanofiber composed of the ordered flexible and rigid micro-block regions [91]. Copyright 2008, Reproduced with permission from IOP Publishing.

Accepted Manuscript

ACCEPTED MANUSCRIPT

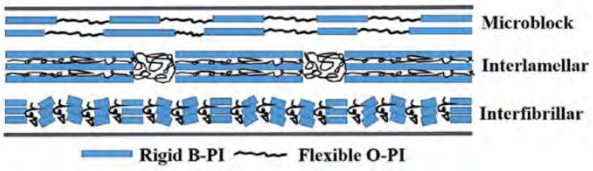

Fig 22. Schematic representation showing the microstructure of blend-PI nanofiber with rigid and flexible components [96]. Copyright 2014, Reproduced with permission from Royal Society of Chemistry.

Accepted Manuscript

ACCEPTED MANUSCRIPT

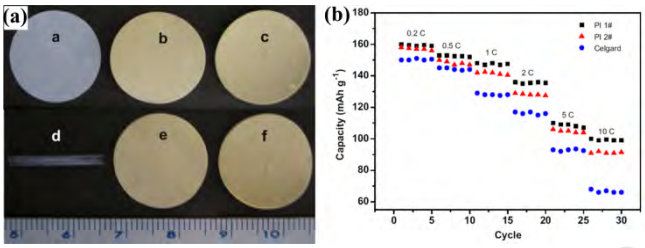

Fig 23. a) Digital images of Celgard membrane, PI nanofiber mats/membranes with the thickness values of 40 μm (b) and 100 μm (c) before (a, b, c) and after (d, e, f) the thermal test at 150 °C; b) Rate capability tests for the cells with Celgard membrane and PI nanofiber mat/membrane as separators [95]. Copyright 2013, Reproduced with permission from Elsevier B.V.

Accepted Manuscript

ACCEPTED MANUSCRIPT

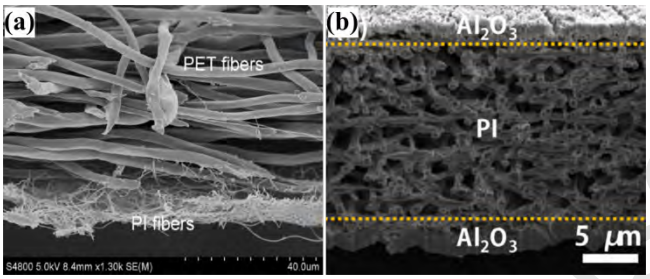

Fig 24. a) SEM image showing the cross-section of PI/PET composite membrane [129]. Copyright 2012, Reproduced with permission from The Electrochemical Society; b) SEM image showing the cross-section of Al_2O_3-PI separator [209]. Copyright 2014, Reproduced with permission from Elsevier B.V.

Accepted Manuscript

ACCEPTED MANUSCRIPT

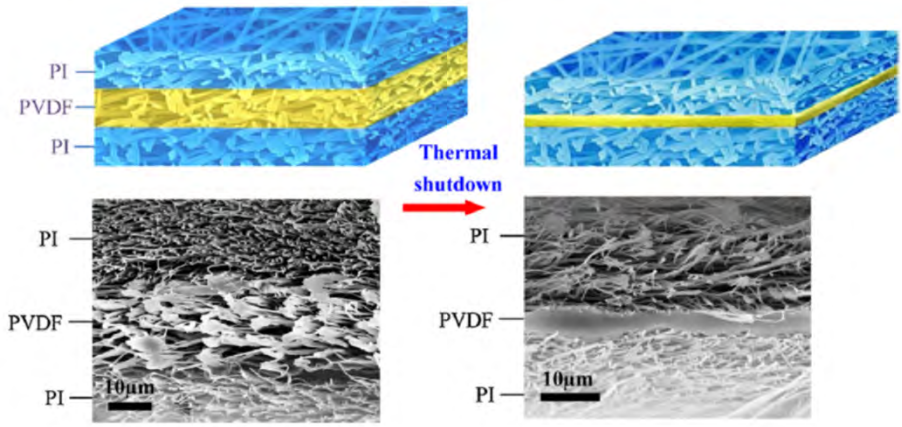

Fig 25. Illustration showing the shutdown behavior of the sandwiched PI/PVDF/PI nanofiber separator [216]. Copyright 2015, Reproduced with permission from Elsevier B.V.

Accepted Manuscript

ACCEPTED MANUSCRIPT

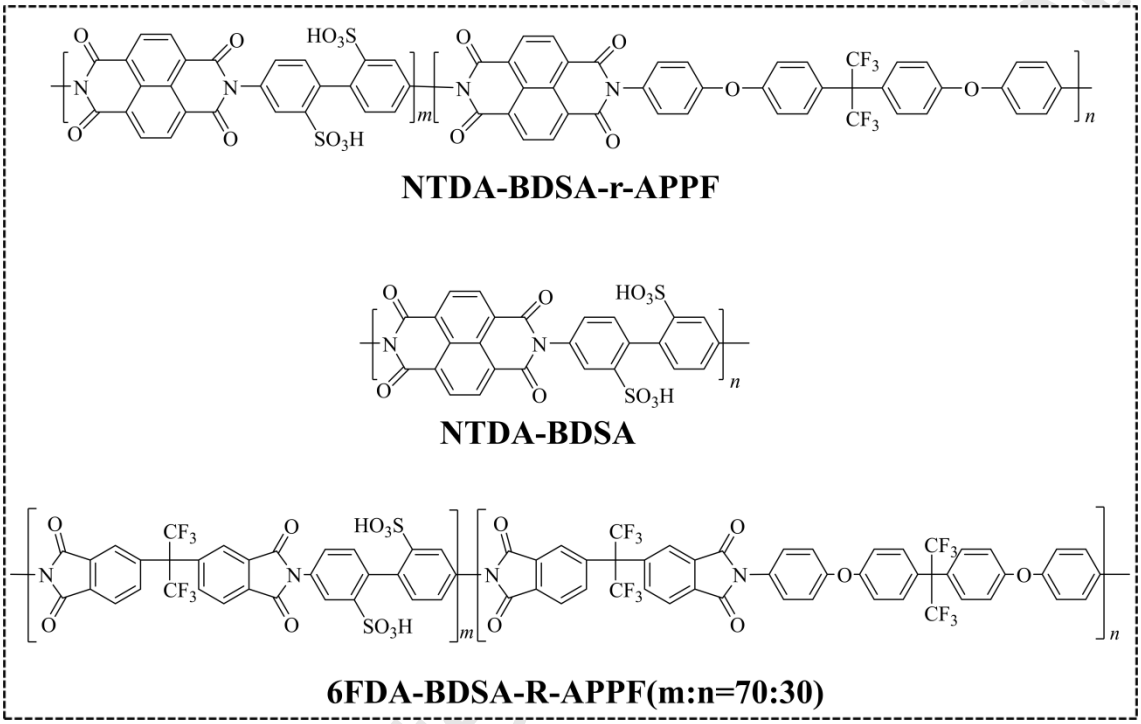

Fig 26. Chemical structures of sulfonated PIs [208, 210].

ACCEPTED MANUSCRIPT

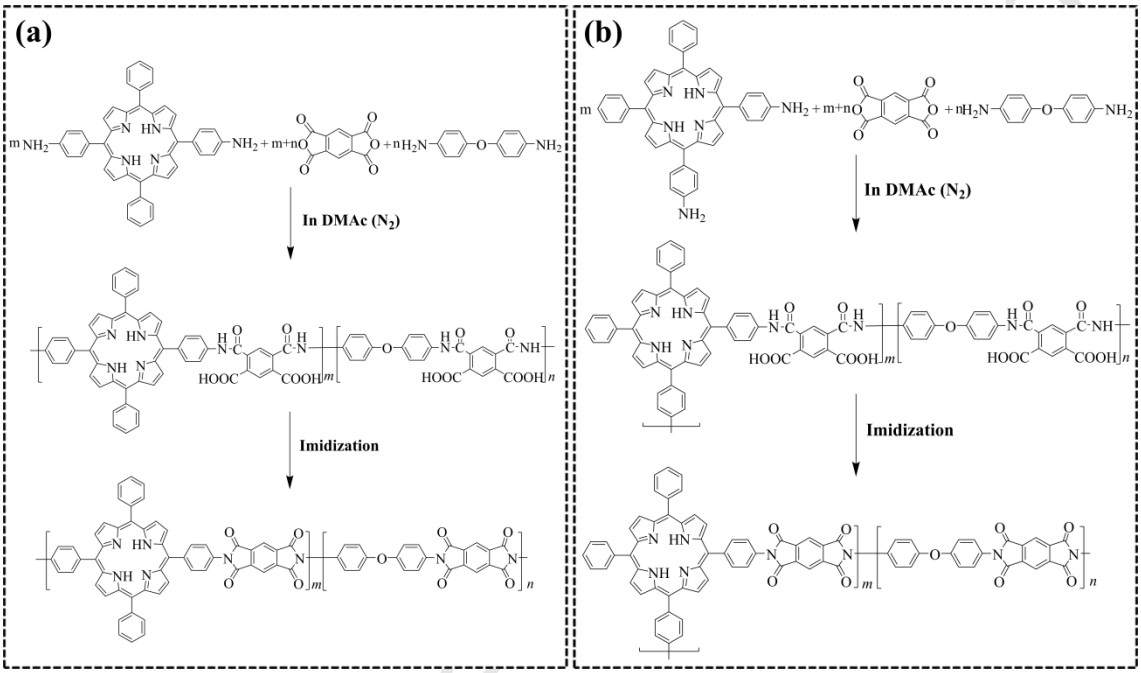

Fig 27. Chemical schemes depicting the syntheses and molecular structures of porphyrinated co-PIs made from *trans*-DATPP (a) and *cis*-DATPP (b) [225]. Copyright 2008, Reproduced with permission from American Chemical Society.

ACCEPTED MANUSCRIPT

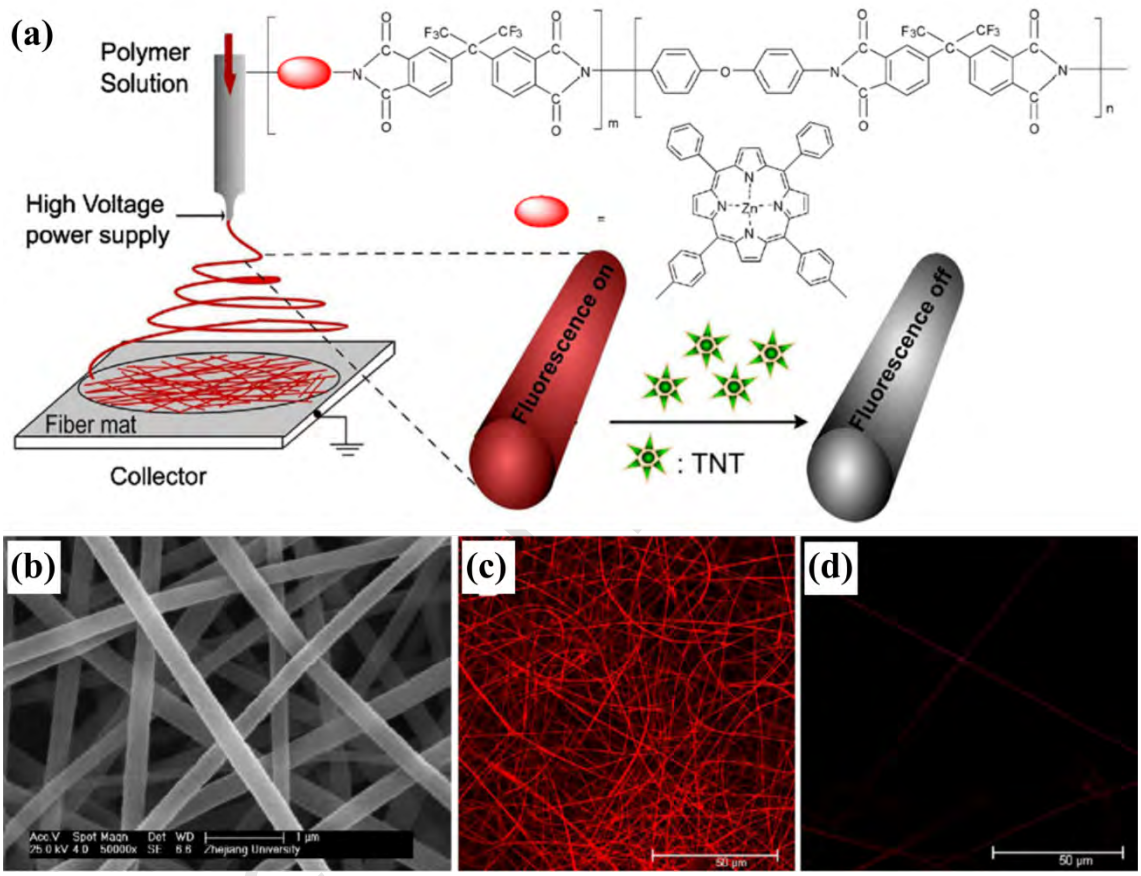

Fig 28. (a) Molecular structure of porphyrinated PI and schematic illustration showing the porphyrinated nanofiber membrane for fluorescent detection of TNT; SEM micrograph (b), and CLSM images of the porphyrinated nanofiber membrane before (c) and after (d) exposing to 10 ppb TNT vapor (λ_{ex} = 488 nm) [127]. Copyright 2013, Reproduced with permission from Elsevier B.V.

ACCEPTED MANUSCRIPT

Fig 29. An example of using the PI nanopaper for flexible antenna [236]. Copyright 2013, Reproduced with permission from Elsevier B.V.

Accepted Manuscript

ACCEPTED MANUSCRIPT

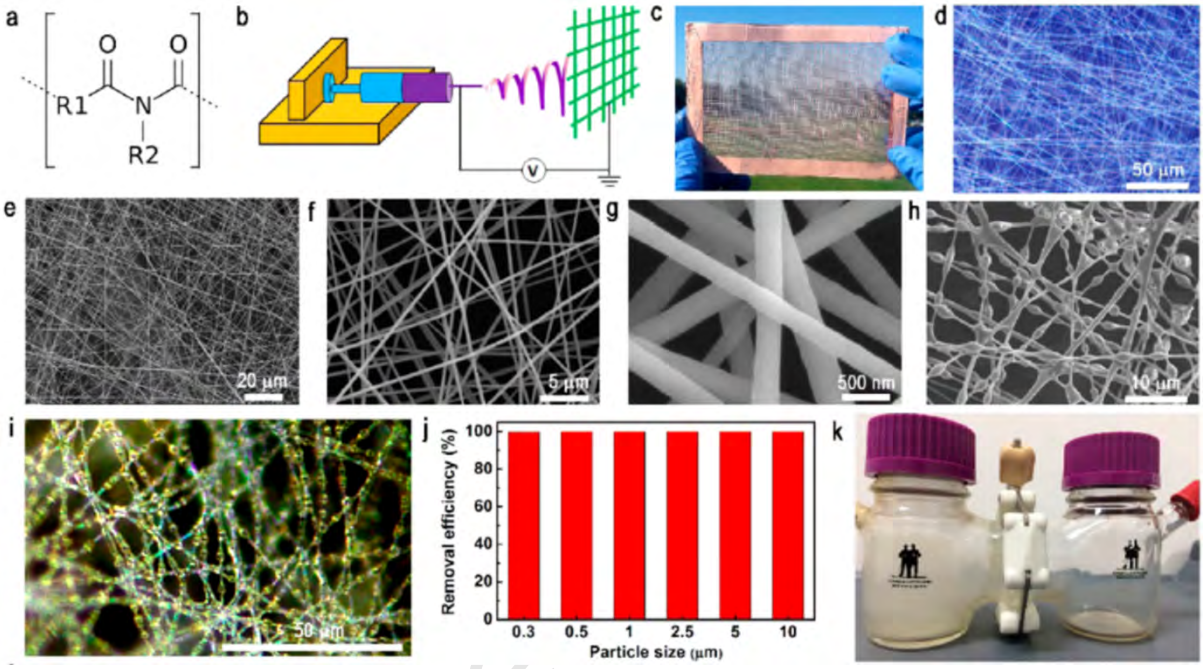

Fig 30. Structure and PM removal performance of PI nanofiber air filters: (a) General molecular structure of PI; (b) Schematic representation showing the fabrication of transparent PI air filters by electrospinning; (c) Photograph of a typical transparent PI air filter with optical transmittance of 70%; (d) OM image of a transparent PI air filter; (e−g) SEM images acquired from the PI air filters with different magnifications; (h) SEM image of a PI air filter with captured PM particles; (i) OM image of a PI air filter with captured PM particles. (j) PM removal efficiencies of the PI air filter with optical transmittance of 50%; (k) Demonstration of using the PI nanofiber air filter to block the PM from the sources (left bottle) entering the environment (right bottle) [241]. Copyright 2016, Reproduced with permission from American Chemical Society.

ACCEPTED MANUSCRIPT

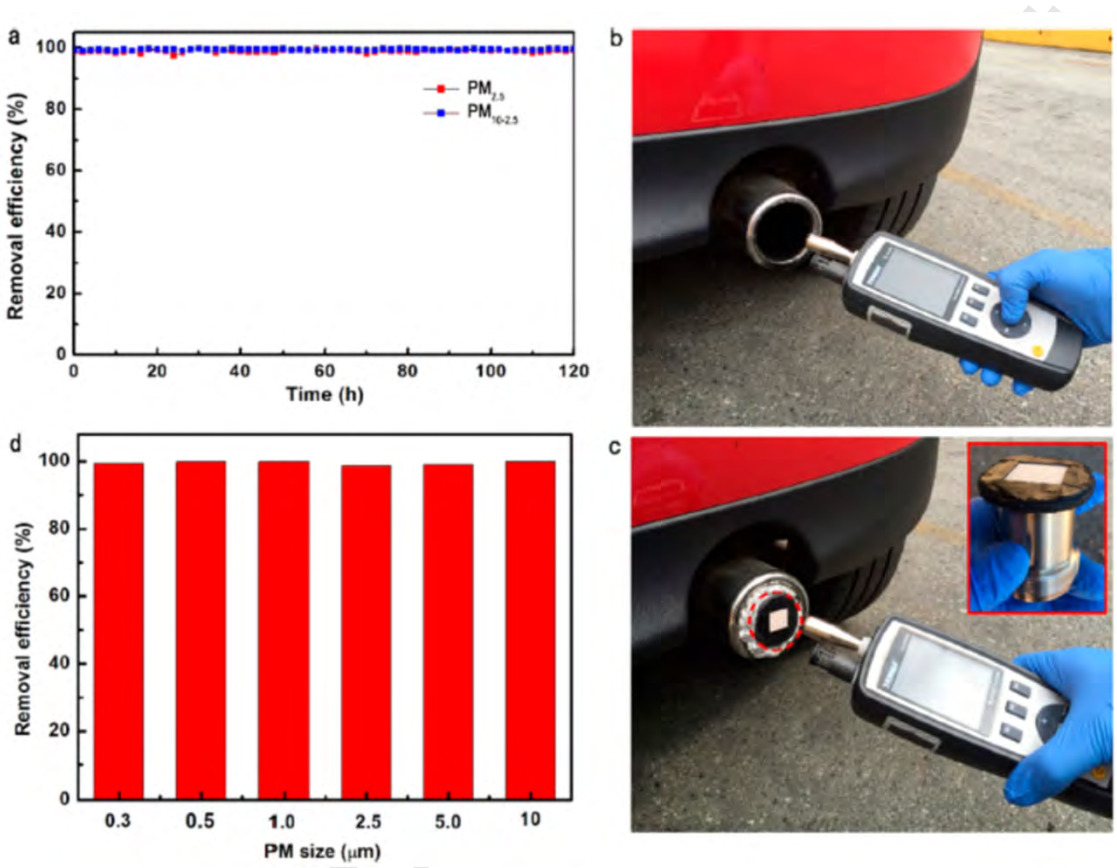

Fig 31. Long-term performance and practical application of PI air filters: (a) Long-term $PM_{2.5}$ and $PM_{2.5-10}$ removal efficiencies by the PI nanofiber air filter with transmittance of 50% under continuous hazardous condition of PM pollution; (b) PM number concentration measurement of vehicle exhaust gas without air filter. (c) PM number concentration measurement of vehicle exhaust gas with air filter; (d) Removal efficiencies of PM particles from vehicle exhaust gas [241]. Copyright 2016, Reproduced with permission from American Chemical Society.

ACCEPTED MANUSCRIPT

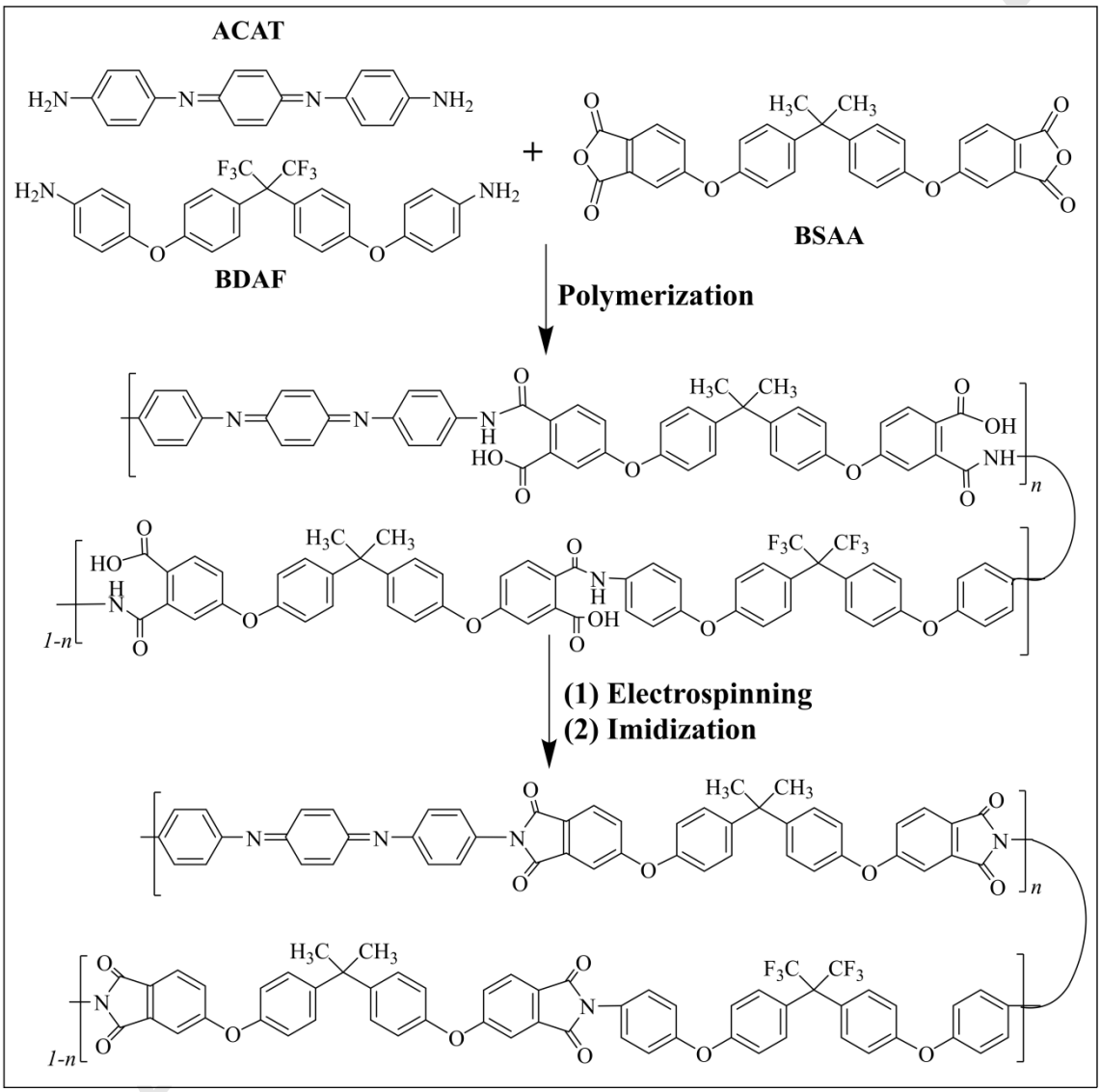

Fig 32. Scheme showing the synthesis of electro-active PAA and PI [256]. Copyright 2011, Reproduced with permission from Royal Society of Chemistry.

ACCEPTED MANUSCRIPT

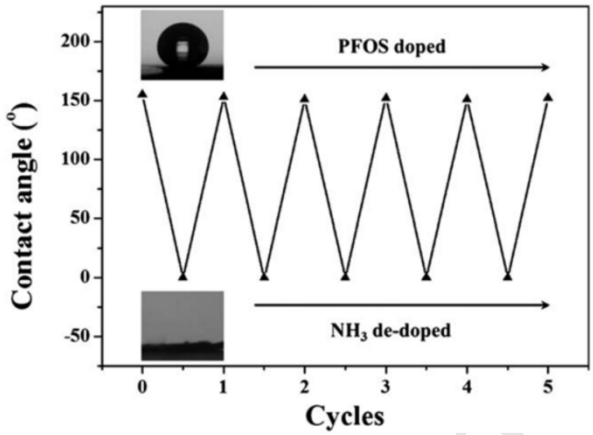

Fig 33. Reversible super-hydrophobic/super-hydrophilic conversions of the EPF through doping with PFOS and de-doping by ammonia gas [256]. Copyright 2011, Reproduced with permission from Royal Society of Chemistry.

Accepted Manuscript

ACCEPTED MANUSCRIPT

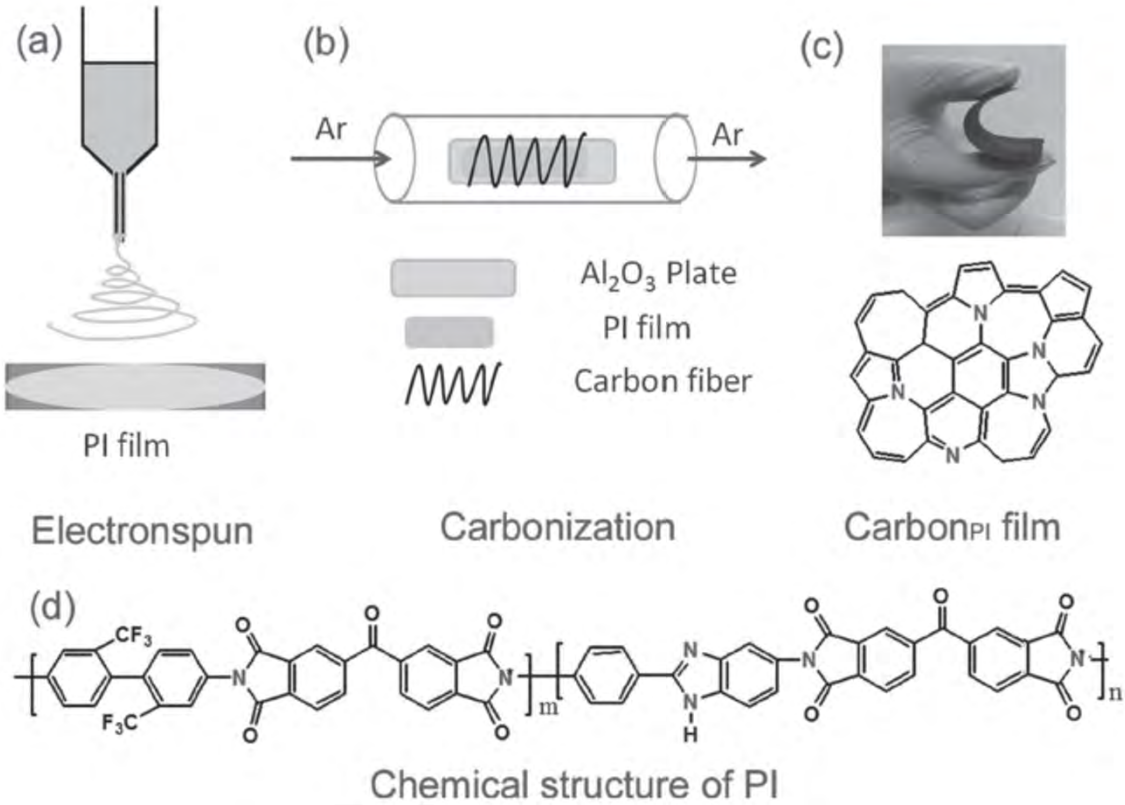

Fig 34. Preparation of carbon nanofiber membrane derived from PI: a) Electrospinning PI membrane; b) Carbonization of PI membrane in a furnace at 1000 °C; c) Photograph of the resulting $Carbon_{PI}$ membrane and molecular structure showing the nitrogen doping; d) Chemical structure of PI polymer [283]. Copyright 2015, Reproduced with permission from John Wiley & Sons, Inc.